
LARK: Learnability-Grounded Trajectory Selection for Efficient Reasoning Distillation

Tianrun Yu¹, Kaixiang Zhao¹, Chih-Chun Chen¹, Amanda Hughes¹
Taylor W. Killian¹, Fenglong Ma², Weitong Zhang³, Porter Jenkins^{1,*}

¹Brigham Young University ²The Pennsylvania State University ³University of North Carolina at Chapel Hill

*Corresponding author: pjenkins@cs.byu.edu

Abstract

We study trajectory selection for reasoning distillation, where teacher-generated reasoning trajectories are selectively used as supervision for a student model. Existing methods rely on heuristics such as trajectory quality or model confidence, but they often overlook whether a trajectory is learnable by the student. In this paper, we present LARK¹, a learnability-grounded method for reasoning trajectory selection. LARK selects trajectories that the student can learn efficiently while preserving the generalization of the full training distribution. At the core of LARK is a learnability factor ρ , which characterizes the rate at which the student’s training loss decreases. To estimate this rate efficiently and maintain generalization, we introduce a learnability proxy and a χ^2 -regularized selection policy that balances learnability and distributional coverage, both with strong theoretical guarantees on their estimation error. Empirically, LARK consistently outperforms data selection baselines across multiple base models and reasoning tasks. Diagnostic analyses show that the LARK score predicts downstream training utility and that LARK-selected trajectories induce faster supervised fine-tuning loss reduction.

1 Introduction

Reasoning distillation has emerged as an effective paradigm for transferring chain-of-thought reasoning abilities from larger teacher Large Language Models (LLMs) to smaller student models [Hsieh et al., 2023, Yuan et al., 2023]. In this setting, a teacher model generates reasoning trajectories, and a student model is fine-tuned to imitate them. Recent studies have shown that *a small set of carefully selected reasoning examples* can yield substantial performance gains [Ye et al., 2025, Muennighoff et al., 2025], often rivaling the use of much larger training sets. These findings suggest that reasoning distillation requires both *generating* sufficient reasoning data and *identifying* the supervision that is most useful for the student.

Many existing data selection methods for reasoning distillation still inherit the classical formulation of data selection in LLM fine-tuning [Xia et al., 2024, Xiao and Chen, 2025], where selection is performed at the question or sample level [Yu et al., 2023, Zhang et al., 2025b, Liu et al., 2024]. However, reasoning distillation presents a finer-grained selection problem. For a single question, we often have multiple candidate reasoning trajectories, generated by different teacher models, sampling runs, or reasoning styles. Even when several trajectories lead to the same correct final answer, they may provide very different training signals to the current student model. A trajectory that appears natural, high-quality, or well aligned with the student model is not necessarily the one that the student can learn from most efficiently.

¹Our code is available at <https://github.com/Tianrun-Yu/LARK>.

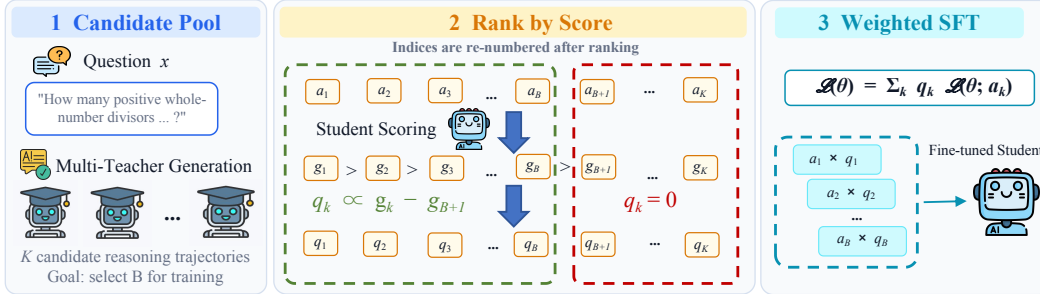


Figure 1: Overview of the LARK pipeline. For each question, multiple teacher-generated reasoning trajectories form a candidate pool. LARK uses the student model to score these trajectories, ranks them by the score, and selects the top- B trajectories for weighted SFT. In the figure, a_k denotes the k -th trajectory after ranking, g_k denotes the practical LARK score \hat{g}_k , and q_k denotes its training weight. The indices in the ranking panel are re-numbered after sorting.

Existing trajectory selection methods largely rely on heuristic criteria. Some methods use external verifiers or LLM-as-a-judge scores to assess reasoning quality [Zheng et al., 2023, Yang et al., 2025], while GRAPE, Local Naturalness, and RSR score candidates using the student model itself [Zhang et al., 2025a, Just et al., 2025, Yang et al., 2026]. Although these methods are useful, they do not explicitly measure whether a trajectory is *learnable* by the student. This gap motivates the central question:

Can we design a principled trajectory selection criterion that ensures distilled reasoning trajectories are learnable by the student model?

We answer this question by proposing **LARK**—**L**earnability-grounded **A**nchor-time **R**anking—a learnability-grounded method for reasoning trajectory selection, as illustrated in Figure 1. LARK identifies the subset of trajectories from which the student model can learn most efficiently. At its core, LARK introduces a principled selection criterion that characterizes trajectory learnability from an optimization perspective, while preserving generalization through χ^2 -regularization. Our contributions are as follows:

- We formulate reasoning trajectory selection as a learnability-grounded policy optimization problem. We introduce the anchor-time learnability rate ρ , which characterizes the decay rate of the post-training loss and thereby turns learnability into a principled optimization objective.
- To estimate the learnability rate ρ efficiently while preventing the selector from hacking the learnability criterion, we use a first-order Taylor expansion around the unselected data distribution and derive a χ^2 -regularized policy optimization problem. Theoretically, we show that this policy optimization implicitly increases data learnability and can be solved in closed form under fixed-budget trajectory selection.
- Empirically, we show that LARK outperforms existing baselines across multiple base models and tasks. Diagnostic analyses further support our theoretical claims and validate the learnability-grounded perspective for trajectory selection.

Notation. Vectors are denoted by lowercase boldface letters, e.g., \mathbf{x} . For a sequential response, $\mathbf{y}_{<t}$ denotes the sequence of tokens preceding the t -th token. We denote by $[n]$ the set $\{1, \dots, n\}$. For two positive sequences $\{a_n\}_{n \geq 1}$ and $\{b_n\}_{n \geq 1}$, we write $a_n = o(b_n)$ if $a_n/b_n \rightarrow 0$ as $n \rightarrow \infty$. We denote the K -dimensional simplex by Δ^K , and $\|\cdot\|$ denotes the Euclidean norm throughout the paper. For two distributions p and q , the χ^2 divergence is defined as $\chi^2(q \| p) = \int_x (q(x) - p(x))^2 / p(x) dx$, with the integral replaced by a summation in the discrete case.

2 Related Work

Reasoning distillation and data selection. Reasoning distillation transfers chain-of-thought traces from stronger teacher models to smaller student models [Hsieh et al., 2023, Yuan et al., 2023]. Recent

work has shown that a small but carefully chosen set of reasoning examples can rival much larger training sets [Yu et al., 2023, Ye et al., 2025, Muennighoff et al., 2025]. This has motivated a growing body of work on data-selection methods that filter examples by diversity, difficulty, uncertainty, or learning impact [Zhang et al., 2025b, Liu et al., 2024, Li et al., 2025].

Most of these methods operate at the question or example level. In contrast, we study a finer-grained problem that arises in reasoning distillation. For a given question, multiple candidate reasoning trajectories may be available. These trajectories can all lead to correct answers while providing substantially different training signals to the student. LARK therefore asks which trajectory, among candidates for the same question, is most learnable for the current student model.

Trajectory selection and optimization-grounded weighting. Existing trajectory-selection methods typically score candidates by either external quality signals or student-side fit. External methods rely on correctness checks, verifiers, or LLM-as-a-judge evaluation to estimate the quality of a reasoning trajectory [Cobbe et al., 2021]. Student-side methods instead use the student model’s own behavior, such as likelihood (GRAPE [Zhang et al., 2025a]), local-context likelihood (Local Naturalness [Just et al., 2025]), or rank-surprisal alignment (RSR [Yang et al., 2026]), to identify trajectories that appear better aligned with the student.

LARK differs from both families by deriving its selection criterion from a local learnability objective. Specifically, it asks whether a trajectory yields a favorable *optimization signal* for the current student. This perspective connects our work to gradient-based data selection rooted in the Polyak–Łojasiewicz framework [Łojasiewicz, 1963, Karimi et al., 2016, Xia et al., 2024], though unlike those methods we avoid per-trajectory backward passes by using a forward-pass proxy. For multi-trajectory selection, we adopt a χ^2 -regularized weighting that is related in spirit to regularized alignment and offline optimization [Rafailov et al., 2023, Huang et al., 2024, Xie et al., 2022], yielding a closed-form, budgeted rule.

3 Preliminaries

3.1 Supervised Fine-Tuning for Reasoning Distillation

We consider the supervised fine-tuning (SFT) of the student model. Let \mathbf{x} be the question and $\mathbf{y}_k = (y_1^k, \dots, y_{|a_k|}^k)^\top$ denote the k -th trajectory from the teacher with length $|a_k|$. The SFT loss is defined by

$$\ell(\boldsymbol{\theta}, \mathbf{y}_k) = \frac{1}{|a_k|} \sum_{t=1}^{|a_k|} -\log \pi_{\boldsymbol{\theta}}(y_t \mid \mathbf{x}, \mathbf{y}_{<t}),$$

where $\pi_{\boldsymbol{\theta}}$ denotes the student language model with parameter $\boldsymbol{\theta}$. Over a set of response candidates $\{\mathbf{y}_k\}_{k=1}^K$, we consider the finite-sum loss over a weight $\mathbf{q} = (q_1, \dots, q_K)^\top$ written by

$$\mathcal{L}(\boldsymbol{\theta}, \mathbf{q}) = \sum_{k=1}^K q_k \cdot \ell(\boldsymbol{\theta}, \mathbf{y}_k), \quad \text{where } \sum_{k=1}^K q_k = 1, q_k \geq 0, \forall k \in [K], \quad (1)$$

where \mathbf{q} encodes which trajectories should be emphasized during the SFT. For instance, when $q_k = \frac{1}{K}$ for all $k \in [K]$, Eq. (1) reduces to the standard SFT loss over K trajectories. When B trajectories are selected for training, it is equivalent to finding a weight vector \mathbf{q} on the simplex Δ^K with the number of non-zero elements exactly equal to B .

3.2 Gradient Flow Loss Decay Identity

We characterize the learnability from the lens of optimization theory, in which Polyak–Łojasiewicz (PL) condition of over-parameterized optimization [Bassily et al., 2018, Liu et al., 2022, Chatterjee, 2022] centers on the ratio of the squared gradient norm to the loss. We write this ratio as

$$\rho(\boldsymbol{\theta}; \mathbf{q}) \triangleq \|\nabla_{\boldsymbol{\theta}} \mathcal{L}(\boldsymbol{\theta}; \mathbf{q})\|^2 / \mathcal{L}(\boldsymbol{\theta}; \mathbf{q}), \quad (2)$$

which we refer to as the *loss decay rate function*. $\rho(\boldsymbol{\theta}, \mathbf{q})$ characterizes the landscape of the optimization process. For instance, when $\rho(\boldsymbol{\theta}, \mathbf{q}) \geq \mu$, Eq. (2) implies $\|\nabla_{\boldsymbol{\theta}} \mathcal{L}\|^2 \geq \mu \mathcal{L}$, which is commonly used in the analysis of over-parameterized optimization [Liu et al., 2022] (where optimal loss $\mathcal{L}^* = 0$).

Decay rate of gradient flow. Let $T > 0$ denote the total fine-tuning time. For a fixed weight vector \mathbf{q} , the *gradient flow* $\phi_{\mathbf{q}} : [0, T] \rightarrow \mathbb{R}^{|\boldsymbol{\theta}|}$ describes the evolution of the parameters when the student is

fine-tuned on the weighted objective $\mathcal{L}(\cdot; \mathbf{q})$, defined as the solution to the ODE

$$\dot{\phi}_{\mathbf{q}}(s) = -\nabla_{\theta} \mathcal{L}(\phi_{\mathbf{q}}(s); \mathbf{q}), \quad \phi_{\mathbf{q}}(0) = \theta_{\text{ref}}, \quad s \in [0, T].$$

Here $\phi_{\mathbf{q}}(0) = \theta_{\text{ref}}$ is the starting point of fine-tuning, $\phi_{\mathbf{q}}(T)$ is the parameter at time T , and s is the continuous gradient-flow time variable. By the chain rule and Eq.(2), we have

$$\frac{d}{ds} \mathcal{L}(\phi_{\mathbf{q}}(s); \mathbf{q}) = -\|\nabla_{\theta} \mathcal{L}(\phi_{\mathbf{q}}(s); \mathbf{q})\|^2 = -\rho(\theta, \mathbf{q}) \mathcal{L}(\theta, \mathbf{q}), \quad \phi_{\mathbf{q}}(0) = \theta_{\text{ref}}.$$

Solving this ordinary differential equation yields

$$\mathcal{L}(\phi_{\mathbf{q}}(T); \mathbf{q}) = \mathcal{L}(\theta_{\text{ref}}; \mathbf{q}) \cdot \exp\left(-\int_0^T \rho(\phi_{\mathbf{q}}(s); \mathbf{q}) ds\right), \quad (3)$$

which implies the integral $\int_0^T \rho(\phi_{\mathbf{q}}(s); \mathbf{q}) ds$ plays an important role in controlling the loss decay.

4 Proposed Method

In this section, we present the methodology of LARK. Specifically, §4.1 establishes that the time-integrated learnability objective in Eq. (3) can be controlled by the anchor-time learnability rate $\rho(\cdot)$ evaluated at the initial student model. §4.2 then approximately optimizes $\rho(\theta_{\text{ref}}; \mathbf{q})$ through local linearization around the uniform prior, develops a forward-pass proxy \hat{g}_k that estimates the local gradient of ρ without backward propagation, and bounds the residual errors by a χ^2 -regularization term to preserve generalization and prevent reward hacking of the learnability criterion. §4.3 combines these pieces into a closed-form, budget-parameterized selection rule with no hyperparameter to tune.

4.1 Estimating the Learnability Objective with Anchor-Relative Condition

As shown in Eq. (3), selecting trajectories that are *learnable* by the student model can be formulated as optimizing the time-integrated learnability objective $\max_{\mathbf{q} \in \Delta^K} \int_0^T \rho(\phi_{\mathbf{q}}(s); \mathbf{q}) ds$, which favors trajectory distributions under which the post-training loss decays rapidly during SFT. However, directly optimizing this objective is infeasible, since it requires tracking the factor ρ along the entire SFT optimization trajectory. To address this challenge, we introduce the following structural condition, which allows the learnability objective to be approximated from a fixed anchor model.

Condition 1. *We say the model satisfies the anchor-relative condition if there exists an absolute constant $\kappa > 0$ such that, for every $\mathbf{q} \in \Delta^K$ and every $s \in [0, T]$, $\rho(\phi_{\mathbf{q}}(s); \mathbf{q}) \geq \kappa \rho(\theta_{\text{ref}}; \mathbf{q})$.*

Under Condition 1, the learnability rate evaluated at the initial student parameters θ_{ref} provides a tractable proxy for the full time-integrated objective. This anchor-relative condition is consistent with the lazy fine-tuning behavior often observed in over-parameterized LLMs during SFT. In this regime, the model parameters remain close to the initialization θ_{ref} , and consequently the learnability rate ρ remains close to its anchor-time value $\rho(\theta_{\text{ref}}; \mathbf{q})$. We provide a theoretical justification of this condition under the neural tangent kernel regime [NTK; Jacot et al., 2018] in Appendix A.2, together with empirical validation in Appendix A.3.

The following proposition then follows naturally; we defer its proof to Appendix A.1.

Proposition 1. *Under Condition 1, for every $\mathbf{q} \in \Delta^K$, the post-training loss of the student model satisfies $\mathcal{L}(\phi_{\mathbf{q}}(T); \mathbf{q}) \leq \mathcal{L}(\theta_{\text{ref}}; \mathbf{q}) \cdot \exp(-\kappa T \cdot \rho(\theta_{\text{ref}}; \mathbf{q}))$.*

Proposition 1 shows that, under the anchor-relative condition, the decay of the SFT loss can be controlled by the learnability rate evaluated at the anchor model θ_{ref} . Therefore, instead of directly optimizing the intractable trajectory-wide objective $\int_0^T \rho(\phi_{\mathbf{q}}(s); \mathbf{q}) ds$, we can optimize the anchor-time surrogate $\max_{\mathbf{q} \in \Delta^K} \rho(\theta_{\text{ref}}; \mathbf{q})$ to encourage faster loss decay for the student model.

4.2 Approximately Optimizing Learnability $\rho(\theta_{\text{ref}}; \mathbf{q})$ through Local Linearization

In practice, directly optimizing $\rho(\theta_{\text{ref}}; \mathbf{q})$ is problematic. As shown in Appendix B.1, this objective induces a quasi-convex maximization problem over the simplex Δ^K , whose optimum is attained at a vertex of the simplex. Consequently, exact maximization would lead to a degenerate solution that places all probability mass on a single trajectory, thereby “hacking” the learnability criterion instead of producing a useful training distribution.

This observation motivates treating the learnability criterion ρ as a *local* indicator around the uniform distribution $\mathbf{p} = (\frac{1}{K}, \dots, \frac{1}{K}) \in \mathbb{R}^K$ which corresponds to standard SFT without trajectory selection. Rather than globally maximizing $\rho(\boldsymbol{\theta}_{\text{ref}}; \mathbf{q})$, we restrict attention to distributions \mathbf{q} in a neighborhood of \mathbf{p} and locally linearize the objective around \mathbf{p} . The first-order Taylor expansion gives

$$\begin{aligned} \rho(\boldsymbol{\theta}_{\text{ref}}; \mathbf{q}) - \rho(\boldsymbol{\theta}_{\text{ref}}; \mathbf{p}) &= \langle \nabla_{\mathbf{q}} \rho(\boldsymbol{\theta}_{\text{ref}}; \mathbf{q}), \mathbf{q} - \mathbf{p} \rangle + o(\|\mathbf{q} - \mathbf{p}\|_2) \\ &= \sum_{k=1}^K \underbrace{\frac{\partial}{\partial q_k} \rho(\boldsymbol{\theta}_{\text{ref}}; \mathbf{q}) \Big|_{\mathbf{q}=\mathbf{p}}}_{g_k^*} \cdot (q_k - p_k) + \underbrace{o(\|\mathbf{q} - \mathbf{p}\|_2)}_{R_2(\mathbf{p}, \mathbf{q})}. \end{aligned} \quad (4)$$

Two steps remain for optimizing Eq. (4). First, we need to estimate the first-order derivative g_k^* in a computationally efficient manner. Second, we need to bound the residual $R_2(\mathbf{p}, \mathbf{q})$ carefully.

4.2.1 Estimating gradient g_k^*

According to the definition of ρ , $g_k^* = \frac{\partial}{\partial q_k} \rho(\boldsymbol{\theta}_{\text{ref}}; \mathbf{q}) = \frac{\partial}{\partial q_k} \frac{\|\sum_i q_i \mathbf{g}_i\|^2}{\sum_i q_i \ell_i}$, where $\mathbf{g}_i = \nabla_{\boldsymbol{\theta}} \ell_i$ and $\ell_i = \ell(\boldsymbol{\theta}, \mathbf{y}_i)$. With detailed derivations deferred to Appendix B.3, we can write

$$g_k^* = \frac{2\mathbf{g}_k^\top \sum_i q_i \mathbf{g}_i}{\sum_i q_i \ell_i} - \frac{\|\sum_i q_i \mathbf{g}_i\|^2}{\sum_j q_j \ell_k} \cdot \frac{\ell_k}{\sum_i q_i \ell_i} \Big|_{\mathbf{q}=\mathbf{p}} = \frac{2\mathbf{g}_k^\top \sum_i \mathbf{g}_i}{\sum_i \ell_i} - \frac{\|\sum_i \mathbf{g}_i\|^2}{\sum_i \ell_i} \cdot \frac{\ell_k}{\sum_i \ell_i}, \quad (5)$$

where the second equality follows from $q_k = p_k = \frac{1}{K}$. Based on Eq. (5), we make two observations. First, in many practical overparameterized networks, the per-trajectory gradients \mathbf{g}_k are nearly orthogonal in high-dimensional parameter space, i.e., $\mathbf{g}_k^\top \mathbf{g}_j \approx \delta_{jk} \|\mathbf{g}_k\|^2$. Second, for the single-trajectory ρ -factor defined in Eq. (2), denoted by $\rho_k^* = \|\mathbf{g}_k\|^2 / \ell_k$, the gradient norm can be written as $\|\mathbf{g}_k\|^2 = \rho_k^* \ell_k$. Plugging these observations into Eq. (5), g_k^* can be approximated by

$$g_k^* \approx \frac{2\|\mathbf{g}_k\|^2}{\sum_i \ell_i} - \frac{\sum_j \|\mathbf{g}_j\|^2}{\sum_i \ell_i} \cdot \frac{\ell_k}{\sum_i \ell_i} = \frac{\ell_k}{\sum_i \ell_i} \left(2\rho_k^* - \frac{\sum_i \rho_i^* \ell_i}{\sum_i \ell_i} \right). \quad (6)$$

In practice, calculating ρ_k^* requires backward propagation to compute $\|\mathbf{g}_k\|^2$, which is computationally expensive at selection time. Fortunately, we can avoid this gradient computation by leveraging the softmax structure of the last layer in next-token prediction, as stated in the following lemma:

Lemma 1 (Forward-pass ρ_k^* estimation, informal). *For any $k \in [K]$, let $\boldsymbol{\pi}_t^k \in \Delta^{|\mathcal{V}|}$ be the probability vector produced by the student model for the t -th token, conditioned on the question \mathbf{x} and the previous response tokens $\mathbf{y}_{<t}^k$, and let $\boldsymbol{\delta}(y_t^k) \in \Delta^{|\mathcal{V}|}$ be the one-hot vector corresponding to the ground-truth token from the teacher model. Let $\hat{\rho}_k \triangleq \frac{\sum_t \|\boldsymbol{\pi}_t^k - \boldsymbol{\delta}(y_t^k)\|^2}{\ell_k}$, then under standard structural conditions, there exist absolute positive constants C_1, C_2 where $\hat{\rho}_k \in [C_1 \rho_k^*, C_2 \rho_k^*]$.*

Lemma 1 suggests that ρ_k^* can be estimated in a well-controlled manner by the forward-pass quantity $\hat{\rho}_k$, without explicitly computing gradients. We defer the detailed proof to Appendix B.4. Substituting $\hat{\rho}_k$ into Eq. (5) yields our practical estimator of the local gradient:

$$\hat{g}_k = \frac{\ell_k}{\sum_i \ell_i} \left(2\hat{\rho}_k - \frac{\sum_i \hat{\rho}_i \ell_i}{\sum_i \ell_i} \right), \text{ where } \hat{\rho}_k \triangleq \frac{\sum_t \|\boldsymbol{\pi}_t^k - \boldsymbol{\delta}(y_t^k)\|^2}{\ell_k}. \quad (7)$$

4.2.2 Bounding residuals $R(\mathbf{p}, \mathbf{q})$

We next control the residual errors introduced by the local linearization and the gradient estimation. More precisely, substituting g_k^* with \hat{g}_k in Eq. (4) yields

$$\rho(\boldsymbol{\theta}_{\text{ref}}; \mathbf{q}) - \rho(\boldsymbol{\theta}_{\text{ref}}; \mathbf{p}) = \sum_{k=1}^K \hat{g}_k \cdot (q_k - p_k) + \underbrace{\sum_{k=1}^K (g_k^* - \hat{g}_k) \cdot (q_k - p_k)}_{R_1(\mathbf{p}, \mathbf{q})} + \underbrace{o(\|\mathbf{q} - \mathbf{p}\|_2)}_{R_2(\mathbf{p}, \mathbf{q})},$$

where R_1 captures the error from estimating the true local gradient g_k^* by \hat{g}_k , and R_2 captures the higher-order error from the Taylor expansion. The following lemma shows that both terms can be controlled by the χ^2 distance from the uniform distribution.

Lemma 2 (χ^2 controls both error terms, informal). *Under standard structural conditions, there exist constants $\alpha_1, \alpha_2 > 0$ such that for all $\mathbf{q} \in \Delta^K$,*

$$|R_1(\mathbf{p}, \mathbf{q})| \leq \alpha_1 \chi^2(\mathbf{q} \parallel \mathbf{p}) + 1, \quad |R_2(\mathbf{p}, \mathbf{q})| \leq \alpha_2 \chi^2(\mathbf{q} \parallel \mathbf{p}). \quad (8)$$

Lemma 2 shows that the residual errors are controlled by the χ^2 distance between the selected distribution \mathbf{q} and the uniform distribution \mathbf{p} , with explicit forward-computable constants α_1, α_2 given in Appendix B.5. This further supports our intuition that optimization should be performed in a local neighborhood around the original, non-selected data distribution \mathbf{p} , to preserve generalization and prevent the selector from drifting toward degenerate solutions. Combining the linearized objective with the residual bounds gives the following lower bound on the original learnability improvement; we defer its proof to Appendix B.6.

Theorem 1 (LARK objective, informal). *There exist absolute constants $\alpha > 0$ and $C \in \mathbb{R}$ such that*

$$\rho(\boldsymbol{\theta}_{\text{ref}}; \mathbf{q}) - \rho(\boldsymbol{\theta}_{\text{ref}}; \mathbf{p}) \geq \sum_{k=1}^K \hat{g}_k \cdot (q_k - p_k) - \alpha \chi^2(\mathbf{q} \parallel \mathbf{p}) + C. \quad (9)$$

Theorem 1 reduces the intractable learnability improvement to a tractable surrogate that depends on \mathbf{q} only through (i) the inner product $\langle \mathbf{q} - \mathbf{p}, \hat{\mathbf{g}} \rangle$ between the trajectory deviation and the forward-pass score vector, and (ii) the χ^2 distance to the uniform prior. The constant C is independent of \mathbf{q} and therefore does not affect the maximizer over Δ^K . This reduction sets the stage for the closed-form selection rule developed in §4.3.

4.3 LARK: Closed-form Solution for Fixed-Budget Trajectory Selection

Theorem 1 reduces the intractable learnability improvement to a tractable χ^2 -regularized optimization based on $\{\hat{g}_k\}$. In practice, many data selection algorithms operate in the fixed-budget setting, where the agent needs to select $B \leq K$ trajectories per question, meaning that the support size of \mathbf{q} is B . This fixed-budget optimization admits a closed-form solution, as stated in the following lemma.

Lemma 3 (B -parameterized closed form). *Sort $\hat{g}_1 \geq \dots \geq \hat{g}_K$ and assume $1 \leq B < K$ with $\hat{g}_B > \hat{g}_{B+1}$. Under the uniform prior $p_k = 1/K$, the maximizer of optimization objective*

$$\hat{\mathbf{q}} = \arg \max_{\mathbf{q} \in \Delta^K, \text{supp}(\mathbf{q})=B} \left\{ \sum_{k=1}^K \hat{g}_k (q_k - p_k) - \frac{\tau(B)}{2} \chi^2(\mathbf{q} \parallel \mathbf{p}) \right\}, \quad (10)$$

with regularizer $\tau(B) = \frac{1}{K} \sum_{j=1}^B (\hat{g}_j - \hat{g}_{B+1})$ takes the closed form $\hat{q}_i = (\hat{g}_i - \hat{g}_{B+1}) / \sum_{j=1}^B (\hat{g}_j - \hat{g}_{B+1})$ for $i \leq B$, and $\hat{q}_i = 0$ otherwise.

Lemma 3 gives a closed-form top- B rule: each selected trajectory is weighted by its score margin above \hat{g}_{B+1} , and $\tau^*(B)$ is fully determined by B with no hyperparameter to tune. Algorithm 1 summarizes the full procedure.

Remark 1 (Soft vs. hard top- B). LARK is a soft top- B rule: weights are proportional to score margins above the threshold, rather than uniform $1/B$ as in hard top- B truncation. This hedges against ranking noise near the boundary; the ablation in §5.3 (Figure 2b) shows it outperforms uniform, proportional, and softmax weighting.

Remark 2 (Heuristic reading of \hat{g}_k). \hat{g}_k favors trajectories on which the student is *confidently wrong in a structured way*: ℓ_k is not small, indicating that the student does not yet predict it well, yet the residual mass $\|\boldsymbol{\pi}_t^k - \boldsymbol{\delta}(y_t^k)\|^2$ concentrates on a few near-miss tokens, providing a clear local correction signal. Although \hat{g}_k is a forward-pass surrogate for the exact directional derivative g_k^* , the two remain tightly aligned: Appendix B.8 gives an explicit error bound on $\|\hat{\mathbf{g}} - \mathbf{g}^*\|_{\mathbf{p}}$ and verifies it on real student models, while the token-level signature is verified in §5.4 (Figure 4).

Algorithm 1: LARK: Learnability-grounded Anchor-time Ranking

Input: Candidates $\{\mathbf{y}_k\}_{k=1}^K$; reference π_{ref} with $\boldsymbol{\theta}_{\text{ref}}$; budget B .

Output: $\mathcal{L}(\boldsymbol{\theta}; \hat{\mathbf{q}}) = \sum_{k=1}^K \hat{q}_k \ell(\boldsymbol{\theta}; \mathbf{y}_k)$.

```

1 for  $k = 1, \dots, K$  do
2   Forward pass of  $\pi_{\text{ref}}$  on  $\mathbf{y}_k$ ; record  $\boldsymbol{\pi}_t^k, p_t$ 
   for  $t \in \{1, \dots, |a_k|\}$ 
3    $\ell_k \leftarrow \frac{1}{|a_k|} \sum_t -\log p_t$ 
4    $\hat{\rho}_k \leftarrow \frac{\sum_t \|\boldsymbol{\pi}_t^k - \boldsymbol{\delta}(y_t^k)\|^2}{\sum_t -\log p_t}$ 
5 for  $k = 1, \dots, K$  do
6    $\hat{g}_k \leftarrow \frac{\ell_k}{\sum_i \ell_i} \left( 2\hat{\rho}_k - \frac{\sum_i \hat{\rho}_i \ell_i}{\sum_i \ell_i} \right)$ 
7 Sort and relabel:  $\hat{g}_1 \geq \dots \geq \hat{g}_K$ 
8 for  $i = 1, \dots, K$  do
9   if  $i \leq B$  then
10     $\hat{q}_i \leftarrow \frac{\hat{g}_i - \hat{g}_{B+1}}{\sum_{j=1}^B (\hat{g}_j - \hat{g}_{B+1})}$ 
11   else
12     $\hat{q}_i \leftarrow 0$ 
13 return  $\mathcal{L}(\boldsymbol{\theta}; \hat{\mathbf{q}}) = \sum_{k=1}^K \hat{q}_k \ell(\boldsymbol{\theta}; \mathbf{y}_k)$ 

```

Table 1: Performance comparison under single-trajectory and multi-trajectory selection. Values are Acc@5 percentages, with mean±std taken across three independent decoding seeds at inference time.

Model	Method	Budget $B = 1$					Budget $B = 3$				
		AIME	AMC	GPQA	MATH-500	Avg	AIME	AMC	GPQA	MATH-500	Avg
Qwen-2.5-7B	BaseModel	18.89±1.92	47.79±4.23	39.56±3.29	56.47±4.80	40.68±3.51	18.89±1.92	47.79±4.23	39.56±3.29	56.47±4.80	40.68±3.51
	Random	21.11±3.85	51.00±3.03	56.90±3.55	64.67±4.41	48.42±3.58	24.44±3.85	61.45±3.61	59.76±3.29	69.67±4.20	53.83±3.64
	Token Length _{max}	13.33±3.33	50.60±3.61	41.08±3.04	60.93±4.10	41.49±3.52	20.00±3.33	57.03±4.23	43.77±3.29	65.73±4.40	46.63±3.81
	Rule-based Quality _{max}	21.11±1.92	56.63±3.61	48.15±3.04	65.27±3.70	47.79±3.01	28.89±1.92	67.07±3.03	53.54±3.54	70.73±4.10	55.06±3.10
	LLM-judged Quality _{max}	22.22±1.92	56.22±4.23	50.34±3.29	65.80±3.90	48.65±3.29	26.67±3.33	62.25±3.03	53.03±3.54	69.60±3.70	52.89±3.40
	GRAPE _{max}	16.67±3.33	55.02±3.03	49.33±3.79	64.67±3.90	46.42±3.51	25.56±1.92	63.05±3.03	55.05±3.54	71.00±4.20	53.66±3.11
	Local Naturalness _{max}	23.33±3.33	57.83±3.61	51.18±3.55	65.80±3.80	49.54±3.57	27.78±1.92	64.26±3.03	56.23±3.29	70.87±3.81	54.78±2.97
	RSR _{min}	24.44±3.85	59.44±3.03	52.19±3.04	67.33±3.90	50.85±3.35	32.22±3.85	66.27±3.61	56.73±3.29	71.47±3.90	56.67±3.57
	LARK (Ours)	30.00±3.33	65.86±3.03	65.99±3.55	70.20±3.82	58.01±3.42	36.67±3.33	76.31±3.03	67.34±3.29	74.67±3.45	63.74±3.27
Llama-3.2-3B	BaseModel	2.22±1.92	11.24±4.23	11.45±2.04	18.13±3.21	10.76±2.78	2.22±1.92	11.24±4.23	11.45±2.04	18.13±3.21	10.76±2.78
	Random	4.44±3.85	14.86±3.68	40.40±2.81	24.13±3.45	20.96±3.35	3.33±3.33	17.67±3.03	44.61±3.29	27.07±3.80	23.17±3.36
	Token Length _{max}	3.33±3.33	16.47±2.51	38.22±3.55	24.53±4.03	20.64±3.34	2.22±1.92	16.06±3.03	38.72±3.55	25.07±3.84	20.52±3.00
	Rule-based Quality _{max}	2.22±3.85	10.44±3.03	14.48±2.87	19.60±3.93	11.69±3.29	5.56±3.85	15.66±3.61	23.57±2.78	25.73±3.23	17.63±3.28
	LLM-judged Quality _{max}	4.44±1.92	18.88±3.68	41.58±3.04	25.93±3.51	22.71±2.98	3.33±3.33	18.47±3.03	43.43±3.03	27.00±3.50	23.06±3.22
	GRAPE _{max}	2.22±1.92	14.46±3.19	14.31±2.78	21.80±3.90	13.20±2.84	6.67±3.33	20.48±3.19	21.55±2.28	24.87±3.80	18.39±3.11
	Local Naturalness _{max}	6.67±3.33	17.67±4.23	41.08±2.28	25.60±3.22	22.75±3.26	6.67±3.33	20.08±3.03	42.76±3.04	26.60±3.34	24.03±3.17
	RSR _{min}	6.67±3.33	15.66±2.41	42.09±2.54	25.73±3.81	22.54±3.02	5.56±1.92	17.27±3.03	43.77±3.04	27.87±3.92	23.62±2.90
	LARK (Ours)	8.89±1.92	19.28±2.41	48.32±3.04	28.67±3.50	26.29±2.66	8.89±1.92	22.09±2.51	54.55±3.54	31.00±3.22	29.13±2.72
Qwen-2.5-1.5B	BaseModel	0.00±0.00	24.50±4.23	30.64±2.04	38.53±3.21	23.42±2.36	0.00±0.00	24.50±4.23	30.64±2.04	38.53±3.21	23.42±2.36
	Random	1.11±1.92	33.33±2.51	54.38±3.55	42.33±4.03	32.79±2.96	2.22±1.92	32.93±4.23	55.89±3.04	48.53±4.20	34.89±3.28
	Token Length _{max}	0.00±0.00	25.30±3.19	34.51±2.78	42.40±3.90	25.55±2.45	2.22±1.92	25.70±3.68	42.09±2.59	44.20±4.01	28.55±2.96
	Rule-based Quality _{max}	5.56±1.92	29.72±3.03	41.25±2.87	43.40±3.93	29.98±2.85	6.67±3.33	38.55±3.19	46.30±2.28	46.87±3.80	34.60±3.11
	LLM-judged Quality _{max}	3.33±3.33	29.32±2.51	42.93±3.31	44.80±3.82	30.09±3.21	3.33±3.33	35.34±3.03	46.30±3.04	47.47±3.45	33.11±3.21
	GRAPE _{max}	2.22±1.92	35.34±3.68	42.93±2.81	45.73±3.45	31.56±2.90	5.56±1.92	38.15±1.84	46.63±3.09	48.80±3.74	34.79±2.57
	Local Naturalness _{max}	6.67±3.33	36.14±2.41	45.62±2.54	45.73±3.81	33.54±3.02	6.67±3.33	38.96±4.23	46.80±2.54	48.93±3.61	35.34±3.42
	RSR _{min}	4.44±1.92	32.13±3.68	47.14±3.04	45.93±3.51	32.41±2.98	8.89±3.85	36.14±3.61	46.30±2.78	47.73±3.23	34.77±3.28
	LARK (Ours)	7.78±1.92	40.56±4.23	63.13±2.53	49.33±3.50	41.09±2.98	10.00±3.33	42.57±3.03	66.67±3.03	53.33±3.40	43.14±3.20

5 Experiment

We evaluate LARK on reasoning distillation through three research questions. **RQ1** asks whether LARK outperforms heuristic, quality-based, and student-side baselines under single-trajectory ($B=1$) and multi-trajectory ($B=3$) supervision. **RQ2** isolates the contribution of the trajectory score \hat{g}_k and the χ^2 - B weighting rule by holding one fixed and varying the other. **RQ3** asks *why* LARK works, by linking \hat{g}_k to the anchor-time learnability rate ρ , to the SFT loss trajectory, and to downstream training utility, and by analyzing the token-level structure of the trajectories LARK selects. Section 5.1 describes the shared experimental setup, and Sections 5.2–5.4 answer each question in turn.

5.1 Experimental Setup

Candidate pool. We use a fixed set of 5,000 math problems from NuminaMath [Li et al., 2024], each paired with 33 trajectories from 11 teacher models (3 rollouts each); see Appendix C.1. All methods share this pool, so any performance difference reflects the selection rule alone.

Selection budgets. We evaluate each method at $B=1$ (single trajectory per problem) and $B=3$ (three trajectories). Baselines take the top- B under their score with uniform weights $1/B$; LARK applies the χ^2 - B rule of Lemma 3 to obtain weighted \hat{q} from \hat{g}_k computed at the reference student θ_{ref} .

Baselines. We compare LARK against seven methods (Appendix C.2) spanning heuristics, quality-based selection, LLM-based evaluation, and student-side forward-pass scoring: Random, Token Length_{max}, Rule-based Quality_{max}, LLM-judged Quality_{max}, GRAPE_{max} [Zhang et al., 2025a], Local Naturalness_{max} [Just et al., 2025], and RSR_{min} [Yang et al., 2026].

Students, training, evaluation. We fine-tune Qwen-2.5-7B, Qwen-2.5-1.5B [Yang et al., 2024], and Llama-3.2-3B [Grattafiori et al., 2024] via SFT, and evaluate on AIME-2024 [aop, 2024], AMC [Mathematical Association of America, 2025], GPQA-Diamond [Rein et al., 2024], and MATH-500 [Hendrycks et al., 2021] using Acc@5 (5 samples per problem, marked correct if any contains the gold answer). For each method, we run inference under three independent decoding seeds using the corresponding trained checkpoint and evaluation protocol for that method; we report mean±std across these three decoding seeds, so the reported variability reflects inference-time sampling rather than training-seed noise. The Avg column in Table 1 is the unweighted mean across the four benchmarks; per-benchmark numbers are the primary basis of comparison. A train/eval contamination audit appears in Appendix C.5. Training and decoding details are in Appendices C.3–C.4.

5.2 RQ1: Does LARK Outperform Existing Trajectory Selection Methods?

Table 1 compares LARK with all baselines on three students. LARK achieves the best average Acc@5 in all six model-budget settings. On Qwen-2.5-7B, it improves over the strongest baseline RSR by 7.16 points at $B=1$ and 7.07 points at $B=3$, with large gains on AMC and GPQA. The consistent gains under both budgets suggest that LARK improves trajectory quality, not only supervision size. The same trend holds for smaller students: LARK reaches 41.09% / 43.14% on Qwen-2.5-1.5B and 26.29% / 29.13% on Llama-3.2-3B under $B=1$ / $B=3$, suggesting that the score is not tied to one student family or scale. Appendix D.2 provides a budget-scaling analysis for LARK across $B \in \{1, 3, 5, 10, 20\}$.

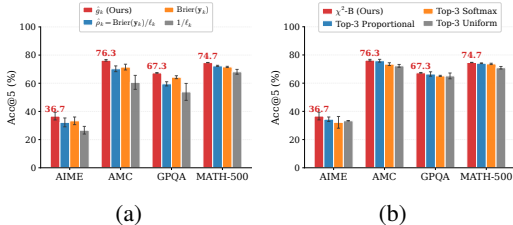


Figure 2: **Ablation of the two LARK components** on Qwen-2.5-7B ($B = 3$). Values are Acc@5 percentages. (a) Score ablation. (b) Weighting ablation.

5.3 RQ2: How Much Does Each Component Contribute?

We ablate the two design choices in LARK: the trajectory score and the weighting rule.

Trajectory score. Fixing the weighting to χ^2 - B , we compare four scores (Figure 2a): the inverse loss $1/\ell_k$, the Brier residual $\sum_t \|\pi_t^k - \delta(y_t^k)\|^2$, the proxy $\hat{\rho}_k$ of Lemma 1, and the induced score \hat{g}_k . The inverse loss is the weakest, confirming that likelihood alone does not characterize learnability; $\hat{\rho}_k$ already improves substantially by combining residual error with loss; and \hat{g}_k is the best across all four benchmarks, since it captures the marginal contribution of each trajectory around \mathbf{p} rather than scoring trajectories in isolation.

Weighting rule. Fixing the score to \hat{g}_k , we vary the weighting at $B=3$ (Figure 2b) over uniform, score-proportional, softmax, and χ^2 - B weights. The χ^2 - B rule consistently outperforms the alternatives, with the largest gains on AIME (where score noise matters most) and on MATH-500 (where the benefit accumulates over many problems). LARK’s improvement therefore comes not only from selecting high- \hat{g}_k trajectories but also from assigning robust weights within the selected support.

Efficiency. LARK is forward-pass only and therefore does not require the per-trajectory backward passes needed to compute the exact directional derivative g_k^* . Its scoring cost matches the lowest-cost student-side baselines, with full complexity analysis and wall-clock measurements reported in Appendix D.1.

5.4 RQ3: Why Does LARK Work?

We provide three pieces of evidence connecting \hat{g}_k to the quantities it is designed to control, then characterize what makes the trajectories LARK selects informative.

\hat{g}_k controls the anchor-time learnability rate. We first verify that maximizing \hat{g}_k actually raises $\rho(\theta_{\text{ref}}; \mathbf{q})$, the quantity LARK is designed to optimize (§4.1). For a representative problem we evaluate $\Delta\rho(\mathbf{q}) = \rho(\theta_{\text{ref}}; \mathbf{q}) - \rho(\theta_{\text{ref}}; \mathbf{p})$ densely over Δ^K and project onto two PCA components (Figure 3a). The LARK selections $\hat{\mathbf{q}}(B)$ for $B \in \{1, \dots, 32\}$ trace a path through the $\Delta\rho > 0$ region (green) and avoid the $\Delta\rho < 0$ region (red): every $\hat{\mathbf{q}}(B)$ satisfies $\rho(\theta_{\text{ref}}; \hat{\mathbf{q}}(B)) \geq \rho(\theta_{\text{ref}}; \mathbf{p})$. The forward-pass surrogate therefore acts as an effective control on the underlying anchor-time learnability rate on real student models.

High \hat{g}_k yields faster SFT loss decay. By Proposition 1, a higher ρ should translate into faster SFT loss decay. We verify this by tracking $\Delta\mathcal{L}_t \triangleq \mathcal{L}_t - \mathcal{L}_0$ on Qwen-2.5-7B at $B=3$. Figure 3b shows that LARK achieves the largest loss reduction throughout training, with the gap visible already in the early stage; heuristic and naturalness baselines reduce the loss more slowly and converge to a shallower plateau, even when starting from a lower initial loss.

\hat{g}_k predicts downstream training utility. We finally check that \hat{g}_k tracks downstream Acc@5 in practice. We group the 33 candidates by their teacher model (11 teachers), fine-tune Qwen-2.5-7B separately on each teacher’s trajectories, and evaluate on AMC. The per-teacher mean of \hat{g}_k is

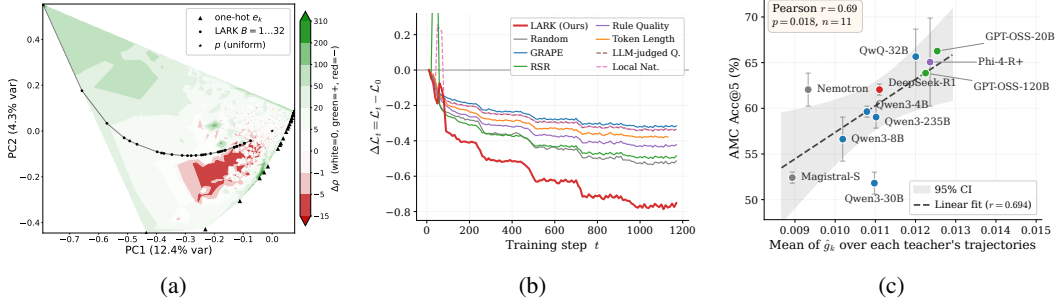


Figure 3: **Three pieces of evidence linking \hat{g}_k to learnability.** (a) $\Delta\rho(q)$ landscape on the simplex (PCA); black dots are $\hat{q}(B)$ for $B=1, \dots, 32$. LARK selections trace the $\Delta\rho \geq 0$ region (green) and avoid $\Delta\rho < 0$ (red). (b) SFT loss reduction $\Delta\mathcal{L}_t = \mathcal{L}_t - \mathcal{L}_0$ on Qwen-2.5-7B ($B=3$); LARK induces the largest SFT loss decay. (c) Per-teacher mean of \hat{g}_k vs. AMC Acc@5.

strongly correlated with downstream AMC accuracy (Figure 3c, Pearson $r = 0.69$, $p = 0.018$): high- \hat{g}_k teachers (GPT-OSS-20B/120B, Phi-4-R+, QwQ-32B) yield students above 65%, while low- \hat{g}_k teachers (Magistral-S, Nemotron) yield students below 55%. The score is predictively valid at the teacher level, capturing a student-side training signal that surface quality and likelihood do not.

Mechanism: confidently wrong, in a structured way.

The three results above establish that maximizing \hat{g}_k raises ρ , accelerates SFT loss decay, and predicts utility, but do not explain *why* the selected trajectories carry strong signal. We compute under θ_{ref} two token-level statistics for each candidate: the mean correct-token probability $\bar{p}(y_t)$, and the wrong-token concentration $\sum_{v \neq y_t} p(v)^2$, which is large when the residual mass falls on a few wrong tokens. Comparing all 33×500 candidates with the LARK-selected top-1 (Figure 4), the selected trajectories have substantially *lower* $\bar{p}(y_t)$ (0.282 vs. 0.449) and *higher* wrong-token concentration (0.107 vs. 0.085, a 26% increase). LARK therefore avoids trajectories the student already predicts confidently and routes supervision toward trajectories on which the student is wrong but in a *structured* way: residual mass concentrates on near-miss tokens close to the gold answer, providing a clear local correction signal. This signature echoes the rank-based view of RSR [Yang et al., 2026], which detects token positions where the gold answer is a near-miss, and clarifies why LARK and RSR end up close in Table 1 despite arising from distinct theoretical objectives. A single-problem walkthrough is given in Appendix D.3.

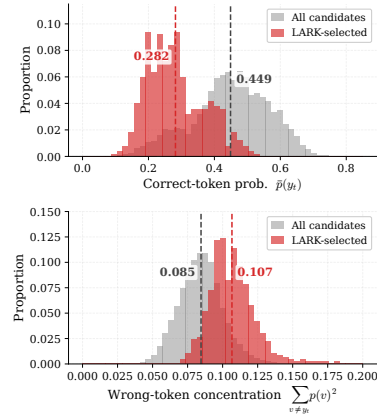


Figure 4: **Token-level behavior** on Qwen-2.5-7B. LARK-selected trajectories have lower correct-token probability $\bar{p}(y_t)$ (top) but higher wrong-token concentration $\sum_{v \neq y_t} p(v)^2$ (bottom).

6 Conclusion

We presented **LARK**, a learnability-grounded method for reasoning trajectory selection in distillation. LARK estimates trajectory learnability with a forward-pass surrogate \hat{g}_k and uses a closed-form χ^2 -regularized soft top- B rule to construct a weighted SFT objective, avoiding expensive per-trajectory backward passes while preserving distributional coverage. Across three student models and four reasoning benchmarks, LARK consistently outperforms strong trajectory selection baselines under both single-trajectory and multi-trajectory budgets. Ablation and diagnostic analyses show that both the learnability score and the weighting rule are important, and that LARK-selected trajectories accelerate SFT loss decay while providing structured local correction signals. Overall, our results support learnability as an effective principle for efficient reasoning distillation, with future extensions to noisier candidate pools and broader reasoning domains.

References

- Aime problems and solutions, 2024. Accessed: 2025-09-13.
- Raef Bassily, Mikhail Belkin, and Siyuan Ma. On exponential convergence of sgd in non-convex over-parametrized learning. *arXiv preprint arXiv:1811.02564*, 2018.
- Sourav Chatterjee. Convergence of gradient descent for deep neural networks. *arXiv preprint arXiv:2203.16462*, 2022.
- Lénaïc Chizat, Edouard Oyallon, and Francis Bach. On lazy training in differentiable programming. In *NeurIPS*, 2019.
- Karl Cobbe, Vineet Kosaraju, Mohammad Bavarian, Mark Chen, Heewoo Jun, Lukasz Kaiser, Matthias Plappert, Jerry Tworek, Jacob Hilton, Reiichiro Nakano, et al. Training verifiers to solve math word problems. *arXiv preprint arXiv:2110.14168*, 2021.
- Simon S Du, Xiyu Zhai, Barnabas Póczos, and Aarti Singh. Gradient descent provably optimizes over-parameterized neural networks. In *ICLR*, 2019.
- Aaron Grattafiori, Abhimanyu Dubey, Abhinav Jauhri, Abhinav Pandey, Abhishek Kadian, Ahmad Al-Dahle, Aiesha Letman, Akhil Mathur, Alan Schelten, Alex Vaughan, et al. The llama 3 herd of models. *arXiv preprint arXiv:2407.21783*, 2024.
- Dan Hendrycks, Collin Burns, Saurav Kadavath, Akul Arora, Steven Basart, Eric Tang, Dawn Song, and Jacob Steinhardt. Measuring mathematical problem solving with the math dataset. *arXiv preprint arXiv:2103.03874*, 2021.
- Cheng-Yu Hsieh, Chun-Liang Li, Chih-Kuan Yeh, Hootan Nakhost, Yasuhisa Fujii, Alex Ratner, Ranjay Krishna, Chen-Yu Lee, and Tomas Pfister. Distilling step-by-step! outperforming larger language models with less training data and smaller model sizes. In *Findings of the Association for Computational Linguistics: ACL 2023*, pages 8003–8017, 2023.
- Audrey Huang, Wenhao Zhan, Tengyang Xie, Jason D Lee, Wen Sun, Akshay Krishnamurthy, and Dylan J Foster. Correcting the myths of kl-regularization: Direct alignment without overoptimization via chi-squared preference optimization. *arXiv preprint arXiv:2407.13399*, 2024.
- Arthur Jacot, Franck Gabriel, and Clément Hongler. Neural tangent kernel: Convergence and generalization in neural networks. In *NeurIPS*, 2018.
- Hoang Anh Just, Myeongseob Ko, and Ruoxi Jia. Distilling reasoning into student llms: Local naturalness for selecting teacher data. *arXiv preprint arXiv:2510.03988*, 2025.
- Hamed Karimi, Julie Nutini, and Mark Schmidt. Linear convergence of gradient and proximal-gradient methods under the polyak-łojasiewicz condition. In *Joint European conference on machine learning and knowledge discovery in databases*, pages 795–811. Springer, 2016.
- Jaehoon Lee, Lechao Xiao, Samuel Schoenholz, Yasaman Bahri, Roman Novak, Jascha Sohl-Dickstein, and Jeffrey Pennington. Wide neural networks of any depth evolve as linear models under gradient descent. In *NeurIPS*, 2019.
- Jia Li, Edward Beeching, Lewis Tunstall, Ben Lipkin, Roman Soletskyi, Shengyi Huang, Kashif Rasul, Longhui Yu, Albert Q Jiang, Ziju Shen, et al. Numinamath: The largest public dataset in ai4maths with 860k pairs of competition math problems and solutions. *Hugging Face repository*, 13(9):9, 2024.
- Xuefeng Li, Haoyang Zou, and Pengfei Liu. Limr: Less is more for rl scaling. *arXiv preprint arXiv:2502.11886*, 2025.
- Chaoyue Liu, Libin Zhu, and Mikhail Belkin. Loss landscapes and optimization in over-parameterized non-linear systems and neural networks. *Applied and Computational Harmonic Analysis*, 59: 85–116, 2022.

- Liangxin Liu, Xuebo Liu, Derek F Wong, Dongfang Li, Ziyi Wang, Baotian Hu, and Min Zhang. Selectit: Selective instruction tuning for large language models via uncertainty-aware self-reflection. *arXiv preprint arXiv:2402.16705*, 2024.
- Stanislaw Lojasiewicz. A topological property of real analytic subsets. *Coll. du CNRS, Les équations aux dérivées partielles*, 117(87-89):2, 1963.
- Sadhika Malladi, Alexander Wettig, Dingli Yu, Danqi Chen, and Sanjeev Arora. A kernel-based view of language model fine-tuning. In *ICML*, 2023.
- Mathematical Association of America. American mathematics competitions, 2025. Accessed: 2025-09-13.
- Niklas Muennighoff, Zitong Yang, Weijia Shi, Xiang Lisa Li, Li Fei-Fei, Hannaneh Hajishirzi, Luke Zettlemoyer, Percy Liang, Emmanuel Candès, and Tatsunori B Hashimoto. s1: Simple test-time scaling. In *Proceedings of the 2025 Conference on Empirical Methods in Natural Language Processing*, pages 20286–20332, 2025.
- Rafael Rafailov, Archit Sharma, Eric Mitchell, Christopher D Manning, Stefano Ermon, and Chelsea Finn. Direct preference optimization: Your language model is secretly a reward model. *Advances in neural information processing systems*, 36:53728–53741, 2023.
- David Rein, Betty Li Hou, Asa Cooper Stickland, Jackson Petty, Richard Yuanzhe Pang, Julien Dirani, Julian Michael, and Samuel R Bowman. Gpqa: A graduate-level google-proof q&a benchmark. In *First conference on language modeling*, 2024.
- Mengzhou Xia, Sadhika Malladi, Suchin Gururangan, Sanjeev Arora, and Danqi Chen. Less: Selecting influential data for targeted instruction tuning. *arXiv preprint arXiv:2402.04333*, 2024.
- Quan Xiao and Tianyi Chen. A unified understanding of offline data selection and online self-refining generation for post-training llms. *arXiv preprint arXiv:2511.21056*, 2025.
- Tengyang Xie, Dylan J Foster, Yu Bai, Nan Jiang, and Sham M Kakade. The role of coverage in online reinforcement learning. *arXiv preprint arXiv:2210.04157*, 2022.
- An Yang, Beichen Zhang, Binyuan Hui, Bofei Gao, Bowen Yu, Chengpeng Li, Dayiheng Liu, Jianhong Tu, Jingren Zhou, Junyang Lin, et al. Qwen2. 5-math technical report: Toward mathematical expert model via self-improvement. *arXiv preprint arXiv:2409.12122*, 2024.
- An Yang, Anfeng Li, Baosong Yang, Beichen Zhang, Binyuan Hui, Bo Zheng, Bowen Yu, Chang Gao, Chengen Huang, Chenxu Lv, et al. Qwen3 technical report. *arXiv preprint arXiv:2505.09388*, 2025.
- Yuming Yang, Mingyoung Lai, Wanxu Zhao, Xiaoran Fan, Zhiheng Xi, Mingqi Wu, Chiyue Huang, Jun Zhao, Haijun Lv, Jian Tong, et al. Which reasoning trajectories teach students to reason better? a simple metric of informative alignment. *arXiv preprint arXiv:2601.14249*, 2026.
- Yixin Ye, Zhen Huang, Yang Xiao, Ethan Chern, Shijie Xia, and Pengfei Liu. Limo: Less is more for reasoning. *arXiv preprint arXiv:2502.03387*, 2025.
- Longhui Yu, Weisen Jiang, Han Shi, Jincheng Yu, Zhengying Liu, Yu Zhang, James T Kwok, Zhenguo Li, Adrian Weller, and Weiyang Liu. Metamath: Bootstrap your own mathematical questions for large language models. *arXiv preprint arXiv:2309.12284*, 2023.
- Zheng Yuan, Hongyi Yuan, Chengpeng Li, Guanting Dong, Keming Lu, Chuanqi Tan, Chang Zhou, and Jingren Zhou. Scaling relationship on learning mathematical reasoning with large language models. *arXiv preprint arXiv:2308.01825*, 2023.
- Biao Zhang and Rico Sennrich. Root mean square layer normalization. *Advances in neural information processing systems*, 32, 2019.
- Dylan Zhang, Qirun Dai, and Hao Peng. The best instruction-tuning data are those that fit. *arXiv preprint arXiv:2502.04194*, 2025a.

Jia Zhang, Chen-Xi Zhang, Yao Liu, Yi-Xuan Jin, Xiao-Wen Yang, Bo Zheng, Yi Liu, and Lan-Zhe Guo. D3: Diversity, difficulty, and dependability-aware data selection for sample-efficient llm instruction tuning. *arXiv preprint arXiv:2503.11441*, 2025b.

Lianmin Zheng, Wei-Lin Chiang, Ying Sheng, Siyuan Zhuang, Zhanghao Wu, Yonghao Zhuang, Zi Lin, Zhuohan Li, Dacheng Li, Eric Xing, et al. Judging llm-as-a-judge with mt-bench and chatbot arena. *Advances in neural information processing systems*, 36:46595–46623, 2023.

A	Anchor-Time Analysis of the Learnability Objective	13
A.1	Proof of the Anchor-Time Loss Decay Bound	13
A.2	NTK-Based Justification of the Trajectory Bound	14
A.3	Empirical Verification of the Trajectory Bound	17
B	Theoretical Analysis of LARK	18
B.1	Quasiconvexity of $\rho(\boldsymbol{\theta}_{\text{ref}}; \mathbf{q})$ and Collapse to One-Hot	19
B.2	Notation and Structural Assumptions	20
B.3	Auxiliary Lemmas	21
B.4	Proof of Lemma 1 (Forward-pass ρ_k^* Estimation)	25
B.5	Proof of Lemma 2 (χ^2 Controls Both Error Terms)	26
B.6	Proof of Theorem 1 (LARK Objective)	29
B.7	Proof of Lemma 3 (B -Parameterized Closed Form)	30
B.8	Theoretical and Empirical Validation of the Surrogate $\hat{\mathbf{g}}$	31
C	Experimental Details	33
C.1	Candidate Pool	33
C.2	Trajectory Selection Baselines	33
C.3	Implementation Details	35
C.4	Evaluation Protocol	36
C.5	Train/Eval Contamination Audit	38
D	Diagnostic Analyses of LARK	39
D.1	Computational Cost	39
D.2	Selection Budget Scaling	40
D.3	Case Study: A Single-Problem Walkthrough	40
E	Limitations	43

A Anchor-Time Analysis of the Learnability Objective

This appendix supports the anchor-time reduction in Section 4.1. We first prove the post-training loss bound (Appendix A.1). We then provide a theoretical justification of the anchor-relative trajectory bound through the NTK lazy-training framework (Appendix A.2), and verify it empirically on real SFT trajectories (Appendix A.3).

A.1 Proof of the Anchor-Time Loss Decay Bound

Proof of Proposition 1. Fix any $\mathbf{q} \in \Delta^K$. By the gradient-flow decay identity (3) and Condition 1, which gives $\rho(\phi_{\mathbf{q}}(s); \mathbf{q}) \geq \kappa \cdot \rho(\boldsymbol{\theta}_{\text{ref}}; \mathbf{q})$ for every $s \in [0, T]$, we have

$$\int_0^T \rho(\phi_{\mathbf{q}}(s); \mathbf{q}) ds \geq \int_0^T \kappa \cdot \rho(\boldsymbol{\theta}_{\text{ref}}; \mathbf{q}) ds = \kappa T \cdot \rho(\boldsymbol{\theta}_{\text{ref}}; \mathbf{q}).$$

Substituting into (3) and using the non-negativity of $\mathcal{L}(\boldsymbol{\theta}_{\text{ref}}; \mathbf{q})$ together with the monotonicity of $x \mapsto \exp(-x)$ on \mathbb{R} ,

$$\mathcal{L}(\phi_{\mathbf{q}}(T); \mathbf{q}) = \mathcal{L}(\boldsymbol{\theta}_{\text{ref}}; \mathbf{q}) \cdot \exp\left(-\int_0^T \rho(\phi_{\mathbf{q}}(s); \mathbf{q}) ds\right) \leq \mathcal{L}(\boldsymbol{\theta}_{\text{ref}}; \mathbf{q}) \cdot \exp(-\kappa T \cdot \rho(\boldsymbol{\theta}_{\text{ref}}; \mathbf{q})). \quad (11)$$

Since $\mathbf{q} \in \Delta^K$ was arbitrary, the bound holds for every $\mathbf{q} \in \Delta^K$. \square

A.2 NTK-Based Justification of the Trajectory Bound

We provide a theoretical justification of Condition 1 through the Neural Tangent Kernel (NTK) framework. Under standard NTK lazy-training conditions for pretrained language model fine-tuning, combined with a local non-degeneracy condition on the ground-truth probability, we derive a strictly positive constant κ for which Condition 1 provably holds.

Note on terminology. Throughout this subsection, we distinguish between two kinds of structural premises. *Condition 1* is the anchor-relative condition stated in the main text, which we aim to justify. *Assumptions A.1–A.4* below are standard NTK lazy-training premises, which we use to derive Condition 1 as a theorem (Proposition 2).

NTK setup. We adopt the token-level objects from Section 4.2. For each candidate trajectory \mathbf{y}_k , recall the per-token residual $\delta_t = \pi_t - \mathbf{e}_{y_t} \in \mathbb{R}^V$ and the stacked residual matrix $\Delta_k = [\delta_1, \dots, \delta_{|a_k|}]^\top \in \mathbb{R}^{|a_k| \times V}$, with $p_t = \pi_t(y_t)$ the probability assigned to the ground-truth token. We additionally introduce the following appendix-only objects.

Logits Jacobian. For trajectory \mathbf{y}_k , define

$$J_k(\boldsymbol{\theta}) \triangleq \frac{\partial}{\partial \boldsymbol{\theta}} \text{vec}(\mathbf{z}_1, \dots, \mathbf{z}_{|a_k|}) \in \mathbb{R}^{|a_k|V \times |\boldsymbol{\theta}|}. \quad (12)$$

Vectorized residual. Let $\boldsymbol{\Delta}_k(\boldsymbol{\theta}) \triangleq \text{vec}(\Delta_k(\boldsymbol{\theta})) \in \mathbb{R}^{|a_k|V}$.

Weighted NTK matrix and weighted residual. Given $\mathbf{q} \in \Delta^K$, let

$$\tilde{J}(\boldsymbol{\theta}; \mathbf{q}) \triangleq \begin{pmatrix} \sqrt{q_1/|a_1|} J_1(\boldsymbol{\theta}) \\ \vdots \\ \sqrt{q_K/|a_K|} J_K(\boldsymbol{\theta}) \end{pmatrix}, \quad \tilde{\boldsymbol{\Delta}}(\boldsymbol{\theta}; \mathbf{q}) \triangleq \begin{pmatrix} \sqrt{q_1/|a_1|} \boldsymbol{\Delta}_1(\boldsymbol{\theta}) \\ \vdots \\ \sqrt{q_K/|a_K|} \boldsymbol{\Delta}_K(\boldsymbol{\theta}) \end{pmatrix}, \quad (13)$$

and define the weighted empirical NTK matrix

$$\Theta(\boldsymbol{\theta}; \mathbf{q}) \triangleq \tilde{J}(\boldsymbol{\theta}; \mathbf{q}) \tilde{J}(\boldsymbol{\theta}; \mathbf{q})^\top. \quad (14)$$

NTK identity. By the standard chain rule for softmax cross-entropy ($\nabla_{\mathbf{z}_t} \ell_t = \delta_t$, see Section 4.2), the weighted gradient admits the factorization

$$\nabla_{\boldsymbol{\theta}} \mathcal{L}(\boldsymbol{\theta}; \mathbf{q}) = \tilde{J}(\boldsymbol{\theta}; \mathbf{q})^\top \tilde{\boldsymbol{\Delta}}(\boldsymbol{\theta}; \mathbf{q}),$$

which yields the NTK identity

$$\|\nabla_{\boldsymbol{\theta}} \mathcal{L}(\boldsymbol{\theta}; \mathbf{q})\|^2 = \tilde{\boldsymbol{\Delta}}(\boldsymbol{\theta}; \mathbf{q})^\top \Theta(\boldsymbol{\theta}; \mathbf{q}) \tilde{\boldsymbol{\Delta}}(\boldsymbol{\theta}; \mathbf{q}). \quad (15)$$

When some $q_k = 0$, the corresponding trajectory block contributes neither to the weighted loss nor to its gradient. The zero-weight blocks are therefore harmless in the identity above, but they should not be used to impose full-matrix positive definiteness. This is why Assumption A.3 below conditions the NTK only along the residual directions that enter the weighted objective.

Assumptions. We adopt four conditions for the NTK analysis of language model fine-tuning.

Assumption A.1 (Lazy training). There exists a constant $R > 0$ such that, for every $\mathbf{q} \in \Delta^K$,

$$\sup_{s \in [0, T]} \|\phi_{\mathbf{q}}(s) - \boldsymbol{\theta}_{\text{ref}}\| \leq R. \quad (16)$$

Assumption A.2 (NTK stability). There exists $\epsilon \in (0, 1)$ such that, for every $\mathbf{q} \in \Delta^K$ and every $\boldsymbol{\theta} \in B(\boldsymbol{\theta}_{\text{ref}}, R)$,

$$(1 - \epsilon) \Theta(\boldsymbol{\theta}_{\text{ref}}; \mathbf{q}) \preceq \Theta(\boldsymbol{\theta}; \mathbf{q}) \preceq (1 + \epsilon) \Theta(\boldsymbol{\theta}_{\text{ref}}; \mathbf{q}). \quad (17)$$

Assumption A.3 (Residual-direction NTK conditioning at anchor). There exist constants $0 < \lambda_- \leq \lambda_+ < \infty$ such that, for every $\mathbf{q} \in \Delta^K$ and every $\boldsymbol{\theta} \in B(\boldsymbol{\theta}_{\text{ref}}, R)$,

$$\tilde{\Delta}(\boldsymbol{\theta}; \mathbf{q})^\top \Theta(\boldsymbol{\theta}_{\text{ref}}; \mathbf{q}) \tilde{\Delta}(\boldsymbol{\theta}; \mathbf{q}) \geq \lambda_- \|\tilde{\Delta}(\boldsymbol{\theta}; \mathbf{q})\|^2, \quad (18)$$

and

$$\tilde{\Delta}(\boldsymbol{\theta}_{\text{ref}}; \mathbf{q})^\top \Theta(\boldsymbol{\theta}_{\text{ref}}; \mathbf{q}) \tilde{\Delta}(\boldsymbol{\theta}_{\text{ref}}; \mathbf{q}) \leq \lambda_+ \|\tilde{\Delta}(\boldsymbol{\theta}_{\text{ref}}; \mathbf{q})\|^2. \quad (19)$$

Assumption A.4 (Bounded ground-truth probability). There exist constants $0 < p_- \leq p_+ < 1$ such that, for every $\boldsymbol{\theta} \in B(\boldsymbol{\theta}_{\text{ref}}, R)$, every $\mathbf{q} \in \Delta^K$, every $k \in [K]$, and every token position t ,

$$p_- \leq p_t(\boldsymbol{\theta}) \leq p_+. \quad (20)$$

Assumption A.1 encodes lazy fine-tuning behavior, classical in NTK theory [Jacot et al., 2018, Chizat et al., 2019] and supported empirically for pre-trained transformer fine-tuning by Malladi et al. [2023]. *Assumption A.2* requires the empirical NTK matrix to remain near-constant within the lazy ball, with rate $O(1/\sqrt{m})$ at width m [Lee et al., 2019, Jacot et al., 2018], and is supported empirically by Malladi et al. [2023] for fine-tuning. *Assumption A.3* is a residual-direction conditioning condition: it does not require the full weighted NTK matrix to be positive definite in directions corresponding to zero-weight trajectories, but only requires non-degenerate curvature along the residual directions that determine the weighted loss and its gradient. *Assumption A.4* is a local non-degeneracy condition on teacher-forced token probabilities: $p_t > 0$ holds strictly under finite logits, while $p_t < 1$ excludes already-converged tokens for which the residual signal vanishes.

Loss-residual relation. Before establishing the main result, we relate the loss $\mathcal{L}(\boldsymbol{\theta}; \mathbf{q})$ to the squared residual norm $\|\tilde{\Delta}(\boldsymbol{\theta}; \mathbf{q})\|^2$. The relation depends only on *Assumption A.4*, and the constants ν_-, ν_+ are derived explicitly from p_-, p_+ .

Lemma 4 (Loss-residual two-sided bound). *Under Assumption A.4, for every $\boldsymbol{\theta} \in B(\boldsymbol{\theta}_{\text{ref}}, R)$ and every $\mathbf{q} \in \Delta^K$,*

$$\nu_- \|\tilde{\Delta}(\boldsymbol{\theta}; \mathbf{q})\|^2 \leq \mathcal{L}(\boldsymbol{\theta}; \mathbf{q}) \leq \nu_+ \|\tilde{\Delta}(\boldsymbol{\theta}; \mathbf{q})\|^2, \quad (21)$$

where

$$\nu_- = \frac{1}{2}, \quad \nu_+ = \frac{\log(1/p_-)}{(1 - p_+)^2}. \quad (22)$$

Proof. We first establish corresponding pointwise bounds at the token level: for every token position t , with $p \triangleq p_t \in [p_-, p_+]$,

$$\frac{1}{2} \|\delta_t\|^2 \leq \ell_t \leq \frac{\log(1/p_-)}{(1 - p_+)^2} \|\delta_t\|^2. \quad (23)$$

Lower bound.

$$\begin{aligned} \|\delta_t\|^2 &\stackrel{(a)}{=} (1 - p)^2 + \sum_{v \neq y_t} \pi_t(v)^2 \\ &\stackrel{(b)}{\leq} (1 - p)^2 + \left(\max_{v \neq y_t} \pi_t(v) \right) \sum_{v \neq y_t} \pi_t(v) \\ &\stackrel{(c)}{\leq} (1 - p)^2 + (1 - p) \cdot (1 - p) = 2(1 - p)^2 \\ &\stackrel{(d)}{\leq} 2(1 - p) \stackrel{(e)}{\leq} 2\ell_t, \end{aligned} \quad (24)$$

where (a) is the definition $\delta_t = \pi_t - \mathbf{e}_{y_t}$ together with $\pi_t(y_t) = p$; (b) uses $\sum_v a_v^2 \leq \max_v a_v \cdot \sum_v a_v$ for non-negative $\{a_v\}$; (c) uses both $\max_{v \neq y_t} \pi_t(v) \leq \sum_{v \neq y_t} \pi_t(v) = 1 - p$ and $\sum_{v \neq y_t} \pi_t(v) = 1 - p$; (d) uses $1 - p \leq 1$; and (e) uses the elementary inequality $-\log p \geq 1 - p$ for $p \in (0, 1]$.

Upper bound.

$$\begin{aligned} \ell_t &\stackrel{(f)}{=} -\log p \stackrel{(g)}{\leq} \log(1/p_-) \\ &\stackrel{(h)}{=} \frac{\log(1/p_-)}{(1-p_+)^2} (1-p_+)^2 \stackrel{(i)}{\leq} \frac{\log(1/p_-)}{(1-p_+)^2} (1-p)^2 \stackrel{(j)}{\leq} \frac{\log(1/p_-)}{(1-p_+)^2} \|\delta_t\|^2, \end{aligned} \quad (25)$$

where (f) is the definition of ℓ_t ; (g) uses $p \geq p_-$ and the monotonicity of $-\log$; (h) is multiplication and division by $(1-p_+)^2 > 0$; (i) uses $(1-p_+)^2 \leq (1-p)^2$ from $p \leq p_+ < 1$; and (j) uses $\|\delta_t\|^2 \geq (1-p)^2$ from the y_t -th coordinate.

Aggregation. Summing (23) over $t = 1, \dots, |a_k|$ and dividing by $|a_k|$ yields

$$\nu_- \|\Delta_k\|^2 / |a_k| \leq \mathcal{L}(\theta; \mathbf{y}_k) \leq \nu_+ \|\Delta_k\|^2 / |a_k|,$$

where $\|\Delta_k\|^2 = \sum_t \|\delta_t\|^2$. Multiplying by q_k and summing over k gives

$$\nu_- \sum_{k=1}^K \frac{q_k}{|a_k|} \|\Delta_k\|^2 \leq \mathcal{L}(\theta; \mathbf{q}) \leq \nu_+ \sum_{k=1}^K \frac{q_k}{|a_k|} \|\Delta_k\|^2, \quad (26)$$

and the result follows from

$$\sum_k (q_k / |a_k|) \|\Delta_k\|^2 = \|\tilde{\Delta}(\theta; \mathbf{q})\|^2.$$

□

Main result. We now establish the main result.

Proposition 2 (NTK-based justification of Condition 1). *Under Assumptions A.1–A.4, Condition 1 holds with*

$$\kappa = \frac{(1-\epsilon)\lambda_- \nu_-}{\lambda_+ \nu_+} = \frac{(1-\epsilon)\lambda_- (1-p_+)^2}{2\lambda_+ \log(1/p_-)} > 0. \quad (27)$$

Proof. Fix any $\mathbf{q} \in \Delta^K$ and $s \in [0, T]$, and set $\theta = \phi_{\mathbf{q}}(s)$. Assumption A.1 gives $\theta \in B(\theta_{\text{ref}}, R)$.

Writing $\tilde{\Delta} \triangleq \tilde{\Delta}(\theta; \mathbf{q})$,

$$\begin{aligned} \|\nabla_{\theta} \mathcal{L}(\theta; \mathbf{q})\|^2 &\stackrel{(a)}{=} \tilde{\Delta}^{\top} \Theta(\theta; \mathbf{q}) \tilde{\Delta} \\ &\stackrel{(b)}{\geq} (1-\epsilon) \tilde{\Delta}^{\top} \Theta(\theta_{\text{ref}}; \mathbf{q}) \tilde{\Delta} \\ &\stackrel{(c)}{\geq} (1-\epsilon) \lambda_- \|\tilde{\Delta}\|^2, \end{aligned} \quad (28)$$

where (a) is the NTK identity (15); (b) applies the lower-bound part of Assumption A.2; and (c) applies the residual-direction lower bound (18) from Assumption A.3. Combined with the upper bound $\mathcal{L}(\theta; \mathbf{q}) \leq \nu_+ \|\tilde{\Delta}\|^2$ from Lemma 4,

$$\rho(\theta; \mathbf{q}) = \frac{\|\nabla_{\theta} \mathcal{L}(\theta; \mathbf{q})\|^2}{\mathcal{L}(\theta; \mathbf{q})} \geq \frac{(1-\epsilon)\lambda_- \|\tilde{\Delta}\|^2}{\nu_+ \|\tilde{\Delta}\|^2} = \frac{(1-\epsilon)\lambda_-}{\nu_+}. \quad (29)$$

Writing $\tilde{\Delta}_{\text{ref}} \triangleq \tilde{\Delta}(\theta_{\text{ref}}; \mathbf{q})$,

$$\begin{aligned} \|\nabla_{\theta} \mathcal{L}(\theta_{\text{ref}}; \mathbf{q})\|^2 &\stackrel{(d)}{=} \tilde{\Delta}_{\text{ref}}^{\top} \Theta(\theta_{\text{ref}}; \mathbf{q}) \tilde{\Delta}_{\text{ref}} \\ &\stackrel{(e)}{\leq} \lambda_+ \|\tilde{\Delta}_{\text{ref}}\|^2, \end{aligned} \quad (30)$$

where (d) is (15) at θ_{ref} and (e) applies the residual-direction upper bound (19) from Assumption A.3. Combined with the lower bound $\mathcal{L}(\theta_{\text{ref}}; \mathbf{q}) \geq \nu_- \|\tilde{\Delta}_{\text{ref}}\|^2$ from Lemma 4,

$$\rho(\theta_{\text{ref}}; \mathbf{q}) = \frac{\|\nabla_{\theta} \mathcal{L}(\theta_{\text{ref}}; \mathbf{q})\|^2}{\mathcal{L}(\theta_{\text{ref}}; \mathbf{q})} \leq \frac{\lambda_+ \|\tilde{\Delta}_{\text{ref}}\|^2}{\nu_- \|\tilde{\Delta}_{\text{ref}}\|^2} = \frac{\lambda_+}{\nu_-}. \quad (31)$$

Combining (29) and (31), both being positive,

$$\frac{\rho(\phi_{\mathbf{q}}(s); \mathbf{q})}{\rho(\boldsymbol{\theta}_{\text{ref}}; \mathbf{q})} \stackrel{(f)}{\geq} \frac{(1 - \epsilon) \lambda_- / \nu_+}{\lambda_+ / \nu_-} = \frac{(1 - \epsilon) \lambda_- \nu_-}{\lambda_+ \nu_+}, \quad (32)$$

where (f) uses the lower bound on the numerator from (29) and the upper bound on the denominator from (31). Since \mathbf{q} and s were arbitrary,

$$\inf_{s \in [0, T]} \rho(\phi_{\mathbf{q}}(s); \mathbf{q}) \geq \frac{(1 - \epsilon) \lambda_- \nu_-}{\lambda_+ \nu_+} \cdot \rho(\boldsymbol{\theta}_{\text{ref}}; \mathbf{q}), \quad (33)$$

which is Condition 1 with

$$\kappa = \frac{(1 - \epsilon) \lambda_- \nu_-}{\lambda_+ \nu_+}.$$

Substituting $\nu_- = 1/2$ and $\nu_+ = \log(1/p_-)/(1 - p_+)^2$ from Lemma 4 yields (27). \square

Remark on κ . The expression

$$\kappa = \frac{(1 - \epsilon) \lambda_- (1 - p_+)^2}{2 \lambda_+ \log(1/p_-)}$$

admits a clean interpretation. The ratio λ_-/λ_+ is the effective condition number of the empirical NTK along the residual directions that determine the weighted loss; $1 - \epsilon$ captures NTK stability along the trajectory; and $(1 - p_+)^2/\log(1/p_-)$ is a geometric correction accounting for the cross-entropy loss, arising from the unbounded growth of $-\log p$ near $p = 0$. Under squared loss, this last factor reduces to a constant and κ collapses to $(1 - \epsilon) \lambda_-/\lambda_+$, recovering the classical NTK convergence-rate dependence on the kernel condition number [Jacot et al., 2018, Du et al., 2019]. The post-training loss bound in Proposition 1 thus holds with this κ , providing theoretical justification for using $\rho(\boldsymbol{\theta}_{\text{ref}}; \mathbf{q})$ as the anchor-time selection objective in Section 4.1.

A.3 Empirical Verification of the Trajectory Bound

Experimental setup. Condition 1 quantifies over all $\mathbf{q} \in \Delta^K$, with no restriction on the candidate pool of the weighted SFT loss in Eq. (1): the pool may consist of the K trajectories of a single question, or of (question, trajectory) pairs aggregated across multiple questions. In actual deployment, LARK is not applied to a single question in isolation but to mini-batches drawn from a corpus of questions, where each batch induces a weight vector over the (question, trajectory) pairs it contains. We therefore verify Condition 1 directly in the corpus-level regime in which LARK is deployed.

Model and anchor. We verify on Qwen-2.5-7B, the main student model used in Section 5.1. The pre-trained checkpoint serves as the anchor parameter $\boldsymbol{\theta}_{\text{ref}}$.

Verification corpus. From the 5,000 NuminaMath training questions used in Section 5.1, we randomly sample 500 questions $\{\mathbf{x}_n\}_{n=1}^{500}$ as the verification corpus. Each \mathbf{x}_n retains its full pool of 33 candidate trajectories (11 teachers \times 3 rollouts). For each \mathbf{x}_n and each budget $B \in \{1, 3, 5, 10, 20\}$, we apply the LARK selection rule (Lemma 3) to obtain a weight vector $\hat{\mathbf{q}}_n^{(B)}$. Stacking and rescaling the 500 per-question weights yields a corpus-level weight vector $\mathbf{Q}^{(B)} \in \Delta^{500 \times 33}$, with the corresponding weighted SFT loss

$$\mathcal{L}_{\text{total}}(\boldsymbol{\theta}; B) \triangleq \mathcal{L}(\boldsymbol{\theta}; \mathbf{Q}^{(B)}) = \frac{1}{500} \sum_{n=1}^{500} \mathcal{L}(\boldsymbol{\theta}; \hat{\mathbf{q}}_n^{(B)}). \quad (34)$$

We treat $\mathbf{Q}^{(B)}$ directly as the weight vector \mathbf{q} in Condition 1, so the corpus-level quantities ρ_t and $\hat{\kappa}^{(B)}$ defined below are instantiations of Condition 1 at $\mathbf{Q}^{(B)}$.

SFT training. For each budget $B \in \{1, 3, 5, 10, 20\}$, we run mini-batch SFT on $\mathcal{L}_{\text{total}}(\cdot; B)$ starting from $\boldsymbol{\theta}_{\text{ref}}$, using the same hyperparameters as the main experiments. Full training details are deferred to Appendix C.3.

Recorded quantities. At each training step $t \in \{0, 1, \dots, T_{\text{max}}\}$, we record the corpus-level decay rate

$$\rho_t \triangleq \frac{\|\nabla_{\boldsymbol{\theta}} \mathcal{L}_{\text{total}}(\boldsymbol{\theta}_t; B)\|^2}{\mathcal{L}_{\text{total}}(\boldsymbol{\theta}_t; B)}, \quad (35)$$

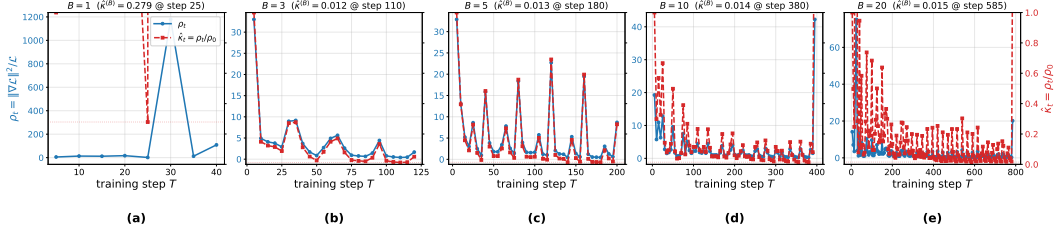


Figure 5: Empirical verification of Condition 1 on Qwen-2.5-7B for $B \in \{1, 3, 5, 10, 20\}$. Blue: ρ_t (left axis); red dashed: $\hat{\kappa}_t = \rho_t / \rho_0$ (right axis). Panel titles report $\hat{\kappa}^{(B)} = \min_t \hat{\kappa}_t$ and the step at which it is attained.

and the anchor-relative ratio $\hat{\kappa}_t \triangleq \rho_t / \rho_0$, which is the discrete-time analog of $\rho(\phi_{\mathbf{Q}^{(B)}}(s); \mathbf{Q}^{(B)}) / \rho(\theta_{\text{ref}}; \mathbf{Q}^{(B)})$ in Condition 1. After training, for each B we report the trajectory-wise minimum

$$\hat{\kappa}^{(B)} \triangleq \min_{t \in [0, T_{\max}]} \rho_t / \rho_0, \quad (36)$$

as the empirical estimate of κ in Condition 1 under budget B .

Findings. Figure 5 reports the verification results for $B \in \{1, 3, 5, 10, 20\}$. Each panel plots the corpus-level decay rate ρ_t (blue solid, left axis) and the anchor-relative ratio $\hat{\kappa}_t = \rho_t / \rho_0$ (red dashed, right axis) against the training step t . The trajectory-wise minimum $\hat{\kappa}^{(B)}$ and the step at which it is attained are annotated in each panel title.

We highlight three observations from the results.

- *Condition 1 holds across all configurations.* For every B , the trajectory-wise minimum $\hat{\kappa}^{(B)}$ is strictly positive ($\hat{\kappa}^{(B)} \in [0.012, 0.279]$), confirming that ρ along the SFT trajectory does not collapse to zero relative to its anchor-time value. This empirically validates the existence of a positive κ in Condition 1.
- *Smallest budget yields the largest $\hat{\kappa}$.* The minimum ratio at $B = 1$ ($\hat{\kappa}^{(1)} = 0.279$) substantially exceeds the values for $B \geq 3$ (which fall in the range 0.012–0.015). Single-trajectory training produces a more stable ρ trajectory and a tighter anchor-relative bound, while multi-trajectory training induces more oscillatory ρ_t but still maintains a positive lower bound.
- *$\hat{\kappa}^{(B)}$ stabilizes for moderate B .* For $B \in \{3, 5, 10, 20\}$, the minimum ratio remains within a narrow range (0.012–0.015), indicating that beyond a small budget, the corpus-level anchor-relative bound depends only weakly on B .

On the early-step transient in ρ_t . A closer look at Figure 5 reveals that, for $B \geq 3$, ρ_t is non-monotone: it exhibits a sharp transient spike during the first $\sim 10\%$ of training steps (reaching values an order of magnitude above ρ_0) before settling to a positive plateau. Two factors are consistent with this behavior. First, the empirical NTK $\Theta(\theta_t; \mathbf{q})$ adapts most rapidly during the warmup phase of SFT, before the lazy-training regime of Assumption A.1 fully takes effect; the looser NTK stability in this early window admits larger fluctuations of ρ_t around its anchor-time value. Second, weighted multi-trajectory gradients $\nabla_{\theta} \mathcal{L}(\theta_t; \mathbf{q})$ admit cancellation across trajectory blocks with different residual directions, which can produce non-monotone $\|\nabla_{\theta} \mathcal{L}\|^2$ in early steps. Crucially, the empirical $\hat{\kappa}^{(B)}$ reported in the panel titles is the trajectory-wise *minimum* of ρ_t / ρ_0 over the entire training run, which already absorbs this transient: even at the lowest point of the trajectory, ρ_t / ρ_0 remains bounded away from zero, which is exactly what Condition 1 requires. The transient therefore tightens (rather than relaxes) the empirical estimate of κ .

B Theoretical Analysis of LARK

This appendix collects the formal statements, proofs, and supporting derivations for the theoretical claims in Section 4.2 (the local linearization analysis of LARK) and Section 4.3 (the closed-form selection rule).

We begin in Appendix B.1 by establishing that $\rho(\boldsymbol{\theta}_{\text{ref}}; \mathbf{q})$ is quasiconvex on Δ^K and that its (constrained or unconstrained) maximum collapses to a one-hot solution; this is the formal justification for the local-linearization strategy adopted in Section 4.2. Appendix B.2 fixes the additional notation and structural assumptions used by the rest of the appendix. Appendix B.3 collects auxiliary lemmas (gradient identities and bounds at the LM-head and backbone, together with the Taylor decomposition of ρ around \mathbf{p}) that are reused by the subsequent proofs. Appendices B.4, B.5, B.6, and B.7 respectively give the formal versions and full proofs of Lemma 1 (forward-pass ρ_k^* estimation), Lemma 2 (χ^2 controls both R_1 and R_2), Theorem 1 (the LARK objective lower bound), and Lemma 3 (the B -parameterized closed form). Finally, Appendix B.8 provides a quantitative error bound on the surrogate \hat{g}_k relative to the exact directional derivative g_k^* , together with empirical evidence that the two are tightly correlated on real student models.

B.1 Quasiconvexity of $\rho(\boldsymbol{\theta}_{\text{ref}}; \mathbf{q})$ and Collapse to One-Hot

Throughout this subsection, fix $\boldsymbol{\theta} = \boldsymbol{\theta}_{\text{ref}}$ and recall from Section 4.2 that $\mathbf{g}_k = \nabla_{\boldsymbol{\theta}} \ell_k$ with $\ell_k = \ell(\boldsymbol{\theta}_{\text{ref}}, \mathbf{y}_k) > 0$. Define

$$N(\mathbf{q}) \triangleq \left\| \sum_k q_k \mathbf{g}_k \right\|^2 = \mathbf{q}^\top G \mathbf{q}, \quad D(\mathbf{q}) \triangleq \sum_k q_k \ell_k, \quad (37)$$

where $G \in \mathbb{R}^{K \times K}$ with $G_{ij} = \langle \mathbf{g}_i, \mathbf{g}_j \rangle$ is the gradient Gram matrix. Since $G \succeq 0$, $N(\mathbf{q})$ is a convex quadratic in \mathbf{q} , and $D(\mathbf{q}) > 0$ is affine, so $\rho(\boldsymbol{\theta}_{\text{ref}}; \mathbf{q}) = N(\mathbf{q})/D(\mathbf{q})$.

Proposition 3 (Quasiconvexity of $\rho(\boldsymbol{\theta}_{\text{ref}}; \mathbf{q})$). $\rho(\boldsymbol{\theta}_{\text{ref}}; \mathbf{q})$ is quasiconvex in $\mathbf{q} \in \Delta^K$.

Proof. It suffices to show that for every $c \geq 0$, the sublevel set $\mathcal{S}_c \triangleq \{\mathbf{q} \in \Delta^K : \rho(\boldsymbol{\theta}_{\text{ref}}; \mathbf{q}) \leq c\}$ is convex. We have

$$\begin{aligned} \mathbf{q} \in \mathcal{S}_c &\stackrel{(a)}{\iff} \rho(\boldsymbol{\theta}_{\text{ref}}; \mathbf{q}) \leq c \\ &\stackrel{(b)}{\iff} \frac{N(\mathbf{q})}{D(\mathbf{q})} \leq c \\ &\stackrel{(c)}{\iff} N(\mathbf{q}) \leq c \cdot D(\mathbf{q}) \\ &\stackrel{(d)}{\iff} \mathbf{q}^\top G \mathbf{q} - c \sum_k q_k \ell_k \leq 0, \end{aligned} \quad (38)$$

where (a) is the definition of \mathcal{S}_c ; (b) substitutes $\rho(\boldsymbol{\theta}_{\text{ref}}; \mathbf{q}) = N(\mathbf{q})/D(\mathbf{q})$; (c) multiplies both sides by $D(\mathbf{q}) > 0$; and (d) substitutes the definitions of N and D from (37). The left-hand side of the final inequality in (38) is the sum of the convex quadratic $\mathbf{q}^\top G \mathbf{q}$ (since $G \succeq 0$) and the affine term $-c \sum_k q_k \ell_k$, hence convex in \mathbf{q} . Therefore \mathcal{S}_c is the intersection of a convex sublevel set with the convex set Δ^K , which is convex. \square

Corollary 1 (Maximum at a vertex). $\max_{\mathbf{q} \in \Delta^K} \rho(\boldsymbol{\theta}_{\text{ref}}; \mathbf{q})$ is attained at an extreme point of Δ^K .

Proof. We have

$$\begin{aligned} \max_{\mathbf{q} \in \Delta^K} \rho(\boldsymbol{\theta}_{\text{ref}}; \mathbf{q}) &\stackrel{(a)}{=} \max_{\mathbf{q} \in \Delta^K} \rho(\boldsymbol{\theta}_{\text{ref}}; \mathbf{q}) \Big|_{\text{extreme point}} \\ &\stackrel{(b)}{=} \max_{k \in [K]} \rho(\boldsymbol{\theta}_{\text{ref}}; \mathbf{e}_k), \end{aligned} \quad (39)$$

where (a) follows because every $\mathbf{q} \in \Delta^K$ can be written as a convex combination of the extreme points $\{\mathbf{e}_1, \dots, \mathbf{e}_K\}$, namely $\mathbf{q} = \sum_{k=1}^K q_k \mathbf{e}_k$, and quasiconvexity implies $\rho(\boldsymbol{\theta}_{\text{ref}}; \mathbf{q}) \leq \max_{k \in [K]: q_k > 0} \rho(\boldsymbol{\theta}_{\text{ref}}; \mathbf{e}_k) \leq \max_{k \in [K]} \rho(\boldsymbol{\theta}_{\text{ref}}; \mathbf{e}_k)$. The reverse inequality is immediate since each $\mathbf{e}_k \in \Delta^K$. Hence the maximum over Δ^K is attained at an extreme point. Step (b) identifies the extreme points of Δ^K as the standard basis vectors $\{\mathbf{e}_1, \dots, \mathbf{e}_K\}$. \square

Corollary 2 (One-hot optimum).

$$\max_{\mathbf{q} \in \Delta^K} \rho(\boldsymbol{\theta}_{\text{ref}}; \mathbf{q}) = \max_{k \in [K]} \rho(\boldsymbol{\theta}_{\text{ref}}; \mathbf{e}_k) = \max_{k \in [K]} \frac{\|\mathbf{g}_k\|^2}{\ell_k} = \max_{k \in [K]} \rho_k^*. \quad (40)$$

Proof. We have

$$\begin{aligned} \max_{\mathbf{q} \in \Delta^K} \rho(\boldsymbol{\theta}_{\text{ref}}; \mathbf{q}) &\stackrel{(a)}{=} \max_{k \in [K]} \rho(\boldsymbol{\theta}_{\text{ref}}; \mathbf{e}_k) \\ &\stackrel{(b)}{=} \max_{k \in [K]} \frac{N(\mathbf{e}_k)}{D(\mathbf{e}_k)} = \max_{k \in [K]} \frac{\|\mathbf{g}_k\|^2}{\ell_k} \stackrel{(c)}{=} \max_{k \in [K]} \rho_k^*, \end{aligned} \quad (41)$$

where (a) applies Corollary 1; (b) substitutes $\mathbf{q} = \mathbf{e}_k$ into the definitions in (37), giving $N(\mathbf{e}_k) = \|\mathbf{g}_k\|^2$ and $D(\mathbf{e}_k) = \ell_k$; and (c) uses the definition $\rho_k^* = \|\mathbf{g}_k\|^2/\ell_k$ from Section 4.2. \square

B.2 Notation and Structural Assumptions

This subsection fixes the additional notation and structural assumptions used throughout Appendices B.3–B.8.

B.2.1 Notation

Symbols inherited from the main text. We use the same symbols as Section 4.2: \mathbf{x} is the question; $\mathbf{y}_k = (y_1^k, \dots, y_{|a_k|}^k)$ is the k -th candidate trajectory, of length $|a_k|$; $\boldsymbol{\pi}_t^k \in \Delta^{|\mathcal{V}|}$ is the predictive distribution of the reference student π_{ref} at position t under teacher forcing; $\boldsymbol{\delta}(y_t^k) \in \Delta^{|\mathcal{V}|}$ is the one-hot vector for the ground-truth token; $\ell_k = \ell(\boldsymbol{\theta}_{\text{ref}}, \mathbf{y}_k)$ is the length-normalized cross-entropy of trajectory \mathbf{y}_k ; $\mathbf{g}_k = \nabla_{\boldsymbol{\theta}} \ell_k$ is its gradient; $\rho_k^* = \|\mathbf{g}_k\|^2/\ell_k$ is the per-trajectory rate; $\hat{\rho}_k$ is its forward-pass proxy (see Lemma 1); \hat{g}_k and g_k^* are the surrogate and exact directional derivatives at \mathbf{p} ; R_1, R_2 are the residual terms in (4); $\mathbf{p} = (1/K, \dots, 1/K) \in \Delta^K$ is the uniform prior.

Parameter decomposition. We split the student parameters as $\boldsymbol{\theta} = (\mathbf{W}_{\text{out}}, \boldsymbol{\theta}_{\text{rest}})$, where $\mathbf{W}_{\text{out}} \in \mathbb{R}^{|\mathcal{V}| \times d}$ is the LM head matrix and $\boldsymbol{\theta}_{\text{rest}}$ collects all backbone parameters. For each trajectory \mathbf{y}_k and position t , the backbone produces a hidden state $\mathbf{h}_t \in \mathbb{R}^d$, the LM head produces logits $\mathbf{z}_t = \mathbf{W}_{\text{out}} \mathbf{h}_t \in \mathbb{R}^{|\mathcal{V}|}$, and $\boldsymbol{\pi}_t^k = \text{softmax}(\mathbf{z}_t)$. The token-level loss is $\ell_t = -\log \pi_t^k(y_t^k)$, so that $\ell_k = \frac{1}{|a_k|} \sum_t \ell_t$.

Token-level residual. We write the per-token prediction residual as $\boldsymbol{\delta}_t \triangleq \boldsymbol{\pi}_t^k - \boldsymbol{\delta}(y_t^k) \in \mathbb{R}^{|\mathcal{V}|}$, which coincides with $\nabla_{\mathbf{z}_t} \ell_t$ by the standard softmax–cross-entropy identity (see Lemma 5 below).

Stacked matrices. For each trajectory \mathbf{y}_k we collect the per-token residuals and hidden states into matrices

$$\boldsymbol{\Delta} \triangleq [\boldsymbol{\delta}_1, \dots, \boldsymbol{\delta}_{|a_k|}]^\top \in \mathbb{R}^{|a_k| \times |\mathcal{V}|}, \quad \mathbf{H} \triangleq [\mathbf{h}_1, \dots, \mathbf{h}_{|a_k|}]^\top \in \mathbb{R}^{|a_k| \times d}. \quad (42)$$

We also write $\mathbf{J}_H(\mathbf{y}_k) \triangleq [\partial \mathbf{h}_t / \partial \boldsymbol{\theta}_{\text{rest}}]_{t=1}^{|a_k|} \in \mathbb{R}^{|a_k| d \times |\boldsymbol{\theta}_{\text{rest}}|}$ for the sequence-level Jacobian of the hidden states with respect to the backbone parameters. The dependence on \mathbf{y}_k is suppressed when the trajectory is clear from context.

Aggregated quantities. Two aggregations of the per-token residual norms appear repeatedly. Define the (length-normalized) Brier score

$$\text{Brier}(\mathbf{y}_k) \triangleq \frac{1}{|a_k|} \sum_{t=1}^{|a_k|} \|\boldsymbol{\delta}_t\|^2 = \frac{\|\boldsymbol{\Delta}\|_F^2}{|a_k|}. \quad (43)$$

With this notation, the forward-pass proxy of Lemma 1 can be written as

$$\hat{\rho}_k = \frac{\sum_t \|\boldsymbol{\delta}_t\|^2}{\sum_t \ell_t} = \frac{\text{Brier}(\mathbf{y}_k)}{\ell_k}, \quad (44)$$

so that the $1/|a_k|$ factors cancel exactly in numerator and denominator.

Multi-trajectory quantities. Across the candidate pool, write $G \in \mathbb{R}^{K \times K}$ for the gradient Gram matrix with $G_{ij} = \langle \mathbf{g}_i, \mathbf{g}_j \rangle$, and let $\boldsymbol{\ell} = (\ell_1, \dots, \ell_K)^\top$. We use the shorthands

$$\bar{\mathbf{g}} \triangleq \frac{1}{K} \sum_k \mathbf{g}_k, \quad \bar{\ell} \triangleq \frac{1}{K} \sum_k \ell_k, \quad (45)$$

together with $\hat{\rho}_{\max} \triangleq \max_i \hat{\rho}_i$, $\ell_{\min} \triangleq \min_i \ell_i$, and $\ell_{\max} \triangleq \max_i \ell_i$. We also write $\|\mathbf{v}\|_{\mathbf{p}}^2 \triangleq \sum_k p_k v_k^2$ for the \mathbf{p} -weighted Euclidean norm; under uniform \mathbf{p} , $\|\mathbf{v}\|_{\mathbf{p}}^2 = \frac{1}{K} \sum_k v_k^2$.

B.2.2 Structural assumptions

We make four structural assumptions on the reference student π_{ref} and its candidate-pool statistics. All four are mild conditions that are either standard in the convergence analysis of deep networks or directly verifiable from a single forward pass.

Assumption B.1 (Hidden-state norm stability). There exist constants $0 < C_- \leq C_+$ such that for every candidate trajectory \mathbf{y}_k and every token position t ,

$$C_-^2 \leq \|\mathbf{h}_t\|^2 \leq C_+^2. \quad (46)$$

Remark 3. This holds naturally in modern LLMs employing RMSNorm [Zhang and Sennrich, 2019], which constrains hidden-state norms to a tight interval; we have $C_+/C_- \approx 1$ in practice.

Assumption B.2 (Local Jacobian conditioning). There exists $\Lambda > 0$ such that for every candidate trajectory \mathbf{y}_k ,

$$\lambda_{\max}(\mathbf{J}_H(\mathbf{y}_k)\mathbf{J}_H(\mathbf{y}_k)^\top) \leq \Lambda. \quad (47)$$

Remark 4. This is a standard local Lipschitz continuity assumption on the backbone, widely adopted in convergence analyses of SFT [Liu et al., 2022].

Assumption B.3 (Matrix cosine alignment). There exists $\zeta_- > 0$ such that for every candidate trajectory \mathbf{y}_k ,

$$\zeta(\mathbf{y}_k) \triangleq \frac{\|\Delta^\top \mathbf{H}\|_F^2}{\|\Delta\|_F^2 \cdot \|\mathbf{H}\|_F^2} \geq \zeta_- > 0. \quad (48)$$

Remark 5. $\zeta(\mathbf{y}_k)$ is the squared Frobenius cosine similarity between the residual matrix Δ and the hidden-state matrix \mathbf{H} . Assumption B.3 requires that the joint signal between prediction residuals and hidden states does not degenerate, and is verifiable from a single forward pass.

Assumption B.4 (Strictly positive trajectory loss). $\ell_{\min} = \min_{i \in [K]} \ell_i > 0$.

Remark 6. Under finite logits, $\ell_t > 0$ at every token, so $\ell_k > 0$ for every trajectory and Assumption B.4 holds automatically. We state it explicitly because it is needed in Appendix B.5 to ensure the Hessian of $\rho(\theta_{\text{ref}}; \mathbf{q})$ is uniformly bounded over Δ^K via $D(\mathbf{q}) = \ell^\top \mathbf{q} \geq \ell_{\min}$.

B.3 Auxiliary Lemmas

This subsection collects building-block lemmas that are reused by the proofs in Appendices B.4–B.6. Lemmas 5–7 are the gradient identity and gradient norm bounds for the LM head and the backbone; they are the main tools for the proof of Lemma 1 in Appendix B.4. Lemma 8 gives the Taylor decomposition of $\rho(\theta_{\text{ref}}; \mathbf{q})$ around the uniform prior \mathbf{p} , together with the closed form of g_k^* and the definition of \hat{g}_k in terms of forward-pass quantities; this is the starting identity for the proof of Lemma 2 in Appendix B.5. Lemma 9 provides a forward-computable upper bound on the entries of the gradient Gram matrix G via the proxy $\hat{\rho}_i$, which controls every G -dependent quantity that appears in the proof of Lemma 2. Finally, Lemma 10 gives the closed-form Hessian of ρ on Δ^K , used to bound the second-order remainder R_2 .

B.3.1 LM head and backbone gradient identities and bounds

Lemma 5 (LM head gradient). *Let $\ell_t = -\log \pi_t^k(y_t^k)$, $\boldsymbol{\pi}_t^k = \text{softmax}(\mathbf{z}_t)$, and $\mathbf{z}_t = \mathbf{W}_{\text{out}}\mathbf{h}_t$. Then*

$$\frac{\partial \ell_t}{\partial \mathbf{W}_{\text{out}}} = \boldsymbol{\delta}_t \mathbf{h}_t^\top \in \mathbb{R}^{|\mathcal{V}| \times d}, \quad \frac{\partial \ell_t}{\partial \mathbf{h}_t} = \mathbf{W}_{\text{out}}^\top \boldsymbol{\delta}_t. \quad (49)$$

Proof. We prove the first identity; the second is immediate from the chain rule applied to $\mathbf{z}_t = \mathbf{W}_{\text{out}} \mathbf{h}_t$. For any direction $\mathbf{U} \in \mathbb{R}^{|\mathcal{V}| \times d}$,

$$\begin{aligned}
\left\langle \frac{\partial \ell_t}{\partial \mathbf{W}_{\text{out}}}, \mathbf{U} \right\rangle_F &\stackrel{(a)}{=} \left\langle \frac{\partial \ell_t}{\partial \mathbf{z}_t}, \frac{\partial \mathbf{z}_t}{\partial \mathbf{W}_{\text{out}}} [\mathbf{U}] \right\rangle \\
&\stackrel{(b)}{=} \left\langle \frac{\partial \ell_t}{\partial \mathbf{z}_t}, \mathbf{U} \mathbf{h}_t \right\rangle \\
&\stackrel{(c)}{=} \sum_{v=1}^{|\mathcal{V}|} \frac{\partial \ell_t}{\partial z_{t,v}} [\mathbf{U} \mathbf{h}_t]_v \\
&\stackrel{(d)}{=} \sum_{v=1}^{|\mathcal{V}|} (\pi_t^k(v) - \mathbf{1}[v = y_t^k]) [\mathbf{U} \mathbf{h}_t]_v \\
&\stackrel{(e)}{=} \langle \boldsymbol{\pi}_t^k - \boldsymbol{\delta}(y_t^k), \mathbf{U} \mathbf{h}_t \rangle \\
&\stackrel{(f)}{=} \langle \boldsymbol{\delta}_t \mathbf{h}_t^\top, \mathbf{U} \rangle_F, \tag{50}
\end{aligned}$$

where (a) is the chain rule for the Fréchet derivative; (b) follows from the linearity of $\mathbf{z}_t = \mathbf{W}_{\text{out}} \mathbf{h}_t$ in \mathbf{W}_{out} , giving $\frac{\partial \mathbf{z}_t}{\partial \mathbf{W}_{\text{out}}} [\mathbf{U}] = \mathbf{U} \mathbf{h}_t$; (c) expands the inner product componentwise; (d) is the standard softmax-cross-entropy gradient identity, $\partial \ell_t / \partial z_{t,v} = \pi_t^k(v) - \mathbf{1}[v = y_t^k]$, obtained by applying the quotient rule to $\pi_t^k(y_t^k) = e^{z_{t,y_t^k}} / \sum_{v'} e^{z_{t,v'}}$; (e) recognizes the sum as $\langle \boldsymbol{\delta}_t, \mathbf{U} \mathbf{h}_t \rangle$ with $\boldsymbol{\delta}_t = \boldsymbol{\pi}_t^k - \boldsymbol{\delta}(y_t^k)$; and (f) uses the trace identity $\langle \mathbf{a}, \mathbf{B} \mathbf{c} \rangle = \langle \mathbf{a} \mathbf{c}^\top, \mathbf{B} \rangle_F$. Since \mathbf{U} was arbitrary, $\partial \ell_t / \partial \mathbf{W}_{\text{out}} = \boldsymbol{\delta}_t \mathbf{h}_t^\top$. \square

Lemma 6 (LM head gradient bounds). *Under Assumptions B.1 and B.3, for every candidate trajectory \mathbf{y}_k ,*

$$\zeta_- C_-^2 \text{Brier}(\mathbf{y}_k) \leq \|\nabla_{\mathbf{W}_{\text{out}}} \ell_k\|_F^2 \leq C_+^2 \text{Brier}(\mathbf{y}_k). \tag{51}$$

Proof. By Lemma 5 and the definition $\ell_k = \frac{1}{|a_k|} \sum_t \ell_t$,

$$\nabla_{\mathbf{W}_{\text{out}}} \ell_k = \frac{1}{|a_k|} \sum_t \boldsymbol{\delta}_t \mathbf{h}_t^\top = \frac{1}{|a_k|} \boldsymbol{\Delta}^\top \mathbf{H}, \tag{52}$$

where the second equality follows from the definitions of $\boldsymbol{\Delta}, \mathbf{H}$ in (42). Hence $\|\nabla_{\mathbf{W}_{\text{out}}} \ell_k\|_F^2 = \|\boldsymbol{\Delta}^\top \mathbf{H}\|_F^2 / |a_k|^2$.

Lower bound.

$$\begin{aligned}
\|\nabla_{\mathbf{W}_{\text{out}}} \ell_k\|_F^2 &\stackrel{(a)}{=} \frac{\|\boldsymbol{\Delta}^\top \mathbf{H}\|_F^2}{|a_k|^2} \\
&\stackrel{(b)}{\geq} \frac{\zeta_- \|\boldsymbol{\Delta}\|_F^2 \|\mathbf{H}\|_F^2}{|a_k|^2} \\
&\stackrel{(c)}{\geq} \frac{\zeta_- |a_k| \text{Brier}(\mathbf{y}_k) \cdot |a_k| C_-^2}{|a_k|^2} \\
&= \zeta_- C_-^2 \text{Brier}(\mathbf{y}_k), \tag{53}
\end{aligned}$$

where (a) is (52); (b) applies Assumption B.3, which gives $\|\boldsymbol{\Delta}^\top \mathbf{H}\|_F^2 \geq \zeta_- \|\boldsymbol{\Delta}\|_F^2 \|\mathbf{H}\|_F^2$; and (c) substitutes $\|\boldsymbol{\Delta}\|_F^2 = |a_k| \text{Brier}(\mathbf{y}_k)$ from (43) together with $\|\mathbf{H}\|_F^2 = \sum_t \|\mathbf{h}_t\|^2 \geq |a_k| C_-^2$ from Assumption B.1.

Upper bound.

$$\begin{aligned}
\|\nabla_{\mathbf{W}_{\text{out}}} \ell_k\|_F^2 &\stackrel{(d)}{=} \frac{\|\boldsymbol{\Delta}^\top \mathbf{H}\|_F^2}{|a_k|^2} \\
&\stackrel{(e)}{\leq} \frac{\|\boldsymbol{\Delta}\|_F^2 \|\mathbf{H}\|_F^2}{|a_k|^2} \\
&\stackrel{(f)}{\leq} \frac{|a_k| \text{Brier}(\mathbf{y}_k) \cdot |a_k| C_+^2}{|a_k|^2} \\
&= C_+^2 \text{Brier}(\mathbf{y}_k), \tag{54}
\end{aligned}$$

where (d) is (52); (e) is the matrix Cauchy–Schwarz inequality $\|\Delta^\top \mathbf{H}\|_F^2 \leq \|\Delta\|_F^2 \|\mathbf{H}\|_F^2$; and (f) substitutes $\|\Delta\|_F^2 = |a_k| \text{Brier}(\mathbf{y}_k)$ from (43) together with $\|\mathbf{H}\|_F^2 = \sum_t \|\mathbf{h}_t\|^2 \leq |a_k| C_+^2$ from Assumption B.1. \square

Lemma 7 (Backbone gradient bound). *Under Assumptions B.1 and B.2, for every candidate trajectory \mathbf{y}_k ,*

$$\|\nabla_{\boldsymbol{\theta}_{\text{rest}}} \ell_k\|^2 \leq \frac{\Lambda \|\mathbf{W}_{\text{out}}\|_{\text{op}}^2}{|a_k|} \text{Brier}(\mathbf{y}_k). \quad (55)$$

Proof. By the chain rule together with the second identity of Lemma 5, $\partial \ell_t / \partial \mathbf{h}_t = \mathbf{W}_{\text{out}}^\top \boldsymbol{\delta}_t$, hence

$$\nabla_{\boldsymbol{\theta}_{\text{rest}}} \ell_k = \mathbf{J}_H(\mathbf{y}_k)^\top \text{vec}\left(\frac{1}{|a_k|} \Delta \mathbf{W}_{\text{out}}\right). \quad (56)$$

Then

$$\begin{aligned} \|\nabla_{\boldsymbol{\theta}_{\text{rest}}} \ell_k\|^2 &\stackrel{(a)}{\leq} \lambda_{\max}(\mathbf{J}_H(\mathbf{y}_k) \mathbf{J}_H(\mathbf{y}_k)^\top) \left\| \text{vec}\left(\frac{1}{|a_k|} \Delta \mathbf{W}_{\text{out}}\right) \right\|^2 \\ &\stackrel{(b)}{\leq} \frac{\Lambda}{|a_k|^2} \|\Delta \mathbf{W}_{\text{out}}\|_F^2 \\ &\stackrel{(c)}{\leq} \frac{\Lambda \|\mathbf{W}_{\text{out}}\|_{\text{op}}^2}{|a_k|^2} \|\Delta\|_F^2 \\ &\stackrel{(d)}{=} \frac{\Lambda \|\mathbf{W}_{\text{out}}\|_{\text{op}}^2}{|a_k|} \text{Brier}(\mathbf{y}_k), \end{aligned} \quad (57)$$

where (a) uses $\|\mathbf{A}^\top \mathbf{v}\|^2 \leq \lambda_{\max}(\mathbf{A} \mathbf{A}^\top) \|\mathbf{v}\|^2$ with $\mathbf{A} = \mathbf{J}_H(\mathbf{y}_k)$; (b) applies Assumption B.2 together with the identity $\|\text{vec}(\mathbf{M})\|^2 = \|\mathbf{M}\|_F^2$; (c) uses the submultiplicativity $\|\Delta \mathbf{W}_{\text{out}}\|_F \leq \|\mathbf{W}_{\text{out}}\|_{\text{op}} \|\Delta\|_F$; and (d) substitutes $\|\Delta\|_F^2 = |a_k| \text{Brier}(\mathbf{y}_k)$ from (43). \square

B.3.2 Taylor decomposition of $\rho(\boldsymbol{\theta}_{\text{ref}}; \mathbf{q})$

The next lemma packages the algebraic preliminaries for the linearization argument: the closed form of the exact directional derivative g_k^* , the definition of the forward-pass surrogate \hat{g}_k , and the resulting decomposition of the change in ρ into a linear term plus two residuals.

Lemma 8 (Taylor decomposition). *Let $N(\mathbf{q}) \triangleq \|\sum_k q_k \mathbf{g}_k\|^2 = \mathbf{q}^\top G \mathbf{q}$ and $D(\mathbf{q}) \triangleq \sum_k q_k \ell_k = \boldsymbol{\ell}^\top \mathbf{q}$, so that $\rho(\boldsymbol{\theta}_{\text{ref}}; \mathbf{q}) = N(\mathbf{q})/D(\mathbf{q})$. Then:*

(i) (Closed form of g_k^* .) *The exact directional derivative at \mathbf{p} satisfies*

$$g_k^* = \frac{\partial}{\partial q_k} \frac{N(\mathbf{q})}{D(\mathbf{q})} \Big|_{\mathbf{q}=\mathbf{p}} = \frac{2 \mathbf{g}_k^\top \bar{\mathbf{g}}}{\bar{\ell}} - \frac{\rho(\boldsymbol{\theta}_{\text{ref}}; \mathbf{p}) \ell_k}{\bar{\ell}}. \quad (58)$$

(ii) (Forward-pass surrogate.) *Applying the diagonal approximations $\mathbf{g}_k^\top \bar{\mathbf{g}} \approx \|\mathbf{g}_k\|^2 / K$ and $\|\bar{\mathbf{g}}\|^2 \approx \frac{1}{K^2} \sum_i \|\mathbf{g}_i\|^2$ in (58), and substituting the proxy $\hat{\rho}_i$ for $\rho_i^* = \|\mathbf{g}_i\|^2 / \ell_i$, gives*

$$\hat{g}_k = \frac{\ell_k}{\sum_i \ell_i} \left(2\hat{\rho}_k - \frac{\sum_i \hat{\rho}_i \ell_i}{\sum_i \ell_i} \right). \quad (59)$$

(iii) (Decomposition.) *Setting $\boldsymbol{\eta} \triangleq \hat{\mathbf{g}} - \mathbf{g}^*$, the change in ρ admits the decomposition*

$$\rho(\boldsymbol{\theta}_{\text{ref}}; \mathbf{q}) - \rho(\boldsymbol{\theta}_{\text{ref}}; \mathbf{p}) = \langle \mathbf{q} - \mathbf{p}, \hat{\mathbf{g}} \rangle + R_1 + R_2, \quad (60)$$

where

$$R_1 \triangleq -\langle \mathbf{q} - \mathbf{p}, \boldsymbol{\eta} \rangle, \quad R_2 \triangleq \rho(\boldsymbol{\theta}_{\text{ref}}; \mathbf{q}) - \rho(\boldsymbol{\theta}_{\text{ref}}; \mathbf{p}) - \langle \mathbf{q} - \mathbf{p}, \mathbf{g}^* \rangle \quad (61)$$

are the surrogate substitution error and the second-order Taylor remainder, respectively.

Proof. For (i), apply the quotient rule to $N(\mathbf{q})/D(\mathbf{q})$:

$$\frac{\partial}{\partial q_k} \frac{N(\mathbf{q})}{D(\mathbf{q})} = \frac{D(\mathbf{q}) \cdot 2 \mathbf{g}_k^\top \sum_i q_i \mathbf{g}_i - N(\mathbf{q}) \ell_k}{D(\mathbf{q})^2}. \quad (62)$$

Evaluating at $\mathbf{q} = \mathbf{p}$ with $p_k = 1/K$ gives $\sum_i p_i \mathbf{g}_i = \bar{\mathbf{g}}$, $D(\mathbf{p}) = \bar{\ell}$, and $N(\mathbf{p})/D(\mathbf{p}) = \rho(\boldsymbol{\theta}_{\text{ref}}; \mathbf{p})$, yielding (58).

For (ii), substitute $\mathbf{g}_k^\top \bar{\mathbf{g}} \approx \|\mathbf{g}_k\|^2/K$ and $\rho(\boldsymbol{\theta}_{\text{ref}}; \mathbf{p}) = \|\bar{\mathbf{g}}\|^2/\bar{\ell} \approx \frac{1}{K^2 \bar{\ell}} \sum_i \|\mathbf{g}_i\|^2$ into (58), and replace each $\|\mathbf{g}_i\|^2 = \rho_i^* \ell_i$ by $\hat{\rho}_i \ell_i$. Using $K \bar{\ell} = \sum_i \ell_i$ and simplifying gives (59).

For (iii), expand $\rho(\boldsymbol{\theta}_{\text{ref}}; \mathbf{q}) - \rho(\boldsymbol{\theta}_{\text{ref}}; \mathbf{p}) = \langle \mathbf{q} - \mathbf{p}, \mathbf{g}^* \rangle + R_2$ by definition of R_2 , and add and subtract $\langle \mathbf{q} - \mathbf{p}, \hat{\mathbf{g}} \rangle$ to obtain (60) with R_1 as in (61). \square

B.3.3 Forward-computable bound on the gradient Gram matrix

The next lemma upgrades the per-trajectory bound of Lemma 1 to a uniform, forward-computable bound on every entry of the gradient Gram matrix G . It is the main tool that lets us replace gradient-dependent quantities (such as $\mathbf{g}_k^\top \bar{\mathbf{g}}$, $\|\bar{\mathbf{g}}\|^2$, and $\|G\|_{\text{op}}$) by forward-only quantities throughout the proofs of Lemma 2 and Theorem 1.

Lemma 9 (Gram-matrix entry bound). *Assume Assumptions B.1–B.3, and let*

$$E_+ \triangleq C_+^2 \max_{i \in [K]} (1 + \varepsilon_{\text{head}}(|a_i|)), \quad \varepsilon_{\text{head}}(|a_i|) = \frac{\Lambda \|\mathbf{W}_{\text{out}}\|_{\text{op}}^2}{C_+^2 |a_i|}, \quad (63)$$

so that Lemma 1 yields the uniform inequality $\rho_i^* \leq E_+ \hat{\rho}_i$ for every $i \in [K]$. Then for every $i, j \in [K]$,

$$|G_{ij}| \leq \sqrt{G_{ii} G_{jj}} = \sqrt{\rho_i^* \rho_j^* \ell_i \ell_j} \leq E_+ \sqrt{\hat{\rho}_i \hat{\rho}_j \ell_i \ell_j}. \quad (64)$$

Proof. We have

$$\begin{aligned} |G_{ij}| &\stackrel{(a)}{\leq} \sqrt{G_{ii} G_{jj}} \\ &\stackrel{(b)}{=} \sqrt{\rho_i^* \rho_j^* \ell_i \ell_j} \\ &\stackrel{(c)}{\leq} E_+ \sqrt{\hat{\rho}_i \hat{\rho}_j \ell_i \ell_j}, \end{aligned} \quad (65)$$

where (a) is the entry-wise Cauchy–Schwarz bound for inner products, $|\langle \mathbf{g}_i, \mathbf{g}_j \rangle| \leq \|\mathbf{g}_i\| \|\mathbf{g}_j\|$; (b) uses $G_{ii} = \|\mathbf{g}_i\|^2 = \rho_i^* \ell_i$ from the definition $\rho_i^* = \|\mathbf{g}_i\|^2/\ell_i$; and (c) applies the upper part of Lemma 1 entry-wise to each of ρ_i^* and ρ_j^* . \square

Remark 7. All bounds derived in Appendix B.5 (the proof of Lemma 2) trace back to (64). In particular, both the off-diagonal residuals appearing in the surrogate substitution error and the operator-norm bound on G used in the Hessian analysis are obtained by summing (64) over the appropriate index sets.

B.3.4 Hessian of ρ on the simplex

Lemma 10 (Hessian formula). *On the relative interior of Δ^K , the Hessian of $\rho(\boldsymbol{\theta}_{\text{ref}}; \mathbf{q}) = N(\mathbf{q})/D(\mathbf{q})$ in \mathbf{q} is*

$$\nabla_{\mathbf{q}}^2 \rho(\boldsymbol{\theta}_{\text{ref}}; \mathbf{q}) = \frac{1}{D(\mathbf{q})} \left[2G - \boldsymbol{\ell} (\nabla \rho)^\top - (\nabla \rho) \boldsymbol{\ell}^\top \right], \quad (66)$$

where $\nabla \rho = (2G\mathbf{q} - \rho \boldsymbol{\ell})/D(\mathbf{q})$.

Proof. The quotient rule applied to $\rho = N/D$ gives $\nabla \rho = (\nabla N - \rho \nabla D)/D = (2G\mathbf{q} - \rho \boldsymbol{\ell})/D$, or equivalently $D \nabla \rho = 2G\mathbf{q} - \rho \boldsymbol{\ell}$. Differentiating both sides with respect to \mathbf{q} , using $\nabla D = \boldsymbol{\ell}$ and the product rule $\nabla(D \nabla \rho) = \boldsymbol{\ell} (\nabla \rho)^\top + D \nabla^2 \rho$, gives

$$\boldsymbol{\ell} (\nabla \rho)^\top + D \nabla^2 \rho = 2G - (\nabla \rho) \boldsymbol{\ell}^\top. \quad (67)$$

Solving for $\nabla^2 \rho$ and noting that the left-hand side is symmetric (which forces the symmetrized form of the rank-2 correction) yields (66). \square

B.4 Proof of Lemma 1 (Forward-pass ρ_k^* Estimation)

This subsection states and proves the formal version of Lemma 1. The informal version in Section 4.2 asserts the existence of absolute positive constants C_1, C_2 with $\hat{\rho}_k \in [C_1 \rho_k^*, C_2 \rho_k^*]$. The formal statement below makes the constants C_1, C_2 explicit in terms of the structural quantities of Assumptions B.1–B.3.

Lemma 11 (Formal version of Lemma 1). *Under Assumptions B.1–B.3, for every candidate trajectory \mathbf{y}_k ,*

$$C_1 \rho_k^* \leq \hat{\rho}_k \leq C_2 \rho_k^*, \quad (68)$$

where

$$C_1 \triangleq \frac{1}{E_+}, \quad C_2 \triangleq \frac{1}{\zeta_- C_-^2}, \quad E_+ \triangleq C_+^2 \max_{i \in [K]} (1 + \varepsilon_{\text{head}}(|a_i|)), \quad (69)$$

and the LM-head correction term is

$$\varepsilon_{\text{head}}(|a_i|) \triangleq \frac{\Lambda \|\mathbf{W}_{\text{out}}\|_{\text{op}}^2}{C_+^2 |a_i|}. \quad (70)$$

Proof. Since $\boldsymbol{\theta} = (\mathbf{W}_{\text{out}}, \boldsymbol{\theta}_{\text{rest}})$ are disjoint parameter blocks,

$$\|\nabla_{\boldsymbol{\theta}} \ell_k\|^2 = \|\nabla_{\mathbf{W}_{\text{out}}} \ell_k\|_F^2 + \|\nabla_{\boldsymbol{\theta}_{\text{rest}}} \ell_k\|^2. \quad (71)$$

Using the equivalent form $\hat{\rho}_k = \text{Brier}(\mathbf{y}_k)/\ell_k$ from (44) together with $\rho_k^* = \|\nabla_{\boldsymbol{\theta}} \ell_k\|^2/\ell_k$ from Section 4.2, it suffices to relate $\|\nabla_{\boldsymbol{\theta}} \ell_k\|^2$ to $\text{Brier}(\mathbf{y}_k)$.

Upper bound on $\hat{\rho}_k$.

$$\begin{aligned} \rho_k^* &\stackrel{(a)}{=} \frac{\|\nabla_{\boldsymbol{\theta}} \ell_k\|^2}{\ell_k} \\ &\stackrel{(b)}{\geq} \frac{\|\nabla_{\mathbf{W}_{\text{out}}} \ell_k\|_F^2}{\ell_k} \\ &\stackrel{(c)}{\geq} \frac{\zeta_- C_-^2 \text{Brier}(\mathbf{y}_k)}{\ell_k} \\ &\stackrel{(d)}{=} \zeta_- C_-^2 \hat{\rho}_k, \end{aligned} \quad (72)$$

where (a) is the definition $\rho_k^* = \|\nabla_{\boldsymbol{\theta}} \ell_k\|^2/\ell_k$; (b) applies the decomposition (71) and discards the non-negative backbone term $\|\nabla_{\boldsymbol{\theta}_{\text{rest}}} \ell_k\|^2 \geq 0$; (c) applies the lower bound of Lemma 6; and (d) substitutes $\hat{\rho}_k = \text{Brier}(\mathbf{y}_k)/\ell_k$ from (44). Therefore,

$$\hat{\rho}_k \leq \frac{1}{\zeta_- C_-^2} \rho_k^* = C_2 \rho_k^*. \quad (73)$$

Lower bound on $\hat{\rho}_k$.

$$\begin{aligned} \rho_k^* &\stackrel{(e)}{=} \frac{\|\nabla_{\boldsymbol{\theta}} \ell_k\|^2}{\ell_k} \\ &\stackrel{(f)}{=} \frac{\|\nabla_{\mathbf{W}_{\text{out}}} \ell_k\|_F^2 + \|\nabla_{\boldsymbol{\theta}_{\text{rest}}} \ell_k\|^2}{\ell_k} \\ &\stackrel{(g)}{\leq} \frac{1}{\ell_k} \left(C_+^2 \text{Brier}(\mathbf{y}_k) + \frac{\Lambda \|\mathbf{W}_{\text{out}}\|_{\text{op}}^2}{|a_k|} \text{Brier}(\mathbf{y}_k) \right) \\ &\stackrel{(h)}{=} C_+^2 (1 + \varepsilon_{\text{head}}(|a_k|)) \hat{\rho}_k \\ &\stackrel{(i)}{\leq} E_+ \hat{\rho}_k, \end{aligned} \quad (74)$$

where (e) is the definition $\rho_k^* = \|\nabla_{\boldsymbol{\theta}} \ell_k\|^2/\ell_k$; (f) applies the decomposition (71); (g) applies the upper bound of Lemma 6 to the LM-head term and Lemma 7 to the backbone term; (h) substitutes $\hat{\rho}_k = \text{Brier}(\mathbf{y}_k)/\ell_k$ from (44) together with the definition (70) of $\varepsilon_{\text{head}}(|a_k|)$; and (i) follows from the definition of E_+ in (69). Therefore,

$$\hat{\rho}_k \geq \frac{1}{E_+} \rho_k^* = C_1 \rho_k^*. \quad (75)$$

Combining (73) and (75) yields (68). \square

B.5 Proof of Lemma 2 (χ^2 Controls Both Error Terms)

This subsection states and proves the formal version of Lemma 2. We use the Taylor decomposition in Lemma 8. Let $\boldsymbol{\eta} \triangleq \hat{\mathbf{g}} - \mathbf{g}^*$. The two residual terms in (60) are

$$R_1 = -\langle \mathbf{q} - \mathbf{p}, \boldsymbol{\eta} \rangle, \quad R_2 = \rho(\boldsymbol{\theta}_{\text{ref}}; \mathbf{q}) - \rho(\boldsymbol{\theta}_{\text{ref}}; \mathbf{p}) - \langle \mathbf{q} - \mathbf{p}, \mathbf{g}^* \rangle. \quad (76)$$

Since $p_k = 1/K$, we also have

$$\chi^2(\mathbf{q} \parallel \mathbf{p}) = \sum_k \frac{(q_k - p_k)^2}{p_k} = K \|\mathbf{q} - \mathbf{p}\|^2. \quad (77)$$

Let

$$E_+ \triangleq C_+^2 \max_{i \in [K]} (1 + \varepsilon_{\text{head}}(|a_i|)), \quad (78)$$

$$\Delta_\rho \triangleq \max\left(|1 - \zeta_- C_-^2|, \max_{i \in [K]} |C_+^2 (1 + \varepsilon_{\text{head}}(|a_i|)) - 1|\right). \quad (79)$$

By Lemma 11, for all $i \in [K]$, $\rho_i^* \leq E_+ \hat{\rho}_i$ and $|\hat{\rho}_i - \rho_i^*| \leq \Delta_\rho \hat{\rho}_i$. We also define $\hat{\rho}_{\max} \triangleq \max_i \hat{\rho}_i$, $\ell_{\min} \triangleq \min_i \ell_i$, $\ell_{\max} \triangleq \max_i \ell_i$, and $\bar{\ell} \triangleq K^{-1} \sum_i \ell_i$.

Lemma 12 (Formal version of Lemma 2). *Under Assumptions B.1–B.4, for every $\mathbf{q} \in \Delta^K$,*

$$|R_1| \leq \alpha_1 \chi^2(\mathbf{q} \parallel \mathbf{p}) + 1, \quad |R_2| \leq \alpha_2 \chi^2(\mathbf{q} \parallel \mathbf{p}), \quad (80)$$

where

$$\alpha_1 = \frac{1}{4} \left(\frac{3\Delta_\rho \hat{\rho}_{\max}}{\sqrt{K}} + \frac{2E_+ \sqrt{\hat{\rho}_{\max} \ell_{\max} \sum_i \hat{\rho}_i \ell_i}}{\sqrt{K} \bar{\ell}} + \frac{E_+ \ell_{\max} \sum_i \hat{\rho}_i \ell_i}{K \bar{\ell}^2} \right)^2, \quad (81)$$

$$\alpha_2 = \frac{E_+ \sum_i \hat{\rho}_i \ell_i}{K \ell_{\min}} \left(1 + \frac{\sqrt{K} \ell_{\max}}{\ell_{\min}} \right)^2. \quad (82)$$

Proof. We first control R_1 . By Cauchy–Schwarz and (77),

$$\begin{aligned} |R_1| &= \left| \sum_k (q_k - p_k) \eta_k \right| \\ &\leq \sqrt{K \|\mathbf{q} - \mathbf{p}\|^2} \sqrt{\frac{1}{K} \sum_k \eta_k^2} \\ &= \sqrt{\chi^2(\mathbf{q} \parallel \mathbf{p})} \|\boldsymbol{\eta}\|_{\mathbf{p}}, \end{aligned} \quad (83)$$

where $\|\mathbf{v}\|_{\mathbf{p}}^2 \triangleq K^{-1} \sum_k v_k^2$ under the uniform prior. It remains to bound $\|\boldsymbol{\eta}\|_{\mathbf{p}}$.

Introduce the intermediate vector

$$\tilde{\mathbf{g}}_k \triangleq \frac{\ell_k}{\sum_i \ell_i} \left(2\rho_k^* - \frac{\sum_i \rho_i^* \ell_i}{\sum_i \ell_i} \right). \quad (84)$$

This vector keeps the exact per-trajectory rates ρ_i^* but uses the same diagonal approximation that leads to \hat{g}_k . Therefore,

$$\boldsymbol{\eta} = (\hat{\mathbf{g}} - \tilde{\mathbf{g}}) + (\tilde{\mathbf{g}} - \mathbf{g}^*) \triangleq \boldsymbol{\eta}_{\text{prox}} + \boldsymbol{\eta}_{\text{diag}}. \quad (85)$$

For the proxy-substitution term, subtracting (84) from (59) gives

$$\eta_{\text{prox},k} = \frac{\ell_k}{\sum_i \ell_i} \left(2(\hat{\rho}_k - \rho_k^*) - \frac{\sum_i (\hat{\rho}_i - \rho_i^*) \ell_i}{\sum_i \ell_i} \right). \quad (86)$$

Using $|\hat{\rho}_i - \rho_i^*| \leq \Delta_\rho \hat{\rho}_{\max}$ for all i , we obtain

$$|\eta_{\text{prox},k}| \leq \frac{3\Delta_\rho \hat{\rho}_{\max} \ell_k}{\sum_i \ell_i}. \quad (87)$$

Hence

$$\begin{aligned}
\|\boldsymbol{\eta}_{\text{prox}}\|_{\mathbf{p}}^2 &= \frac{1}{K} \sum_k |\eta_{\text{prox},k}|^2 \\
&\leq \frac{(3\Delta_\rho \hat{\rho}_{\max})^2}{K} \frac{\sum_k \ell_k^2}{(\sum_i \ell_i)^2} \\
&\leq \frac{(3\Delta_\rho \hat{\rho}_{\max})^2}{K},
\end{aligned} \tag{88}$$

where the last inequality uses $\sum_k \ell_k^2 \leq (\sum_i \ell_i)^2$. Thus

$$\|\boldsymbol{\eta}_{\text{prox}}\|_{\mathbf{p}} \leq \frac{3\Delta_\rho \hat{\rho}_{\max}}{\sqrt{K}}. \tag{89}$$

We next bound the diagonal-approximation error. Define

$$o_k \triangleq \mathbf{g}_k^\top \bar{\mathbf{g}} - \frac{\|\mathbf{g}_k\|^2}{K} = \frac{1}{K} \sum_{i \neq k} G_{ki}, \quad O \triangleq \|\bar{\mathbf{g}}\|^2 - \frac{1}{K^2} \sum_i \|\mathbf{g}_i\|^2 = \frac{1}{K^2} \sum_{i \neq j} G_{ij}. \tag{90}$$

Combining the closed form of g_k^* in Lemma 8(i) with (84) gives

$$\eta_{\text{diag},k} = \tilde{g}_k - g_k^* = -\frac{2o_k}{\bar{\ell}} + \frac{O\ell_k}{\bar{\ell}^2}. \tag{91}$$

By Lemma 9, $|G_{ij}| \leq E_+ \sqrt{\hat{\rho}_i \hat{\rho}_j \ell_i \ell_j}$. Therefore,

$$\begin{aligned}
K|o_k| &\leq \sum_{i \neq k} |G_{ki}| \\
&\leq E_+ \sqrt{\hat{\rho}_k \ell_k} \sum_{i \neq k} \sqrt{\hat{\rho}_i \ell_i} \\
&\leq E_+ \sqrt{\hat{\rho}_k \ell_k} \sqrt{K \sum_i \hat{\rho}_i \ell_i}.
\end{aligned} \tag{92}$$

Taking the maximum over k yields

$$\max_k |o_k| \leq \frac{E_+ \sqrt{\hat{\rho}_{\max} \ell_{\max}} \sum_i \hat{\rho}_i \ell_i}{\sqrt{K}}. \tag{93}$$

Similarly,

$$\begin{aligned}
K^2|O| &\leq \sum_{i \neq j} |G_{ij}| \\
&\leq E_+ \left(\sum_i \sqrt{\hat{\rho}_i \ell_i} \right)^2 \\
&\leq E_+ K \sum_i \hat{\rho}_i \ell_i,
\end{aligned} \tag{94}$$

and therefore

$$|O| \leq \frac{E_+ \sum_i \hat{\rho}_i \ell_i}{K}. \tag{95}$$

Using (91), (93), (95), and $\|\mathbf{v}\|_{\mathbf{p}} \leq \max_k |v_k|$, we get

$$\begin{aligned}
\|\boldsymbol{\eta}_{\text{diag}}\|_{\mathbf{p}} &\leq \frac{2 \max_k |o_k|}{\bar{\ell}} + \frac{|O| \ell_{\max}}{\bar{\ell}^2} \\
&\leq \frac{2E_+ \sqrt{\hat{\rho}_{\max} \ell_{\max}} \sum_i \hat{\rho}_i \ell_i}{\sqrt{K} \bar{\ell}} + \frac{E_+ \ell_{\max} \sum_i \hat{\rho}_i \ell_i}{K \bar{\ell}^2}.
\end{aligned} \tag{96}$$

Combining (89) and (96) gives

$$\|\boldsymbol{\eta}\|_{\mathbf{p}} \leq \alpha_1^{\text{rms}}, \quad (97)$$

where

$$\alpha_1^{\text{rms}} \triangleq \frac{3\Delta_\rho \hat{\rho}_{\max}}{\sqrt{K}} + \frac{2E_+ \sqrt{\hat{\rho}_{\max} \ell_{\max} \sum_i \hat{\rho}_i \ell_i}}{\sqrt{K} \bar{\ell}} + \frac{E_+ \ell_{\max} \sum_i \hat{\rho}_i \ell_i}{K \bar{\ell}^2}. \quad (98)$$

If $\alpha_1^{\text{rms}} = 0$, then $\boldsymbol{\eta} = \mathbf{0}$ and hence $R_1 = 0$, so the desired bound is trivial. Otherwise, applying Young's inequality with $a = \sqrt{\chi^2(\mathbf{q} \parallel \mathbf{p})}$, $b = \|\boldsymbol{\eta}\|_{\mathbf{p}}$, and $\gamma = (\alpha_1^{\text{rms}})^2/2$ gives

$$\begin{aligned} |R_1| &\leq \sqrt{\chi^2(\mathbf{q} \parallel \mathbf{p})} \|\boldsymbol{\eta}\|_{\mathbf{p}} \\ &\leq \frac{\gamma}{2} \chi^2(\mathbf{q} \parallel \mathbf{p}) + \frac{1}{2\gamma} \|\boldsymbol{\eta}\|_{\mathbf{p}}^2 \\ &\leq \frac{(\alpha_1^{\text{rms}})^2}{4} \chi^2(\mathbf{q} \parallel \mathbf{p}) + 1. \end{aligned} \quad (99)$$

This proves the first bound in (80), with $\alpha_1 = (\alpha_1^{\text{rms}})^2/4$, which is exactly (81).

It remains to control R_2 . By Assumption B.4, $D(\mathbf{q}) = \boldsymbol{\ell}^\top \mathbf{q} \geq \ell_{\min} > 0$ on Δ^K , so $\rho(\boldsymbol{\theta}_{\text{ref}}; \mathbf{q})$ is twice continuously differentiable on the simplex. The second-order Taylor remainder gives

$$|R_2| \leq \frac{M}{2} \|\mathbf{q} - \mathbf{p}\|^2 = \frac{M}{2K} \chi^2(\mathbf{q} \parallel \mathbf{p}), \quad M \triangleq \sup_{\mathbf{q} \in \Delta^K} \|\nabla_{\mathbf{q}}^2 \rho(\boldsymbol{\theta}_{\text{ref}}; \mathbf{q})\|_{\text{op}}. \quad (100)$$

We now bound M . By Lemma 10,

$$\nabla_{\mathbf{q}}^2 \rho = \frac{1}{D(\mathbf{q})} \left[2G - \boldsymbol{\ell}(\nabla \rho)^\top - (\nabla \rho) \boldsymbol{\ell}^\top \right], \quad (101)$$

which implies

$$\|\nabla_{\mathbf{q}}^2 \rho\|_{\text{op}} \leq \frac{2\|G\|_{\text{op}} + 2\|\boldsymbol{\ell}\| \|\nabla \rho\|}{D(\mathbf{q})}. \quad (102)$$

For any $\mathbf{q} \in \Delta^K$,

$$\rho(\boldsymbol{\theta}_{\text{ref}}; \mathbf{q}) = \frac{\mathbf{q}^\top G \mathbf{q}}{D(\mathbf{q})} \leq \frac{\|G\|_{\text{op}} \|\mathbf{q}\|^2}{\ell_{\min}} \leq \frac{\|G\|_{\text{op}}}{\ell_{\min}}, \quad (103)$$

where we used $\|\mathbf{q}\|^2 \leq \sum_k q_k = 1$. Since $\nabla \rho = (2G\mathbf{q} - \rho\boldsymbol{\ell})/D(\mathbf{q})$,

$$\|\nabla \rho\| \leq \frac{2\|G\|_{\text{op}} \|\mathbf{q}\| + \rho \|\boldsymbol{\ell}\|}{D(\mathbf{q})} \leq \frac{\|G\|_{\text{op}}}{\ell_{\min}} \left(2 + \frac{\|\boldsymbol{\ell}\|}{\ell_{\min}} \right). \quad (104)$$

Substituting (104) into (102) and using $D(\mathbf{q}) \geq \ell_{\min}$ gives

$$\|\nabla_{\mathbf{q}}^2 \rho\|_{\text{op}} \leq \frac{2\|G\|_{\text{op}}}{\ell_{\min}} \left(1 + \frac{\|\boldsymbol{\ell}\|}{\ell_{\min}} \right)^2. \quad (105)$$

By Lemma 9,

$$\|G\|_{\text{op}} \leq \|G\|_F \leq E_+ \sqrt{\sum_{i,j} \hat{\rho}_i \hat{\rho}_j \ell_i \ell_j} = E_+ \sum_i \hat{\rho}_i \ell_i. \quad (106)$$

Together with $\|\boldsymbol{\ell}\| \leq \sqrt{K} \ell_{\max}$, this yields

$$M \leq \frac{2E_+ \sum_i \hat{\rho}_i \ell_i}{\ell_{\min}} \left(1 + \frac{\sqrt{K} \ell_{\max}}{\ell_{\min}} \right)^2. \quad (107)$$

Substituting (107) into (100) gives

$$|R_2| \leq \alpha_2 \chi^2(\mathbf{q} \parallel \mathbf{p}),$$

with α_2 as in (82). This proves the second bound in (80) and completes the proof. \square

Remark 8 (Operational meaning of α_1^{rms}). The quantity α_1^{rms} defined in (98) is a \mathbf{p} -weighted RMS bound on the surrogate error:

$$\sqrt{\frac{1}{K} \sum_{k=1}^K |\hat{g}_k - g_k^*|^2} = \|\hat{\mathbf{g}} - \mathbf{g}^*\|_{\mathbf{p}} \leq \alpha_1^{\text{rms}}. \quad (108)$$

The constant $\alpha_1 = (\alpha_1^{\text{rms}})^2/4$ in (81) is the coefficient obtained after absorbing the square-root residual into the χ^2 term through Young's inequality. This is an aggregate bound rather than a per-coordinate one: in the worst case, an individual error $|\hat{g}_k - g_k^*|$ can be as large as $\sqrt{K} \alpha_1^{\text{rms}}$. The use of the RMS norm is natural here because the Cauchy–Schwarz step in (83) pairs $\sqrt{\chi^2(\mathbf{q} \parallel \mathbf{p})}$ with $\|\boldsymbol{\eta}\|_{\mathbf{p}}$.

B.6 Proof of Theorem 1 (LARK Objective)

This subsection states and proves the formal version of Theorem 1. The informal statement in the main text asserts the existence of finite constants $\alpha > 0$ and $C \in \mathbb{R}$, independent of the optimization variable \mathbf{q} , realizing a χ^2 -regularized lower bound on the learnability improvement; the formal version below makes both constants explicit in terms of the constants α_1, α_2 from Lemma 12.

Theorem 2 (Formal version of Theorem 1). *Under Assumptions B.1–B.4, for every $\mathbf{q} \in \Delta^K$,*

$$\rho(\boldsymbol{\theta}_{\text{ref}}; \mathbf{q}) - \rho(\boldsymbol{\theta}_{\text{ref}}; \mathbf{p}) \geq \langle \mathbf{q} - \mathbf{p}, \hat{\mathbf{g}} \rangle - \alpha \chi^2(\mathbf{q} \parallel \mathbf{p}) + C, \quad (109)$$

where

$$\alpha \triangleq \alpha_1 + \alpha_2 > 0, \quad C \triangleq -1, \quad (110)$$

and $\alpha_1, \alpha_2 > 0$ are the explicit constants given by Lemma 12. In particular, α and C are independent of \mathbf{q} .

Proof. By Lemma 8(iii), the change in ρ admits the exact decomposition

$$\rho(\boldsymbol{\theta}_{\text{ref}}; \mathbf{q}) - \rho(\boldsymbol{\theta}_{\text{ref}}; \mathbf{p}) = \langle \mathbf{q} - \mathbf{p}, \hat{\mathbf{g}} \rangle + R_1 + R_2. \quad (111)$$

By Lemma 12, the two residuals satisfy

$$|R_1| \leq \alpha_1 \chi^2(\mathbf{q} \parallel \mathbf{p}) + 1, \quad |R_2| \leq \alpha_2 \chi^2(\mathbf{q} \parallel \mathbf{p}), \quad (112)$$

where $\alpha_1, \alpha_2 > 0$ are given by (81) and (82), respectively. Combining (111) and (112) gives

$$\begin{aligned} \rho(\boldsymbol{\theta}_{\text{ref}}; \mathbf{q}) - \rho(\boldsymbol{\theta}_{\text{ref}}; \mathbf{p}) &\stackrel{(a)}{=} \langle \mathbf{q} - \mathbf{p}, \hat{\mathbf{g}} \rangle + R_1 + R_2 \\ &\stackrel{(b)}{\geq} \langle \mathbf{q} - \mathbf{p}, \hat{\mathbf{g}} \rangle - |R_1| - |R_2| \\ &\stackrel{(c)}{\geq} \langle \mathbf{q} - \mathbf{p}, \hat{\mathbf{g}} \rangle - (\alpha_1 \chi^2(\mathbf{q} \parallel \mathbf{p}) + 1) - \alpha_2 \chi^2(\mathbf{q} \parallel \mathbf{p}) \\ &\stackrel{(d)}{=} \langle \mathbf{q} - \mathbf{p}, \hat{\mathbf{g}} \rangle - (\alpha_1 + \alpha_2) \chi^2(\mathbf{q} \parallel \mathbf{p}) - 1, \end{aligned} \quad (113)$$

where (a) is (111); (b) uses $R_1, R_2 \geq -|R_1|, -|R_2|$; (c) substitutes the bounds (112) from Lemma 12; and (d) collects the two χ^2 terms. Identifying $\alpha = \alpha_1 + \alpha_2$ and $C = -1$ as in (110) yields (109). \square

Remark 9 (Correspondence with the informal constants α and C). Theorem 2 instantiates the informal constants α, C of Theorem 1 as $\alpha = \alpha_1 + \alpha_2$ and $C = -1$, where α_1, α_2 are the forward-computable constants from Lemma 12. The resulting bound depends on \mathbf{q} only through the linear term $\langle \mathbf{q} - \mathbf{p}, \hat{\mathbf{g}} \rangle$ and the χ^2 regularization. Since $C = -1$ is independent of \mathbf{q} , it does not affect the maximizer of the right-hand side over Δ^K . The coefficient α motivates the use of a χ^2 penalty; in the fixed-budget selection rule of Section 4.3, the penalty temperature is calibrated as $\tau(B)$ so that the optimizer has exactly B active trajectories.

B.7 Proof of Lemma 3 (B -Parameterized Closed Form)

Theorem 2 motivates a χ^2 -regularized linear surrogate. In the fixed-budget setting, we calibrate the regularization temperature so that the optimizer has exactly B active coordinates. By the equivalence (77) between the χ^2 -divergence and the squared Euclidean distance under the uniform prior, the corresponding objective can be written as

$$\hat{\mathbf{q}} = \arg \max_{\mathbf{q} \in \Delta^K} \left\{ \langle \mathbf{q} - \mathbf{p}, \hat{\mathbf{g}} \rangle - \frac{\tau K}{2} \|\mathbf{q} - \mathbf{p}\|^2 \right\}, \quad (114)$$

where we write τ for the temperature to be chosen as a function of the budget B .

Proof of Lemma 3. The objective (114) is strictly concave in \mathbf{q} whenever $\tau K > 0$, so the KKT conditions characterize its unique global maximizer over Δ^K . Introduce a Lagrange multiplier $\lambda \in \mathbb{R}$ for the equality constraint $\sum_k q_k = 1$ and KKT multipliers $\mu_k \geq 0$ for the non-negativity constraints $q_k \geq 0$. The Lagrangian is

$$\mathcal{L}(\mathbf{q}, \lambda, \boldsymbol{\mu}) = \langle \mathbf{q} - \mathbf{p}, \hat{\mathbf{g}} \rangle - \frac{\tau K}{2} \|\mathbf{q} - \mathbf{p}\|^2 - \lambda \left(\sum_k q_k - 1 \right) + \sum_k \mu_k q_k. \quad (115)$$

Stationarity and complementary slackness give

$$\hat{g}_k - \tau K(q_k - p_k) - \lambda + \mu_k = 0, \quad \mu_k q_k = 0, \quad \mu_k \geq 0. \quad (116)$$

Since $p_k = 1/K$, these conditions imply the projection form

$$\hat{q}_k = \left[\frac{1}{K} + \frac{\hat{g}_k - \lambda}{\tau K} \right]_+, \quad (117)$$

where $[x]_+ = \max\{x, 0\}$. The threshold λ is determined by the normalization condition $\sum_k \hat{q}_k = 1$.

Sort the scores as $\hat{g}_{(1)} \geq \hat{g}_{(2)} \geq \dots \geq \hat{g}_{(K)}$, where (i) denotes the sorted index. From (117), $\hat{q}_{(i)} > 0$ if and only if $\hat{g}_{(i)} > \lambda - \tau$. Thus an active set of size B is obtained whenever

$$\hat{g}_{(B)} > \lambda - \tau \geq \hat{g}_{(B+1)}. \quad (118)$$

Under the assumption $\hat{g}_{(B)} > \hat{g}_{(B+1)}$, the top- B active set is well-defined. We choose the boundary value

$$\lambda = \hat{g}_{(B+1)} + \tau, \quad (119)$$

which makes the $(B+1)$ -st coordinate exactly inactive while keeping the first B coordinates positive.

Substituting (119) into (117), for every $i \leq B$ we obtain

$$\begin{aligned} \hat{q}_{(i)} &= \frac{1}{K} + \frac{\hat{g}_{(i)} - \hat{g}_{(B+1)} - \tau}{\tau K} \\ &= \frac{\hat{g}_{(i)} - \hat{g}_{(B+1)}}{\tau K}. \end{aligned} \quad (120)$$

For $i > B$, the projection in (117) gives $\hat{q}_{(i)} = 0$. Imposing the simplex normalization on the active coordinates gives

$$1 = \sum_{i=1}^B \hat{q}_{(i)} = \frac{1}{\tau K} \sum_{i=1}^B (\hat{g}_{(i)} - \hat{g}_{(B+1)}). \quad (121)$$

Therefore the budget-calibrated temperature is

$$\tau^*(B) = \frac{1}{K} \sum_{i=1}^B (\hat{g}_{(i)} - \hat{g}_{(B+1)}), \quad (122)$$

which is positive because $\hat{g}_{(B)} > \hat{g}_{(B+1)}$. Substituting (122) into (120) yields

$$\hat{q}_{(i)} = \frac{\hat{g}_{(i)} - \hat{g}_{(B+1)}}{\sum_{j=1}^B (\hat{g}_{(j)} - \hat{g}_{(B+1)})} \quad \text{for } i \leq B, \quad \hat{q}_{(i)} = 0 \quad \text{for } i > B. \quad (123)$$

This is the closed-form B -parameterized weighting rule stated in Lemma 3. \square

B.8 Theoretical and Empirical Validation of the Surrogate $\hat{\mathbf{g}}$

The forward-pass surrogate $\hat{\mathbf{g}}$ is the central computational shortcut underlying the LARK algorithm: it replaces the exact directional derivative $\mathbf{g}^* = \nabla_{\mathbf{q}} \rho(\boldsymbol{\theta}_{\text{ref}}; \mathbf{q})|_{\mathbf{q}=\mathbf{p}}$, whose evaluation requires one backward pass per candidate trajectory, with a quantity computable from forward passes alone. This subsection studies the relationship between $\hat{\mathbf{g}}$ and \mathbf{g}^* from two complementary perspectives: a theoretical RMS error bound and an empirical comparison on real student models.

B.8.1 Theoretical Error Bound

The bounds derived in Appendix B.5 immediately yield a quantitative bound on $\|\hat{\mathbf{g}} - \mathbf{g}^*\|$ in the \mathbf{p} -weighted norm $\|\mathbf{v}\|_{\mathbf{p}}^2 \triangleq K^{-1} \sum_k v_k^2$.

Corollary 3 (\mathbf{p} -weighted RMS error of $\hat{\mathbf{g}}$). *Under Assumptions B.1–B.4,*

$$\|\hat{\mathbf{g}} - \mathbf{g}^*\|_{\mathbf{p}} = \sqrt{\frac{1}{K} \sum_{k=1}^K |\hat{g}_k - g_k^*|^2} \leq \alpha_1^{\text{rms}}, \quad (124)$$

where α_1^{rms} is the RMS upper bound from (98), given by

$$\alpha_1^{\text{rms}} = \underbrace{\frac{3\Delta_\rho \hat{\rho}_{\max}}{\sqrt{K}}}_{\text{proxy term}} + \underbrace{\frac{2E_+ \sqrt{\hat{\rho}_{\max} \ell_{\max} \sum_i \hat{\rho}_i \ell_i}}{\sqrt{K} \bar{\ell}}}_{\text{off-diagonal Gram term}} + \underbrace{\frac{E_+ \ell_{\max} \sum_i \hat{\rho}_i \ell_i}{K \bar{\ell}^2}}_{\text{aggregate off-diagonal term}}. \quad (125)$$

The constant α_1 in Lemma 12 is recovered as $\alpha_1 = (\alpha_1^{\text{rms}})^2/4$.

Proof. By the triangle inequality, $\|\hat{\mathbf{g}} - \mathbf{g}^*\|_{\mathbf{p}} \leq \|\boldsymbol{\eta}_{\text{prox}}\|_{\mathbf{p}} + \|\boldsymbol{\eta}_{\text{diag}}\|_{\mathbf{p}}$, where $\boldsymbol{\eta}_{\text{prox}}$ and $\boldsymbol{\eta}_{\text{diag}}$ are defined in the proof of Lemma 12. Combining the bounds in (89) and (96) gives (124), with α_1^{rms} given by (125). \square

The three terms in (125) correspond to the three sources of surrogate error. The first term, $3\Delta_\rho \hat{\rho}_{\max}/\sqrt{K}$, is the proxy-substitution error: it comes from replacing the exact per-trajectory rates ρ_i^* in the closed form of g_k^* by the forward-pass proxies $\hat{\rho}_i$. Its size is controlled by Δ_ρ , which measures the multiplicative gap between ρ_i^* and $\hat{\rho}_i$ in Lemma 11. The second term, $2E_+ \sqrt{\hat{\rho}_{\max} \ell_{\max} \sum_i \hat{\rho}_i \ell_i}/(\sqrt{K} \bar{\ell})$, controls the per-coordinate off-diagonal Gram residual $o_k = \mathbf{g}_k^\top \bar{\mathbf{g}} - \|\mathbf{g}_k\|^2/K$, which is ignored by the diagonal approximation $\mathbf{g}_k^\top \bar{\mathbf{g}} \approx \|\mathbf{g}_k\|^2/K$. The third term, $E_+ \ell_{\max} \sum_i \hat{\rho}_i \ell_i/(K \bar{\ell}^2)$, controls the aggregate off-diagonal mass $O = \|\bar{\mathbf{g}}\|^2 - K^{-2} \sum_i \|\mathbf{g}_i\|^2$ left over by the approximation $\|\bar{\mathbf{g}}\|^2 \approx K^{-2} \sum_i \|\mathbf{g}_i\|^2$. The latter two terms are small when the per-trajectory gradients are close to orthogonal in parameter space.

The bound in (124) is an aggregate RMS bound across the K candidates, not a per-coordinate guarantee. By the equivalence of finite-dimensional norms,

$$\max_{k \in [K]} |\hat{g}_k - g_k^*| \leq \sqrt{\sum_{k=1}^K |\hat{g}_k - g_k^*|^2} = \sqrt{K} \|\hat{\mathbf{g}} - \mathbf{g}^*\|_{\mathbf{p}} \leq \sqrt{K} \alpha_1^{\text{rms}}. \quad (126)$$

Thus a single coordinate can have a larger error in the worst case, while the RMS error remains controlled. This RMS norm is the relevant quantity for the residual analysis because the Cauchy–Schwarz step in (83) naturally pairs $\sqrt{\chi^2(\mathbf{q}|\mathbf{p})}$ with $\|\boldsymbol{\eta}\|_{\mathbf{p}}$.

B.8.2 Empirical Correlation between $\hat{\mathbf{g}}$ and \mathbf{g}^*

The bound in Corollary 3 is a worst-case guarantee whose constants depend on the structural quantities of Lemma 11. We complement this analysis by directly measuring how well $\hat{\mathbf{g}}$ tracks \mathbf{g}^* on a real student model.

We sample 50 questions uniformly from the candidate pool described in Appendix C.1. For each question, we compute both the LARK surrogate \hat{g}_k and the exact directional derivative $g_k^* = \partial \rho(\boldsymbol{\theta}_{\text{ref}}; \mathbf{q})/\partial q_k|_{\mathbf{q}=\mathbf{p}}$. The exact derivative is obtained by one full-parameter backward pass per

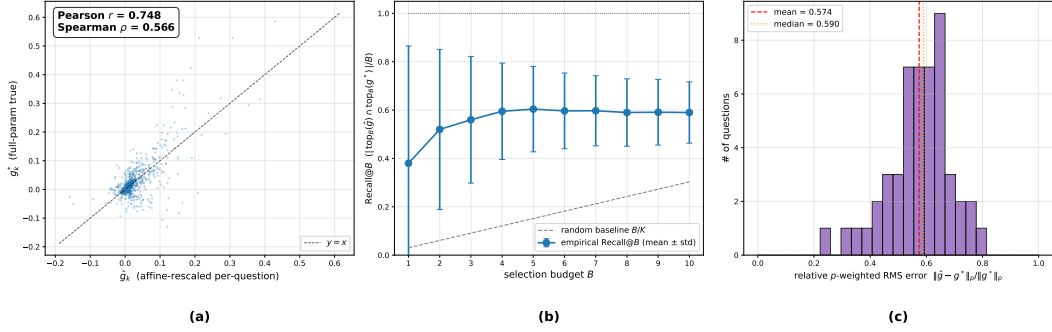


Figure 6: **Empirical correlation between $\hat{\mathbf{g}}$ and \mathbf{g}^* on Qwen-2.5-7B.** (a) Per-question affine-rescaled \hat{g}_k versus exact g_k^* across 50×33 candidates; pooled Pearson $r = 0.748$ and Spearman $\rho = 0.566$. (b) Recall@ B between the top- B rankings of $\hat{\mathbf{g}}$ and \mathbf{g}^* as a function of selection budget B ; the dashed gray line is the random baseline B/K . (c) Histogram of per-question relative \mathbf{p} -weighted RMS error $\|\hat{\mathbf{g}} - \mathbf{g}^*\|_{\mathbf{p}} / \|\mathbf{g}^*\|_{\mathbf{p}}$ across the 50 verification questions; mean 0.574, median 0.590.

candidate trajectory at the anchor model θ_{ref} (Qwen-2.5-7B), rather than by a low-rank or kernel approximation. Across 50 questions and $K = 33$ candidates per question, this produces 1,650 paired values (\hat{g}_k, g_k^*) . To compare values across questions, we apply a per-question affine rescaling that aligns the mean and scale of \hat{g}_k with those of g_k^* . This rescaling preserves within-question rankings and therefore does not affect Recall@ B .

We report three metrics. First, we compute pooled Pearson r and Spearman ρ between the rescaled \hat{g}_k and g_k^* to measure scalar agreement. Second, because LARK uses $\hat{\mathbf{g}}$ primarily through its top- B ranking, we report $\text{Recall@}B \triangleq |\text{top}_B(\hat{\mathbf{g}}) \cap \text{top}_B(\mathbf{g}^*)|/B$ averaged over questions for $B \in \{1, \dots, 10\}$, with random baseline B/K . Third, we report the per-question relative \mathbf{p} -weighted RMS error $\|\hat{\mathbf{g}} - \mathbf{g}^*\|_{\mathbf{p}} / \|\mathbf{g}^*\|_{\mathbf{p}}$, matching the norm used in Corollary 3.

Figure 6(a) shows a clear positive relationship between \hat{g}_k and g_k^* , with pooled Pearson $r = 0.748$ and Spearman $\rho = 0.566$. This indicates that the surrogate captures a substantial portion of the scalar variation in g_k^* after per-question affine rescaling, while the remaining gap is consistent with the off-diagonal Gram interactions omitted by the diagonal approximation in (125).

The ranking agreement is also substantially above chance. As shown in Figure 6(b), Recall@1 ≈ 0.38 , far above the random baseline $1/K \approx 0.03$. At the main experimental budget $B = 3$, Recall@3 ≈ 0.56 , compared with the random baseline $3/K \approx 0.09$. The recall remains around 0.6 for larger budgets, indicating that $\hat{\mathbf{g}}$ preserves meaningful top- B ranking information for the selection rule used by LARK. The error bars also show nontrivial question-level variation, so this result should be interpreted as strong aggregate alignment rather than a perfect per-question match.

Figure 6(c) shows that the relative \mathbf{p} -weighted RMS error concentrates around 0.6 (mean 0.574, median 0.590), which is far below the loose worst-case per-coordinate factor $\sqrt{K} \approx 5.7$ allowed by (126). The empirical error is therefore much smaller than the theoretical worst case, as expected in non-adversarial candidate pools.

Overall, these diagnostics support the use of $\hat{\mathbf{g}}$ as a forward-pass surrogate for top- B trajectory selection. The surrogate is not a high-precision coordinate-wise estimator of \mathbf{g}^* , but it is positively aligned with \mathbf{g}^* at the scalar level and preserves useful top- B ranking information. This is the operative notion of agreement for LARK, since the closed-form selection rule in Lemma 3 depends on the top- B ordering and the score margins above the threshold, rather than on the exact magnitude of every coordinate. The empirical results therefore support the computational tradeoff made by LARK: avoiding K full-parameter backward passes per question while retaining the ranking signal needed for downstream selection.

C Experimental Details

C.1 Candidate Pool

We adopt the trajectory candidate pool released by Yang et al. [2026] without modification. The pool consists of 5,000 mathematical reasoning problems sampled from NuminaMath [Li et al., 2024], each paired with 33 reasoning trajectories produced by 11 teacher models with 3 independent rollouts per teacher. All selection methods in our experiments—including LARK and every baseline in Appendix C.2—operate on this identical pool, so any difference in downstream performance is attributable to the selection rule rather than to differences in the underlying candidate set.

Teacher pool. The 11 teacher models span a range of scales and model families, including both proprietary and open-weight reasoning models: GPT-OSS-20B, GPT-OSS-120B, Phi-4-R+, QwQ-32B, DeepSeek-R1, Qwen3-235B, Qwen3-30B, Qwen3-8B, Qwen3-4B, Nemotron, and Magistral-S. For each (problem, teacher) pair, three independent rollouts are generated, yielding $11 \times 3 = 33$ trajectories per problem. We refer the reader to Yang et al. [2026] for the full inference configuration of each teacher (decoding temperature, top- p , maximum generation length).

Correctness filtering. Every trajectory retained in the pool has been verified to reach the correct final answer under the extraction rule of Yang et al. [2026], which matches the rule described in Appendix C.4. Trajectories whose final answer disagrees with the ground truth are not included. As a result, all 33 candidates for each problem are *correct* reasoning trajectories that nonetheless differ in reasoning style, length, and student-side learnability—a setting that isolates the selection problem from the orthogonal question of correctness verification.

C.2 Trajectory Selection Baselines

We compare LARK against the seven baselines reported in Table 1. Throughout this subsection, let \mathbf{x} denote the prompt (system and user turns), and let $\{\mathbf{y}_k\}_{k=1}^K$ with $K = 33$ denote the candidate trajectories for \mathbf{x} in the pool $\mathcal{C}(\mathbf{x})$ described in Appendix C.1. Each trajectory has length $|a_k|$, with t -th token y_t^k , predictive distribution $\pi_t^k = \pi_\theta(\cdot \mid \mathbf{x}, \mathbf{y}_{<t}^k) \in \Delta^{|\mathcal{V}|}$ under the student π_θ , ground-truth one-hot $\delta(y_t^k) \in \Delta^{|\mathcal{V}|}$, and length-normalized cross-entropy $\ell_k = \frac{1}{|a_k|} \sum_{t=1}^{|a_k|} -\log \pi_t^k(y_t^k)$. Each baseline assigns a scalar score to every candidate \mathbf{y}_k and selects the top- B trajectories under that score with uniform weights $1/B$; LARK instead applies its closed-form χ^2 - B rule to obtain non-uniform weights.

Random. We sample one trajectory uniformly at random from $\{\mathbf{y}_k\}_{k=1}^K$:

$$\mathbf{y}^* \sim \text{Uniform}(\{\mathbf{y}_k\}_{k=1}^K).$$

For $B > 1$, we sample B trajectories without replacement.

Token Length_{max}. We score each candidate by its token length and select the longest:

$$\text{score}_{\text{len}}(\mathbf{y}_k) \triangleq |a_k|, \quad \mathbf{y}^* = \arg \max_{k \in [K]} \text{score}_{\text{len}}(\mathbf{y}_k).$$

Rule-based Quality_{max} (LIMO-style). We implement a lightweight heuristic inspired by LIMO-style filtering [Ye et al., 2025], combining four indicators computed from the assistant text of \mathbf{y}_k : (i) elaborated reasoning (total word length), (ii) self-verification (frequency of “check” and “verify”), (iii) exploratory approach (frequency of “perhaps” and “might”), (iv) adaptive granularity (frequency of “therefore” and “since”). For each candidate, the frequency of each keyword group is normalized by the total word count. We z -score each indicator across the K candidates within the same pool and take a weighted sum:

$$\text{score}_{\text{rule}}(\mathbf{y}_k) = 0.30 \cdot z(\text{len}) + 0.20 \cdot z(\text{selfver}) + 0.25 \cdot z(\text{explore}) + 0.25 \cdot z(\text{granularity}),$$

where $z(\cdot)$ denotes within-pool z -scoring. We select $\mathbf{y}^* = \arg \max_{k \in [K]} \text{score}_{\text{rule}}(\mathbf{y}_k)$.

LLM-judged Quality_{max}. We use Qwen3-32B-Instruct [Yang et al., 2025] as a judge model in non-thinking mode. Given $(\mathbf{x}, \mathbf{y}_k)$, the judge outputs a JSON object with an `overall_score` $s_{\text{judge}}(\mathbf{y}_k) \in [0, 1]$ and a textual `overall_reason`. We select $\mathbf{y}^* = \arg \max_{k \in [K]} s_{\text{judge}}(\mathbf{y}_k)$. The verbatim judge prompt is given below.

Judge Prompt: LLM-as-a-Judge for Trajectory Quality

You are a meticulous and highly critical evaluator of AI reasoning. Your primary goal is to identify and quantify subtle flaws, logical gaps, inefficiencies, and hidden assumptions. Do not default to a high score. Your starting assumption should be critical, and you must rigorously justify every point awarded.

First, please carefully read the following problem statement: <Problem> {question} </Problem>

Now, please carefully read the following candidate’s chain-of-thought reasoning: <Reasoning> {reasoning_to_evaluate} </Reasoning>

When evaluating this reasoning, you must adhere to the following five key evaluation criteria and the scoring rubric below.

Scoring Guidelines and Calibration: You must use the full 0.0 to 1.0 scale. Scores should not be clustered at the top. Use this rubric to anchor your scores:

1.0 (Exceptional/Flawless): Reserved for reasoning that is not only correct but also elegant, insightful, and comprehensive. It is perfectly structured and leaves no room for doubt. This score should be exceedingly rare.

0.8 - 0.9 (Excellent but Imperfect): The core reasoning is valid and well-supported, but there may be very minor, superficial issues (e.g., a trivial typo in a formula that doesn’t affect the outcome, a slightly awkward phrasing). The conclusion is unaffected.

0.5 - 0.7 (Competent but Flawed): The reasoning is generally on the right track but contains noticeable and non-trivial flaws.

0.2 - 0.4 (Poor): The reasoning contains fundamental flaws that largely invalidate the process or conclusion.

0.0 - 0.1 (Unacceptable): The reasoning is completely incorrect, irrelevant, nonsensical, or makes no meaningful attempt to solve the problem.

Evaluation Criteria: Factual Accuracy, Logical Rigor, Solution Completeness, Reasoning Efficiency, Presentation Quality.

For each criterion, give a score from 0.0 to 1.0 (in 0.1 increments) and a brief justification in JSON.

Your output must be a single, valid JSON object with:

```
{
  "dimensional_evaluation": {...},
  "overall_score": <float between 0.0 and 1.0>,
  "overall_reason": "<concise summary>"
}
```

Global Naturalness (GRAPE)_{max} [Zhang et al., 2025a]. GRAPE scores each candidate by the average log-likelihood assigned to its tokens by the student under teacher forcing, equivalently the negative length-normalized cross-entropy:

$$\text{score}_{\text{GRAPE}}(\mathbf{y}_k) \triangleq -\ell_k = \frac{1}{|a_k|} \sum_{t=1}^{|a_k|} \log \pi_t^k(y_t^k).$$

We select $\mathbf{y}^* = \arg \max_{k \in [K]} \text{score}_{\text{GRAPE}}(\mathbf{y}_k)$, which is equivalent to selecting the trajectory of *minimum* length-normalized cross-entropy under the student.

Local Naturalness_{max} [Just et al., 2025]. We follow the Local Naturalness metric. Each trajectory is split into J_k sentence-level steps $\mathbf{y}_k = (\mathbf{s}_1, \dots, \mathbf{s}_{J_k})$, where each \mathbf{s}_j is a contiguous sub-sequence of tokens. With local context size m (we use $m = 4$), we compute

$$\text{score}_{\text{local}}(\mathbf{y}_k) \triangleq \frac{1}{J_k} \sum_{j=1}^{J_k} \left(\frac{1}{|\mathbf{s}_j|} \sum_{u=1}^{|\mathbf{s}_j|} \log \pi_{\theta}(s_{j,u} \mid \mathbf{x}, \mathbf{s}_{j-m:j-1}, \mathbf{s}_{j,<u}) \right),$$

where $\mathbf{s}_{j-m:j-1}$ denotes up to m immediately preceding steps and $s_{j,u}$ is the u -th token of step \mathbf{s}_j . We select $\mathbf{y}^* = \arg \max_{k \in [K]} \text{score}_{\text{local}}(\mathbf{y}_k)$. Unlike GRAPE, this score requires $m + 1$ forward passes per trajectory (one per masked-context rollout); see Appendix D.1.

Rank-Surprisal Ratio (RSR)_{min} [Yang et al., 2026]. RSR computes token-level surprisal and rank under the student. For each token y_t^k with context $\mathbf{c}_t^k = (\mathbf{x}, \mathbf{y}_{<t}^k)$, define the surprisal and rank as

$$s_t^k \triangleq -\log \pi_t^k(y_t^k), \quad r_t^k \triangleq 1 + \sum_{v \in \mathcal{V}} \mathbb{I}[\pi_{\theta}(v \mid \mathbf{c}_t^k) > \pi_t^k(y_t^k)].$$

Ranks are clipped at r_{\max} (we use $r_{\max} = 100$): $\bar{r}_t^k \triangleq \min(r_t^k, r_{\max})$. The trajectory-level score is

$$\text{score}_{\text{RSR}}(\mathbf{y}_k) \triangleq \frac{\sum_{t=1}^{|\mathcal{a}_k|} \bar{r}_t^k}{\sum_{t=1}^{|\mathcal{a}_k|} s_t^k}, \quad \mathbf{y}^* = \arg \min_{k \in [K]} \text{score}_{\text{RSR}}(\mathbf{y}_k).$$

Surprisal and clipped rank are computed from a single forward pass; clipping at r_{\max} avoids the $O(|\mathcal{V}|)$ full sort while remaining exact (Appendix C.3).

C.3 Implementation Details

SFT training. We use a single hyperparameter recipe across all three students (Qwen-2.5-7B, Qwen-2.5-1.5B, Llama-3.2-3B) and across all selection methods, so that any difference in downstream performance can be attributed to the selection rule rather than to per-method training tuning. Each student is fine-tuned with full-parameter SFT under the following configuration:

- **Maximum sequence length:** 32,768 tokens, kept identical across selection scoring, SFT, and evaluation; trajectories exceeding this length (less than 1% of the pool) are truncated from the right.
- **Learning rate:** 1.0×10^{-5} for the main 5,000-trajectory experiments and 5.0×10^{-6} for the 500-trajectory verification of Condition 1 in Appendix A.3, linearly scaled to the smaller dataset to avoid early-step instability.
- **Effective global batch size:** 64 trajectories, realized as 8 GPUs \times per-device batch 1 \times gradient accumulation 8.
- **Epochs:** 5.
- **Optimizer:** AdamW (PyTorch implementation) with default $(\beta_1, \beta_2, \varepsilon) = (0.9, 0.999, 10^{-8})$ and weight decay 0.
- **Learning-rate schedule:** cosine decay with linear warm-up over the first 5% of total steps.
- **Gradient clipping:** max-norm 1.0, delegated to DeepSpeed via `gradient_clipping: auto`.
- **Precision:** bf16 mixed precision throughout, with fp32 communication for ZeRO collectives. We disable bf16 reduced-precision matmul accumulation (`torch.backends.cuda.matmul.allow_bf16_reduced_precision_reduction = False`) to suppress occasional NaN gradients in the LM-head backward on A100; fp16 is never used.
- **Memory and throughput optimizations:** non-reentrant gradient checkpointing, FlashAttention-2, sequence packing with greedy bin-packing and `reset_position_ids`, and Liger fused kernels (RoPE, RMSNorm, SwiGLU). The fused linear-CE kernel is disabled because it is incompatible with sequence packing.

Software stack. Training and inference run inside a single conda environment with PyTorch 2.9.1 (CUDA 12.8), Transformers 4.57.1, PEFT 0.18.0, FlashAttention 2.8.3, Liger-Kernel, and DeepSpeed. Distributed training is launched via `torchrun -nproc_per_node=8` on top of the HuggingFace Trainer, using DeepSpeed ZeRO Stage 2 (`zero2_bf16.json: stage 2, communication_data_type fp32, reduce/allgather_bucket_size = 5 \times 10^8`). Under ZeRO-2, optimizer states and gradients are sharded across the 8 GPUs while parameters are replicated, which is sufficient for the $\leq 8\text{B}$ -parameter students considered. Evaluation uses vLLM 0.15.0 for batched multi-sample decoding, with SGLang 0.5.9 available as a fallback engine.

Hardware and wall-clock. All experiments run on a single node with $8 \times$ NVIDIA A100 80GB (SXM4) GPUs. Each 5,000-trajectory SFT run completes in roughly 3–5 hours depending on the student size, and each 500-trajectory verification run for Appendix D.2 completes in about 25–45 minutes. Aggregating across 3 students, 7 selection baselines (Appendix C.2), and the LARK ablation grid ($\text{top-}B \in \{1, 3, 5, 10\}$ together with χ^2 - and KL-tempered weighting variants), the total training budget is approximately 1,600 A100-hours. Evaluation is sharded across the same 8 GPUs with `tensor_parallel_size=1` per shard, with generations merged across shards afterwards, adding on average ~ 15 minutes per (student, benchmark) pair.

Prompt consistency and truncation. A single chat template is applied throughout the pipeline. The same `tokenizer.apply_chat_template` call is used for (i) selection-time scoring (when computing the forward-pass quantities $\hat{\rho}_k$ and \hat{g}_k on candidate trajectories under θ_{ref}), (ii) SFT example construction (masking out the system and user turns so that only the assistant turn contributes to the loss), and (iii) evaluation prompting (generation prompt appended via `add_generation_prompt=True`). All three stages truncate to the same 32,768-token limit. The reasoning instruction "Please reason step by step, and put your final answer within `\boxed{\}`" is held fixed across selection, training, and evaluation, ensuring that selection scores measured on θ_{ref} remain meaningful for the fine-tuned model under matched prompting.

Reproducibility. We fix the global seed to 42 for random, numpy, and torch in all selection-scoring and Condition 1 verification experiments, and rely on the HuggingFace Trainer default seed of 42 for SFT. All headline numbers in Table 1 are reported as the mean \pm standard deviation over 3 independent evaluation runs that differ only in the sampling seed of the inference engine, with decoding hyperparameters `temperature= 0.6`, `top_p= 0.95`, `repetition_penalty= 1.1`, and maximum generation length 32,768, evaluated under ACC@5 with 5 samples per problem (Appendix C.4). To facilitate reproduction we will release, under an MIT licence, the full training code, the YAML configuration files (`train/configs/sft_full.yaml`, `train/configs/sft_full_500.yaml`, `train/configs/zero2_bf16.json`), the precomputed per-trajectory scores (`data/Q1/<student>/grape_g/scores.json`), and the selection rules used in each ablation.

C.4 Evaluation Protocol

Benchmarks. We evaluate on the same four reasoning benchmarks reported in Section 5.1, which span competition mathematics, grade-level mathematics, and graduate-level science: AIME-2024 [aop, 2024] (30 problems from the 2024 American Invitational Mathematics Examination), AMC [Mathematical Association of America, 2025] (83 problems from the American Mathematics Competitions), MATH-500 [Hendrycks et al., 2021] (500 problems sampled from the MATH test set, which covers algebra, geometry, number theory, probability, and precalculus), and GPQA-Diamond [Rein et al., 2024] (198 multiple-choice questions written by domain experts in physics, chemistry, and biology). The four benchmarks together cover both numeric-answer and multiple-choice formats, which lets us assess whether the improvements brought by LARK transfer beyond the mathematical reasoning domain on which the candidate pool is constructed. The Avg column in Table 1 is the unweighted mean of these four benchmarks; because the four splits differ in the number of problems, the per-benchmark numbers remain the primary basis of comparison.

Decoding configuration. For every benchmark and every fine-tuned student, we generate 5 independent samples per problem with the following decoding parameters:

- `temperature = 0.6`
- `top-p = 0.95`
- `top-k = -1` (no top- k truncation)
- `maximum generation length = 32,768` tokens (matching the SFT context length)

The same decoding configuration is used across all baselines and LARK to ensure that any difference in downstream accuracy is attributable to the selection rule rather than to inference-time differences.

Metric (ACC@5). We report ACC@5 as our primary evaluation metric. For each test problem, we sample 5 independent generations under the decoding configuration above; the problem is marked *correct* if any of the 5 generations contains the correct final answer under the extraction rule described below. ACC@5 captures whether the student model is capable of producing a correct reasoning trajectory for the problem within a small sampling budget, and is less sensitive to single-sample variance than greedy ACC@1. Each experiment is repeated under three independent decoding seeds, with the selected training data and the SFT seed held fixed; we report the mean and standard deviation of ACC@5 across these three decoding seeds, so the reported variability captures inference-time sampling noise rather than training-seed noise.

System prompts. We use a fixed system prompt per benchmark family, distinguishing numeric-answer tasks (AIME, AMC), multiple-choice tasks (GPQA), and free-form-answer tasks (MATH-500). All three prompts share the same overall structure — enforcing English output, separating the reasoning chain from the final answer, and requiring the answer in a `\boxed{...}` environment for unambiguous extraction — and differ only in the answer-format specification.

System Prompt: AIME / AMC (Numeric Answer)

You are an AI mathematician. All content you output MUST be in English. Use the question to deduce the correct numeric answer.
Finish all your reasoning, then on a NEW line output only `\boxed{<number>}`.
 The content inside `\boxed{<number>}` must be the final numeric answer only, with no expressions, variables, or additional text.

System Prompt: GPQA (Multiple Choice)

You are an AI mathematician. All content you output MUST be in English. Use the question to deduce the correct choice.
Finish all your reasoning, then on a NEW line output only `\boxed{<letter>}`.
 The content inside `\boxed{<letter>}` must be exactly one of A, B, C, D.

System Prompt: MATH (Free-form Answer)

You are an AI mathematician. All content you output MUST be in English. Use the question to deduce the correct answer.
Finish all your reasoning, then on a NEW line output only `\boxed{<answer>}`.

Answer extraction rule. We extract the predicted final answer from each generation using the following deterministic rule:

- If the generation contains at least one `\boxed{...}` token, we take the content inside the *last* `\boxed{...}` as the predicted answer. The last (rather than first) occurrence is used because models occasionally produce intermediate boxed expressions during reasoning; only the final boxed value is treated as the answer.
- If the generation contains no `\boxed{...}` token, the generation is treated as *incorrect*, regardless of whether the surrounding text contains a correct value.

For numeric-answer tasks (AIME, AMC), the extracted string is canonicalized by stripping surrounding whitespace and converting fractions a/b to their decimal form before comparison with the ground truth. For multiple-choice tasks (GPQA), the extracted string is uppercased and compared against the gold letter in $\{A, B, C, D\}$. For free-form answers (MATH-500), we follow the canonicalization rules of [Hendrycks et al. \[2021\]](#), which normalize fraction, square-root, and exponent notation prior to string matching.

Efficient scoring for rank-based metrics. The RSR baseline of Appendix C.2 requires the clipped rank $\bar{r}_t^k = \min(r_t^k, r_{\max})$ at every token position. A naive implementation would sort the full $|\mathcal{V}|$ -dimensional logit vector at each token, costing $O(|\mathcal{V}| \log |\mathcal{V}|)$ per token. We avoid this by observing that under rank clipping at r_{\max} , only the relative order of the top- r_{\max} logits matters: any token whose true rank exceeds r_{\max} is mapped to r_{\max} regardless of its exact rank. We therefore extract the top- r_{\max} logits via `torch.topk` (cost $O(|\mathcal{V}| \log r_{\max})$ per token), check whether the gold token y_t^k is among them, and assign \bar{r}_t^k accordingly. This procedure is exact under rank clipping and reduces the per-token cost by a factor of $\log |\mathcal{V}| / \log r_{\max}$, which is roughly $5 \times -6 \times$ for $|\mathcal{V}| \approx 1.5 \times 10^5$ and $r_{\max} = 100$. The same forward pass that produces the surprisal $s_t^k = -\log \pi_t^k(y_t^k)$ is reused to produce the top- r_{\max} logits, so RSR scoring requires only one forward pass per candidate trajectory.

Prompt consistency. We use a consistent chat template across (i) selection-time scoring (when the student model evaluates each candidate trajectory under teacher forcing), (ii) SFT loss formatting (when the model is fine-tuned on the selected trajectories), and (iii) evaluation-time prompting (when the fine-tuned model is queried on benchmark problems). Using the same chat template at all three stages reduces train–test mismatch and ensures that selection scores measured on θ_{ref} remain meaningful for the fine-tuned model. All inputs are truncated to the same maximum sequence length of 32,768 tokens used for SFT.

C.5 Train/Eval Contamination Audit

To ensure that the downstream evaluation results in Table 1 reflect genuine generalization rather than memorization of training-time supervision, we audit the overlap between the 5,000-problem NuminaMath candidate pool of Appendix C.1 and every problem in the evaluation benchmarks of Appendix C.4.

Method. For each evaluation problem we compute the character 8-gram Jaccard similarity against every problem in the candidate pool, after a normalization step that lowercases the text, collapses whitespace, and strips redundant LaTeX spacing macros. We report two statistics: (i) *exact matches* (Jaccard = 1 after normalization), which would indicate verbatim duplication; and (ii) *near-matches* at three progressively stricter thresholds, $J \geq 0.4$, $J \geq 0.7$, and $J \geq 0.85$, to capture different degrees of surface overlap. The metric is sensitive to both surface and structural duplication: an exact-template variant with all numerals changed typically scores $J \in [0.7, 0.95]$, while a fully independent problem on the same topic typically scores $J < 0.2$.

Results. Table 2 summarizes the audit across all four evaluation benchmarks (AIME-2024, AMC, GPQA-Diamond, and MATH-500, broken down by difficulty levels L1–L5). The audit detects 0 exact matches across all 811 evaluation problems. AIME-2024, AMC, GPQA-Diamond, and MATH-L1 contain 0 near-matches at every threshold; GPQA-Diamond is graduate-level physics, chemistry, and biology with no domain overlap with the math-only NuminaMath training pool, while AIME, AMC, and MATH-L1 simply do not appear in the pool under any threshold. MATH-L2 through L5 contain 31 near-matches at $J \geq 0.4$ ($\sim 3.7\%$ of the MATH-500 split), of which only 1 case at $J \geq 0.85$.

Table 2: Train/eval contamination audit. For each evaluation benchmark, we report the number of problems whose character 8-gram Jaccard similarity against the NuminaMath candidate pool of Appendix C.1 exceeds the indicated threshold. *Exact* denotes Jaccard = 1 after text normalization. MATH-L1 through MATH-L5 are the five difficulty levels of MATH-500.

Benchmark	N	Exact	$J \geq 0.4$	$J \geq 0.7$	$J \geq 0.85$
AIME-2024	30	0	0	0	0
AMC	83	0	0	0	0
GPQA-Diamond	198	0	0	0	0
MATH-L1	43	0	0	0	0
MATH-L2	90	0	2	1	1
MATH-L3	105	0	7	1	0
MATH-L4	128	0	16	5	0
MATH-L5	134	0	6	1	0
Total	811	0	31	8	1

Categorization of MATH-L2–L5 near-matches. Manual inspection of all 31 flagged pairs places them in three categories, none of which constitute contamination:

- 1. Template-shared, numerically perturbed.** Same algebraic template, different constants or signs, leading to a different polynomial and a different answer. The highest-similarity case (MATH-L2 #11, $J = 0.869$) asks for the smallest n such that all roots of $z^4 + z^2 + 1 = 0$ are n -th roots of unity, while the closest training problem asks the same question for $z^4 - z^2 + 1 = 0$.
- 2. Template-shared, different question on the same setup.** Same physical or geometric setup, but a different quantity is asked, with no derivable relation between the two answers. For example, MATH-L5 #46 ($J = 0.693$) describes a hot-air balloon held by four ropes anchored at points A, B, C, D ; the training problem on the same setup asks for the length of OH , whereas the evaluation problem asks for the greatest rope length saved by replacing $HC + HD$ with a single rope at a chosen point. These are companion problems from the parent MATH dataset.
- 3. Surface-level template variation.** Same problem stem with different numerical inputs (e.g., coefficients in a quadratic completion task). MATH-L4 #38 ($J = 0.664$) asks to rewrite $x^2 + 2.6x + 3.6$ in the form $(x + b)^2 + c$, while the training problem performs the same operation on $x^2 - 20x + 36$. The procedure is identical but the inputs and outputs differ.

In none of the 31 flagged cases does the answer to a training problem transfer to the corresponding evaluation problem, and no exact duplicates of any AIME-2024, AMC, GPQA-Diamond, or MATH-500 problem appear in the training pool. The downstream Acc@5 results in Table 1 therefore reflect generalization to held-out problems rather than retrieval of memorized supervision.

D Diagnostic Analyses of LARK

This appendix collects additional evaluation results and diagnostic analyses that validate the design choices of LARK beyond the main downstream comparison. Appendix D.1 verifies the efficiency claim through both an asymptotic complexity derivation and a wall-clock measurement on 8 A100 GPUs, showing that LARK matches the lowest cost achieved by any per-trajectory scoring baseline. Appendix D.2 sweeps the selection budget B from 1 to 20 on a 500-problem diagnostic subset and studies how performance changes with the budget. Appendix D.3 zooms into a single training problem to illustrate, end to end, the score landscape over candidate trajectories, the token-level structure of the chosen trajectory, the χ^2 - B weighting it induces, and the resulting weighted SFT objective for that problem.

D.1 Computational Cost

We separate every per-trajectory score into two parts: a single forward pass over the trajectory through the student model, with cost $C_{\text{fwd}}(|a_k|)$, and a per-token post-processing step on the resulting logits. Decomposing the total cost in this way exposes the differences across methods, which would otherwise be hidden by the dominant forward-pass term.

Per-trajectory cost decomposition. A single forward pass through a transformer with L layers, hidden dimension d , and vocabulary size $|\mathcal{V}|$ on a trajectory of length $|a_k|$ has cost

$$C_{\text{fwd}}(|a_k|) = \underbrace{\mathcal{O}(L|a_k|d^2)}_{\text{MLP}} + \underbrace{\mathcal{O}(L|a_k|^2d)}_{\text{attention}} + \underbrace{\mathcal{O}(|a_k| \cdot |\mathcal{V}| \cdot d)}_{\text{LM head}}.$$

After this forward pass, every per-trajectory selection method applies a post-processing operation to the logits at each token. GRAPE computes the cross-entropy of the gold token from a $|\mathcal{V}|$ -dimensional log-sum-exp, with per-token cost $\mathcal{O}(|\mathcal{V}|)$. LARK computes both the cross-entropy and the Brier component $\sum_v \pi_t^k(v)^2$, again with per-token cost $\mathcal{O}(|\mathcal{V}|)$. RSR additionally selects the top- r_{max} entries of each token distribution to form a partial rank statistic, with per-token cost $\mathcal{O}(|\mathcal{V}| \log r_{\text{max}})$. Local Naturalness instead runs $m + 1$ independent forward passes per trajectory (one for each masked rollout), each followed by an $\mathcal{O}(|\mathcal{V}|)$ per-token operation.

Total complexity. Let N denote the number of training problems and K the number of candidate trajectories per problem. Aggregating the forward and the post-processing terms over all NK candidates yields the total cost of each method:

$$\text{GRAPE: } \mathcal{O}(NK \cdot [C_{\text{fwd}}(|a_k|) + |a_k| \cdot |\mathcal{V}|]),$$

$$\text{LARK: } \mathcal{O}(NK \cdot [C_{\text{fwd}}(|a_k|) + |a_k| \cdot |\mathcal{V}|]),$$

$$\text{RSR: } \mathcal{O}(NK \cdot [C_{\text{fwd}}(|a_k|) + |a_k| \cdot |\mathcal{V}| \log r_{\text{max}}]),$$

$$\text{Local Naturalness: } \mathcal{O}(NK \cdot [(m + 1) C_{\text{fwd}}(|a_k|) + |a_k| \cdot |\mathcal{V}|]).$$

LARK matches the lowest cost achieved by GRAPE. RSR adds a $\log r_{\text{max}}$ factor on the per-token term because of its rank selection step, and Local Naturalness multiplies the dominant forward pass by $m + 1$ because of its repeated rollouts. The strict ordering GRAPE = LARK < RSR and GRAPE = LARK < Local Naturalness follows from $|a_k| \cdot |\mathcal{V}| < |a_k| \cdot |\mathcal{V}| \log r_{\text{max}}$ and from $C_{\text{fwd}} < (m + 1) C_{\text{fwd}}$ for $m \geq 1$. We do not assign a model-independent asymptotic formula to LLM-judged Quality because its cost depends on the judge model and serving setup; we therefore report it in the wall-clock comparison.

Empirical wall-clock cost. We benchmark each scoring method by measuring its per-sample wall-clock cost on 8 A100 GPUs.² Figure 7 reports the resulting cost across all five scoring methods.

²Random, Token Length, and Rule-based Quality require no forward pass through the student and run in negligible time, so we omit them from the figure.

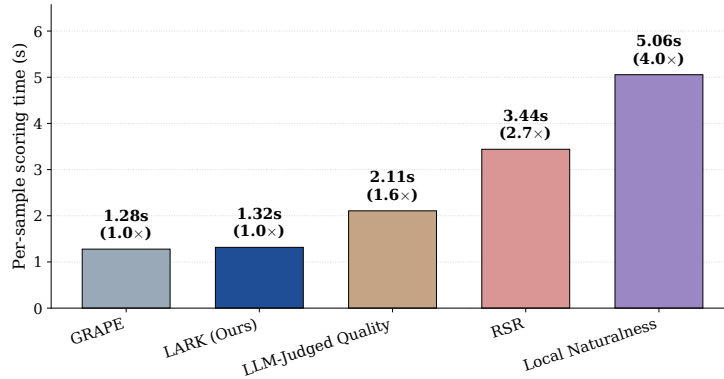


Figure 7: **Per-sample wall-clock cost of trajectory scoring** on 8 A100 GPUs. The number in parentheses is the slowdown relative to the fastest method. LARK is essentially as fast as GRAPE, $1.6\times$ faster than LLM-judged Quality, $2.7\times$ faster than RSR, and $4.0\times$ faster than Local Naturalness. Methods that require no forward pass through the student (Random, Token Length, Rule-based Quality) are omitted because their cost is negligible.

LARK (1.32 s/sample) matches GRAPE (1.28 s/sample) to within 3%, which reflects the fact that they share the same forward pass and differ only by an additional $\mathcal{O}(|\mathcal{V}|)$ Brier sum per token. LLM-judged Quality is $1.6\times$ slower at 2.11 s/sample because of the auxiliary judge call. RSR is $2.7\times$ slower at 3.44 s/sample, which is consistent with the extra $\log r_{\max}$ rank-selection factor in its per-token operation. Local Naturalness is the most expensive at 5.06 s/sample, which is $4.0\times$ slower than LARK and matches the $(m + 1)$ -fold forward-pass cost predicted by the asymptotic analysis. The empirical ordering matches the constant-factor ranking implied by the complexity formulas.

D.2 Selection Budget Scaling

We study how LARK behaves as the number of selected trajectories per question changes. This analysis sweeps the selection budget $B \in \{1, 3, 5, 10, 20\}$ on Qwen-2.5-7B and evaluates the resulting student on AMC Acc@5. Because this sweep is conducted on the same 500-problem subset used for our diagnostic experiments, rather than the full 5,000-problem training set used in Table 1, these results are intended to show the relative trend across budgets rather than to replace the main evaluation results.

For each budget B , we apply the LARK selection rule to choose B trajectories per problem, fine-tune Qwen-2.5-7B with the same SFT protocol described in Appendix C, and report AMC Acc@5 in Figure 8. LARK remains effective across the entire budget range: accuracy increases from 49.4% at $B=1$ to 65.1% at $B=3$, reaches its highest value of 68.7% at $B=10$, and remains strong at 66.3% when $B=20$.

The trend is not strictly monotonic. Moving from $B=1$ to $B=3$ brings a large improvement, indicating that using multiple selected trajectories can provide complementary supervision. However, increasing the budget beyond $B=3$ gives smaller and less stable gains. In particular, $B=5$ underperforms $B=3$, while $B=10$ gives the best result and $B=20$ slightly decreases. This pattern suggests that a small number of carefully selected trajectories already captures most of the useful training signal, while adding more lower-ranked trajectories can introduce weaker or less informative supervision.

Overall, the budget sweep shows that LARK is not sensitive to a single fixed choice of B . The method performs well with a small budget ($B=3$) and remains competitive as the budget increases. This supports the use of a small top- B selection strategy in the main experiments, where the goal is to improve distillation efficiency while avoiding unnecessary supervision from less informative trajectories.

D.3 Case Study: A Single-Problem Walkthrough

While Appendices D.1 and D.2 support the efficiency and budget-scaling analyses of LARK at the aggregate level, this appendix zooms into a single training problem to illustrate the end-to-end

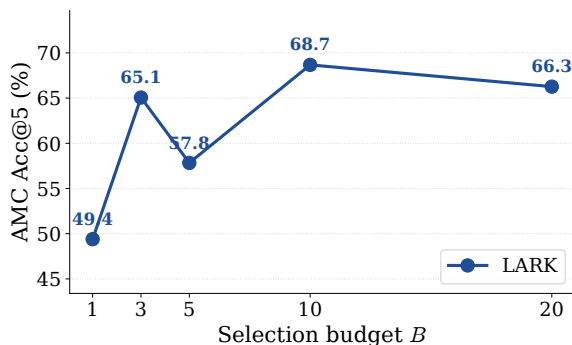


Figure 8: **Selection budget scaling of LARK** on Qwen-2.5-7B, evaluated on AMC after fine-tuning on the 500-problem subset. LARK achieves strong performance across $B \in \{1, 3, 5, 10, 20\}$, with the best result obtained at $B=10$.

behavior of the selection rule. We walk through (i) the problem and its candidate pool, (ii) the LARK score landscape, (iii) the top-1 trajectory selected by LARK, and (iv) the closed-form χ^2 - B weights at $B = 3$.

Problem and candidate pool. We illustrate on problem $\text{pid} = 839$ from the candidate pool of Appendix C.1:

User Question (pid= 839)

If \mathbf{a} , \mathbf{b} , and \mathbf{c} are vectors such that $\|\mathbf{a}\| = \|\mathbf{b}\| = 1$, $\|\mathbf{a} + \mathbf{b}\| = \sqrt{3}$, and

$$\mathbf{c} - \mathbf{a} - 2\mathbf{b} = 3(\mathbf{a} \times \mathbf{b}),$$

then find $\mathbf{b} \cdot \mathbf{c}$.

The ground-truth answer is $\frac{5}{2}$. The pool contains $K = 33$ candidate trajectories produced by 11 teacher models with 3 rollouts each; all reach the correct final answer per the construction of Appendix C.1.

Score landscape. Figure 9 shows the LARK score \hat{g}_k for all 33 candidates, grouped by teacher. The top-1 trajectory is the second rollout of `phi4-reason-plus` (highlighted in red, $\hat{g} = 0.01782$); the same teacher’s third rollout takes rank 2 ($\hat{g} = 0.01687$). Notably, `phi4-reason-plus` rollout 1 ranks only 25 ($\hat{g} = 0.00960$): the within-teacher spread on this teacher alone is $1.86\times$, exceeding the spread between several pairs of teachers. The same pattern recurs across the pool (e.g., `nemotron-super-v15` rollouts span 0.0052 to 0.0078), which underscores that LARK selects at the trajectory level rather than at the teacher level. Teachers commonly perceived as strong on aggregate benchmarks (`deepseek-r1-0528`, `qwen3-235b-2507`, `qwq-32b`) do not contribute any top-3 trajectory on this problem, with their rollouts clustering near the median.

Top-1 trajectory selected by LARK. We quote the top-1 trajectory (`phi4-reason-plus` rollout 2, $\hat{g} = 0.01782$) in full:

Top-1 trajectory selected by LARK (`phi4-reason-plus` rollout 2)

<think>

We are given: Vectors a, b, c . Conditions: $\|a\| = \|b\| = 1$, and $\|a + b\| = \sqrt{3}$. Also $c - a - 2b = 3(a \times b)$. We need find $b \cdot c$.

Step: First, note: $\|a + b\|^2 = (a + b)^2 = a^2 + 2a \cdot b + b^2 = 1 + 2 \cos \theta + 1 = 2 + 2 \cos \theta = 3$. So $2 + 2 \cos \theta = 3 \Rightarrow \cos \theta = 1/2$ so $a \cdot b = 1/2$.

Now, note: $a \times b$ is perpendicular to both a and b . So it is orthogonal to a, b . Then, $c = a + 2b + 3(a \times b)$. Dotting with b : $b \cdot c = b \cdot a + 2b \cdot b + 3b \cdot (a \times b) = a \cdot b + 2 \cdot 1 + 3 \cdot 0 = 1/2 + 2 = 5/2$. So answer: $5/2$.

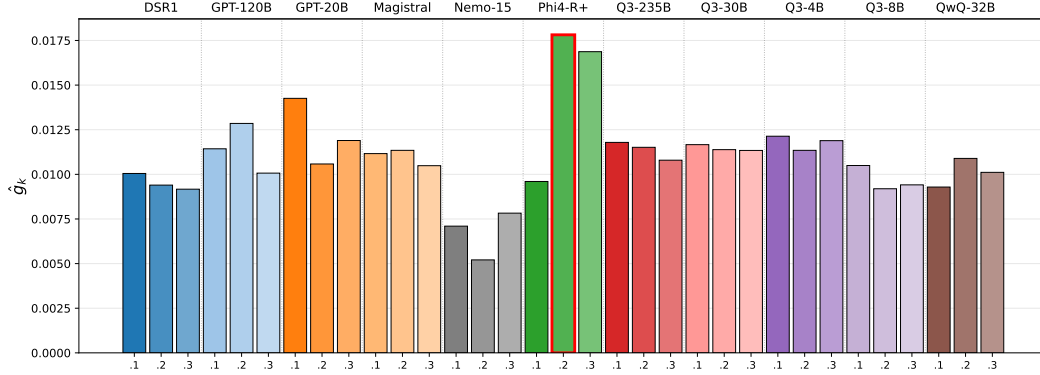


Figure 9: \hat{g}_k for all 33 candidate trajectories on problem pid = 839, grouped by teacher. Each teacher contributes 3 rollouts (indexed .1/.2/.3 along the x -axis). The top-1 trajectory selected by LARK (phi4-reason-plus rollout 2, $\hat{g} = 0.01782$) is highlighted with a red border. Within-teacher variation is comparable to between-teacher variation.

Thus final answer: 5/2. We'll produce answer in box: `\boxed{5/2}`.
`</think>`
`\boxed{\frac{5}{2}}`

The trajectory is substantially more compact than the average candidate in this pool. Importantly, its length-normalized cross-entropy ℓ_k under θ_{ref} is *not* the smallest in the pool; what raises \hat{g}_k appears to be the structure of the residual rather than low loss alone. A qualitative inspection suggests that high-residual tokens around numeric expressions and key algebraic steps carry a large portion of the cumulative Brier mass, matching the heuristic reading of \hat{g}_k in Remark 2.

χ^2 -B weighting at $B = 3$. With $B = 3$, the closed-form χ^2 -B rule gives the weights from the score margins above the threshold $\hat{g}_{(B+1)}$. The four relevant scores on this problem are:

$$\begin{aligned} \hat{g}_{(1)} &= 0.01782 \quad (\text{phi4-reason-plus.2}), \\ \hat{g}_{(2)} &= 0.01687 \quad (\text{phi4-reason-plus.3}), \\ \hat{g}_{(3)} &= 0.01426 \quad (\text{gptoss-20b-high.1}), \\ \hat{g}_{(4)} &= 0.01285 \quad (\text{gptoss-120b-high.2; threshold}). \end{aligned}$$

The score margins above the threshold are

$$\hat{g}_{(1)} - \hat{g}_{(4)} = 0.00497, \quad \hat{g}_{(2)} - \hat{g}_{(4)} = 0.00402, \quad \hat{g}_{(3)} - \hat{g}_{(4)} = 0.00141,$$

summing to $\sum_{j=1}^3 (\hat{g}_{(j)} - \hat{g}_{(4)}) = 0.01040$. The closed-form temperature is therefore $\tau^*(B) = 0.01040/K \approx 3.15 \times 10^{-4}$, and the LARK weights are

$$\hat{q}_{(1)} = 0.478, \quad \hat{q}_{(2)} = 0.387, \quad \hat{q}_{(3)} = 0.136.$$

The contrast with hard top- B truncation (uniform weight $1/B \approx 0.333$ each) is substantial: LARK assigns 43% more weight to the rank-1 trajectory than uniform top-3 would, and only 41% as much weight to the rank-3 trajectory. The asymmetry directly reflects the score gap between the two phi4-reason-plus rollouts and the remainder of the pool. The resulting per-problem contribution to the SFT loss is

$$\mathcal{L}_{\text{SFT}}^{(\text{pid}=839)}(\theta) = 0.478 \ell(\theta; \mathbf{y}_{16}) + 0.387 \ell(\theta; \mathbf{y}_{17}) + 0.136 \ell(\theta; \mathbf{y}_6),$$

with all other 30 candidates carrying zero weight on this problem.

Summary. The walkthrough illustrates three points anchored at a concrete problem: trajectory-level (rather than teacher-level) variation in \hat{g}_k can be the dominant source of selection signal; the LARK-selected trajectory is not the one with the lowest ℓ_k but the one with structured residual signal; and the χ^2 - B weighting deviates substantially from uniform top- B truncation when the top-ranked trajectory is sharply separated from the threshold.

E Limitations

LARK provides a practical and theoretically motivated approach for trajectory-level selection in reasoning distillation. Its forward-pass score makes the method efficient to apply to large candidate pools, and the closed-form weighting rule avoids additional tuning while preserving the benefits of multi-trajectory supervision. The empirical results across multiple student models and benchmarks suggest that learnability is a useful principle for selecting reasoning trajectories.

There are two natural limitations of the present study. First, our experiments use a correctness-verified candidate pool, where all retained trajectories reach the correct final answer. This setting isolates the trajectory-selection problem from the separate problem of correctness verification, but future work could study LARK in noisier pools that include incorrect or partially correct teacher trajectories. Second, due to the computational cost of full-parameter SFT, our reported standard deviations are computed over independent decoding seeds while keeping the training configuration fixed. Running multiple independent SFT seeds would provide an even more complete estimate of training-time variance.